NONLINEAR OPTICAL IMAGE PROCESSING WITH HALFTONE SCREENS

by

Stephen Robert Dashiell

May 1976

Image Processing Institute
University of Southern California
University Park
Los Angeles, California 90007

This research was supported by the Advanced Research Project Agency of the Department of Defense and was monitored by the Air Force Avionics Laboratory under Contract No. F-33615-76-C-1203, ARPA Order No. 3119, and by the Joint Services Electronics Program through the Air Force Office of Scientific Research (AFSC) under Contract No. F-44620-76-C-0061.

UNCLASSIFIED
Security Classification

DOCUMENT CONTROL DATA - R & D

(Security classification of title, body of abstract and indexing annotation must be entered when the overall report is classified)

1. ORIGINATING ACTIVITY (Corporate author) Image Processing Institute University of Southern California, University Park Los Angeles, California 90007	2a. REPORT SECURITY CLASSIFICATION UNCLASSIFIED 2b. GROUP

3. REPORT TITLE

NONLINEAR OPTICAL IMAGE PROCESSING WITH HALFTONE SCREENS

4. DESCRIPTIVE NOTES (Type of report and inclusive dates)
Technical Report, May 1976

5. AUTHOR(S) (First name, middle initial, last name)

Stephen R. Dashiell

6. REPORT DATE	7a. TOTAL NO. OF PAGES	7b. NO. OF REFS
20 May 1976	195	36

8a. CONTRACT OR GRANT NO.	9a. ORIGINATOR'S REPORT NUMBER(S)
F-33615-76-C-1203 b. PROJECT NO. c. ARPA Order No. 3119 d.	USCIPI Report 670 9b. OTHER REPORT NO(S) (Any other numbers that may be assigned this report)

10. DISTRIBUTION STATEMENT

Approved for release: distribution unlimited

11. SUPPLEMENTARY NOTES	12. SPONSORING MILITARY ACTIVITY
	Advanced Research Projects Agency 1400 Wilson Boulevard Arlington, Virginia 22209

13. ABSTRACT

Coherent optical systems are of interest in image or data processing because of their ability to rapidly handle large bandwidth data in parallel. They have been restricted to performing linear operations such as Fourier transformation and convolution, due to the inherent linear nature of an optical system at low power levels. In this dissertation, the combination of a nonlinear halftoning step followed by band pass spatial filtering to yield a specific nonlinear intensity transfer function is explored.

A general analysis of the problem assuming infinite copy film gamma and saturation density is made. A constructive algorithm for designing a halftone cell shape and selecting the diffraction order to yield very general types of non-monotonic nonlinearities is presented. Numerous examples of the synthesis procedure are given.

The design of non-monotonic halftone cells which allow a non-monotonic nonlinearity with an arbitrary number of changes of sign in slope to be obtained in the first diffraction order is considered. An iterative algorithm suitable for computer implementation, and numerous examples of halftone cells designed with this algorithm are given.

The effects of allowing the film gamma and saturation density to become finite are analyzed, and a technique for compensating a priori for some of the resulting degradations is given.

(over)

DD FORM 1 NOV 65 1473

UNCLASSIFIED
Security Classification

14. KEY WORDS	LINK A		LINK B		LINK C	
	ROLE	WT	ROLE	WT	ROLE	WT

Experimental results with general halftone screens made on a plotting flatbed microdensitometer are presented. Logarithmic, exponential, and level slice characteristics have been achieved with monotonic cells. Intensity notch filter and quantization characteristics have been achieved with non-monotonic cells. Other generalizations of the technique are discussed, including the possibliity of real-time nonlinear processing with optical input transducers.

* *

Key Words: Halftone Screens, Image Processing, Nonlinear Optical Processing.

ACKNOWLEDGEMENTS

I would like to express my sincere appreciation to Professor Alexander A. Sawchuk, whose suggestions and guidance made this dissertation possible. Thanks also go to my wife Anne for her love and encouragement during the course of this research.

This research was supported by the Joint Services Electronics Program through the Air Force Office of Scientific Research/AFSC and by the Advanced Research Projects Agency of the Department of Defense monitored by the Air Force Avionics Laboratory, Wright-Patterson Air Force Base.

ABSTRACT

Coherent optical systems are of interest in image or data processing because of their ability to rapidly handle large bandwidth data in parallel. They have been restricted to performing linear operations such as Fourier transformation and convolution, due to the inherent linear nature of an optical system at low power levels. In this dissertation, the combination of a nonlinear halftoning step followed by band pass spatial filtering to yield a specific nonlinear intensity transfer function is explored.

A general analysis of the problem assuming infinite copy film gamma and saturation density is made. A constructive algorithm for designing a halftone cell shape and selecting the diffraction order to yield very general types of nonmonotonic nonlinearities is presented. Numerous examples of the synthesis procedure are given.

The design of non-monotonic halftone cells which allow a non-monotonic nonlinearity with an arbitrary number of changes of sign in slope to be obtained in the first diffraction order is considered. An iterative algorithm suitable for computer implementation, and

numerous examples of halftone cells designed with this algorithm are given.

The effects of allowing the film gamma and saturation density to become finite are analyzed, and a technique for compensating a priori for some of the resulting degradations is given.

Experimental results with general halftone screens made on a plotting flatbed microdensitometer are presented. Logarithmic, exponential, and level slice characteristics have been achieved with monotonic cells. Intensity notch filter and quantization characteristics have been achieved with non-monotonic cells. Other generalizations of the technique are discussed, including the possibility of real-time nonlinear processing with optical input transducers.

TABLE OF CONTENTS

LIST OF FIGURES

CHAPTER 1

INTRODUCTION

Optical information processing systems are capable of performing linear operations such as Fourier transformation and convolution on two-dimensional data in parallel at high speed [1-1]. At the low power levels present in the typical optical processor, only linear operations are possible unless special techniques are employed. Many information processing applications require nonlinear operations to be performed on the data, and these have usually been accomplished digitally. Various techniques however, have been employed to realize nonlinearities optically.

Saturable absorbers and in some cases feedback have been used in an optical system to generate a nonlinear characteristic [1-2,3,4]. This requires working at power levels substantially higher than those usually employed in optical processing systems, due to the high powers required to saturate the saturable absorber. Photochromic materials have been suggested as a possible approach

[1-5]. A theta modulation scheme [1-6] in which brightness levels are locally converted to rotated gratings has been described. By selective spatial filtering of these levels, nonlinear functions can be achieved. Unfortunately there is no straightforward way to optically perform the theta modulation. Multiple isophotes have been achieved with holographic techniques [1-7].

Recently halftone screen preprocessing has been used to achieve nonlinearities, and this is the overall approach taken in this study. The halftone process is a photographic method for representing a picture containing grey tones as a binary picture. This technique has been used in graphics arts for more than 70 years for printing grey tone pictures with printing presses. The grey tones are represented as an area modulation of black dots on a white background which the eye averages to produce the appearance of grey. By preprocessing the photographic input with a halftone screen, the size of these dots can be varied as a function of the density of the original picture to produce the apparent grey tones. Both one-dimensional screens (linear gratings) and two-dimensional screens (arrays of dots) can be used, but the one-dimensional halftoned picture is usually not as good visually as a picture made with a two-dimensional

screen. It will be shown in chapter 2 that when nonlinear transformations in coherent optical systems are the desired result, one-dimensional screens are as useful as two-dimensional screens.

The variation in dot size as a function of input transparency density is the first step of interest in obtaining nonlinear transfer functions. The second step involves diffraction order selection, or equivalently transmitting the energy contained in a specific Fourier component of the halftoned picture. The functional dependence of the second step depends on the diffraction order considered. It will be seen that control of both the diffraction order used and the halftone screen allows a wide variety of nonlinear transfer functions to be realized.

The halftone process is illustrated in the next several figures. Figure 1-1 shows a possible one-dimensional density profile of a typical halftone screen. For a two-dimensional screen, the plot of density vs. y for an (x,y) coordinate system is similar. Figure 1-2 shows a possible input density function. This represents a transition from a light (D=.5) to a dark (D=1.5) region. The input function and the screen function are optically added together to produce the sum

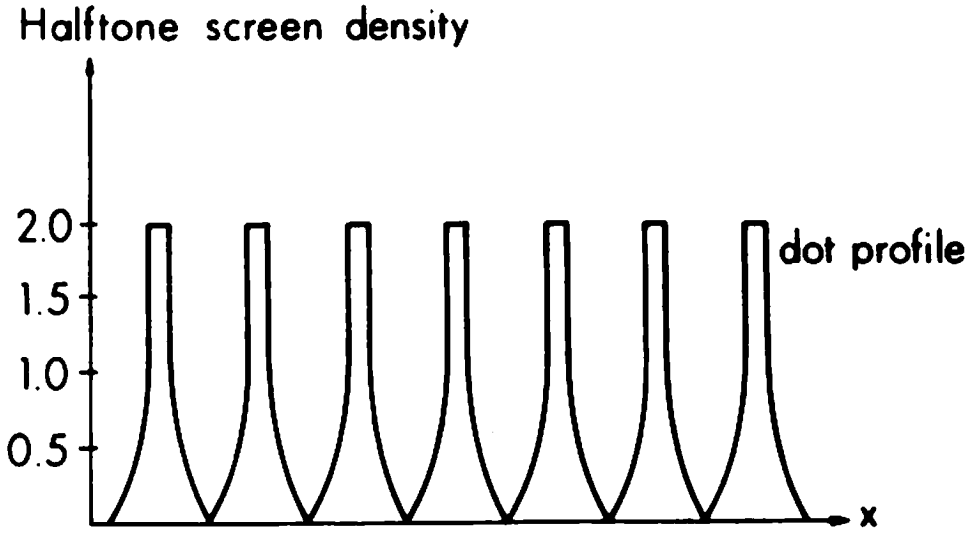

Figure 1-1. A typical density profile for a halftone screen.

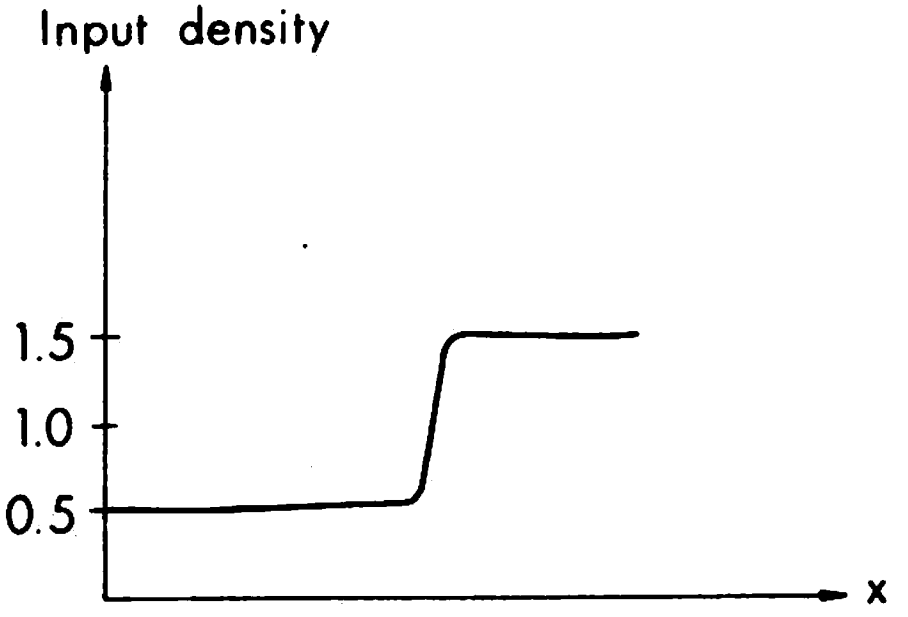

Figure 1-2. Typical input density function containing an edge.

density function shown in Fig. 1-3. The addition is physically accomplished by contacting the halftone screen with the input transparency so a uniform illumination has been transmitted through both. The light transmitted by the pair is then photographically recorded on a high contrast copy film. A typical response for such a film is shown in Fig. 1-4. The D_{clip} shown in Fig. 1-4 indicates the maximum density on Fig. 1-3 through which the copy film can be exposed. The clip level is logarithmically proportional to the controllable uniform illumination used. The effect of varying the illumination is to vary the D_{clip} value which in turn moves the clip level on Fig. 1-3 up or down on the density axis.

The transmission of the copy film is ideally either 1 or Ø because of its high contrast characteristic. The halftoned version of a continuous density distribution such as in Fig. 1-3 will appear as shown in Fig. 1-5. All values of x for which the density is less than the clip level have turned black and hence transmit no light. All values of x for which the density is greater than the clip level do not expose on the film, resulting in unity transmission following photographic processing.

It is this halftoned picture, as shown in profile in Fig. 1-5 which is capable of yielding a nonlinearity when

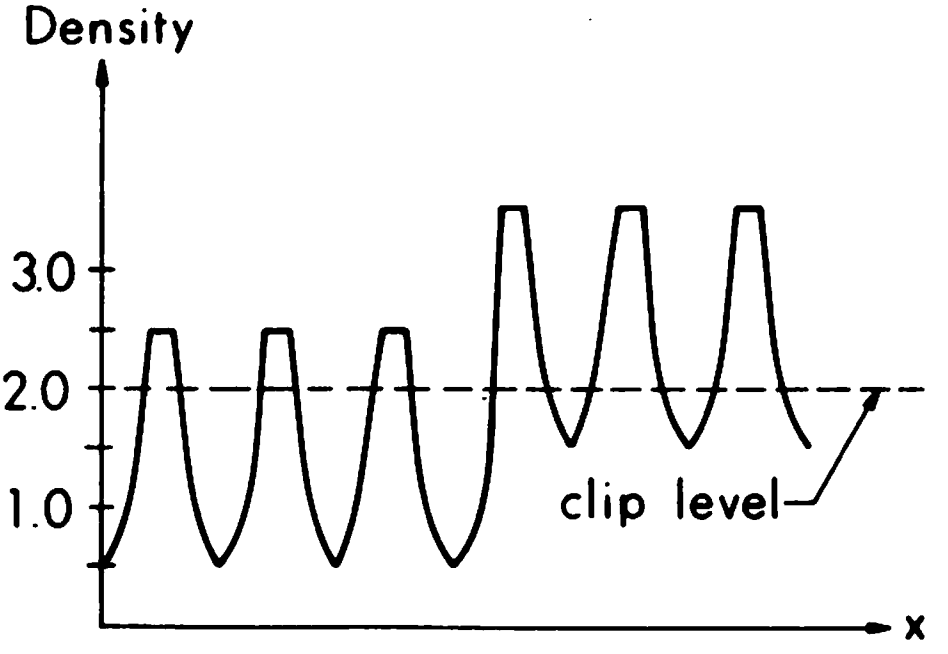

Figure 1-3. Density distribution used as input to the copy film.

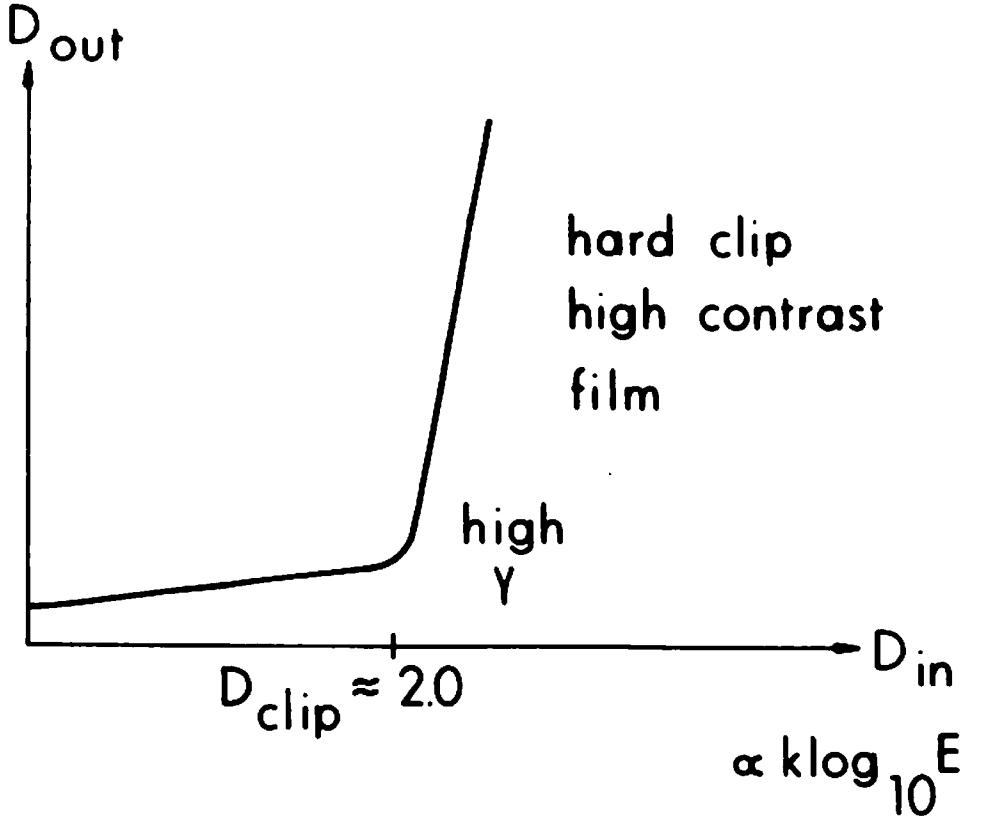

Figure 1-4. Typical response of the copy film.

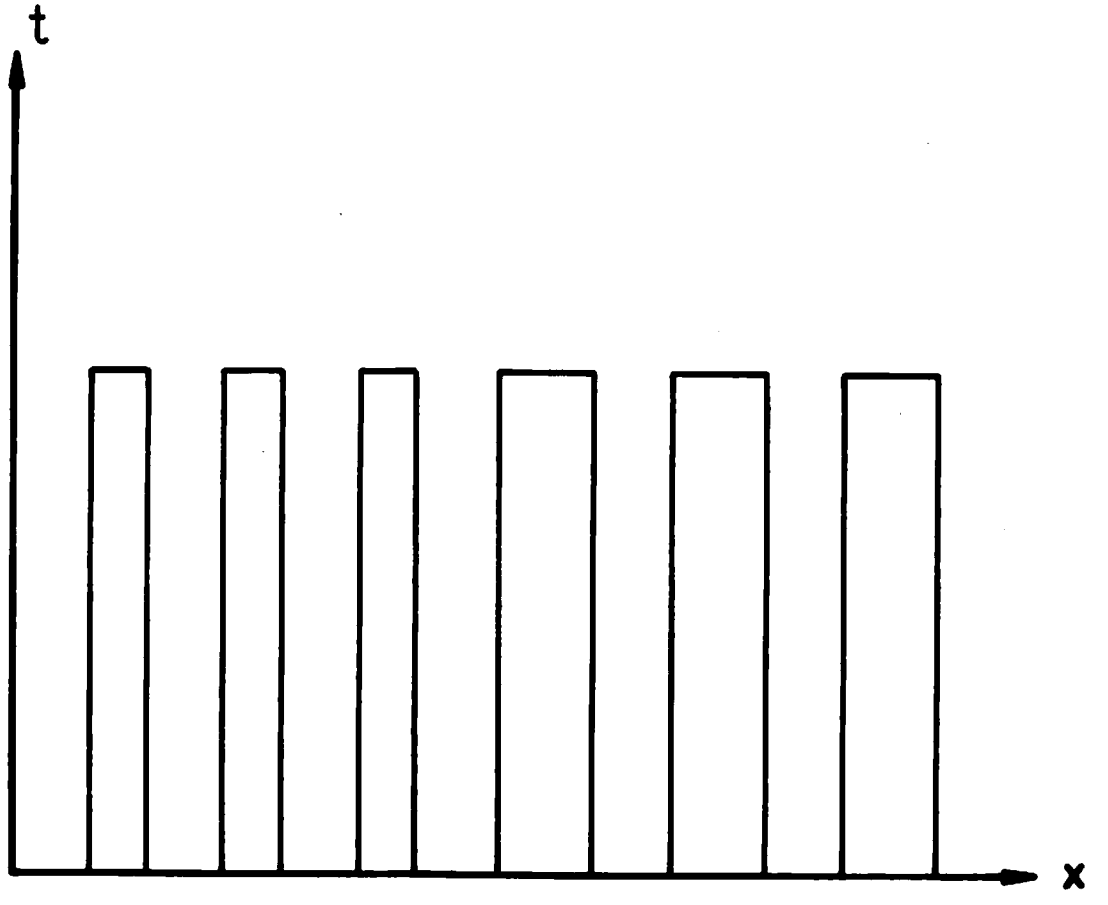

Figure 1-5. Transmission profile of the copy film following photographic processing.

placed in a coherent optical system [1-8] as shown in Fig. 1-6. If this halftoned input picture is made with a two-dimensional halftone screen, the Fourier transform plane will be a two-dimensional array of points of light which will ideally be the centers of distinct spectral islands, each of which contains complete image information. This assumes that the picture is sampled at an adequately high rate. If the sampling rate is not high enough, the spectral islands will not be separable, and aliasing will occur [1-9]. One of these diffraction orders is selected by a spatial filter and retransformed by the second lens to yield the desampled output. As shown in this work, the output will be a nonlinear version of the original picture where the nonlinearity depends on the halftone screen and the diffraction order chosen.

Marquet [1-10] and somewhat later Marquet and Tsujiuchi [1-11] noted that if a halftoned image was desampled in a coherent optical system, various types of nonlinearities could be produced, depending on the diffraction order chosen in the Fourier transform plane. Kato and Goodman [1-12,13] successfully performed a logarithmic transformation with a commercially available halftone screen. More recently Lohmann and Strand [1-14,15,16] have used the halftone technique to perform analog-to-digital conversion, and to generate equidensity

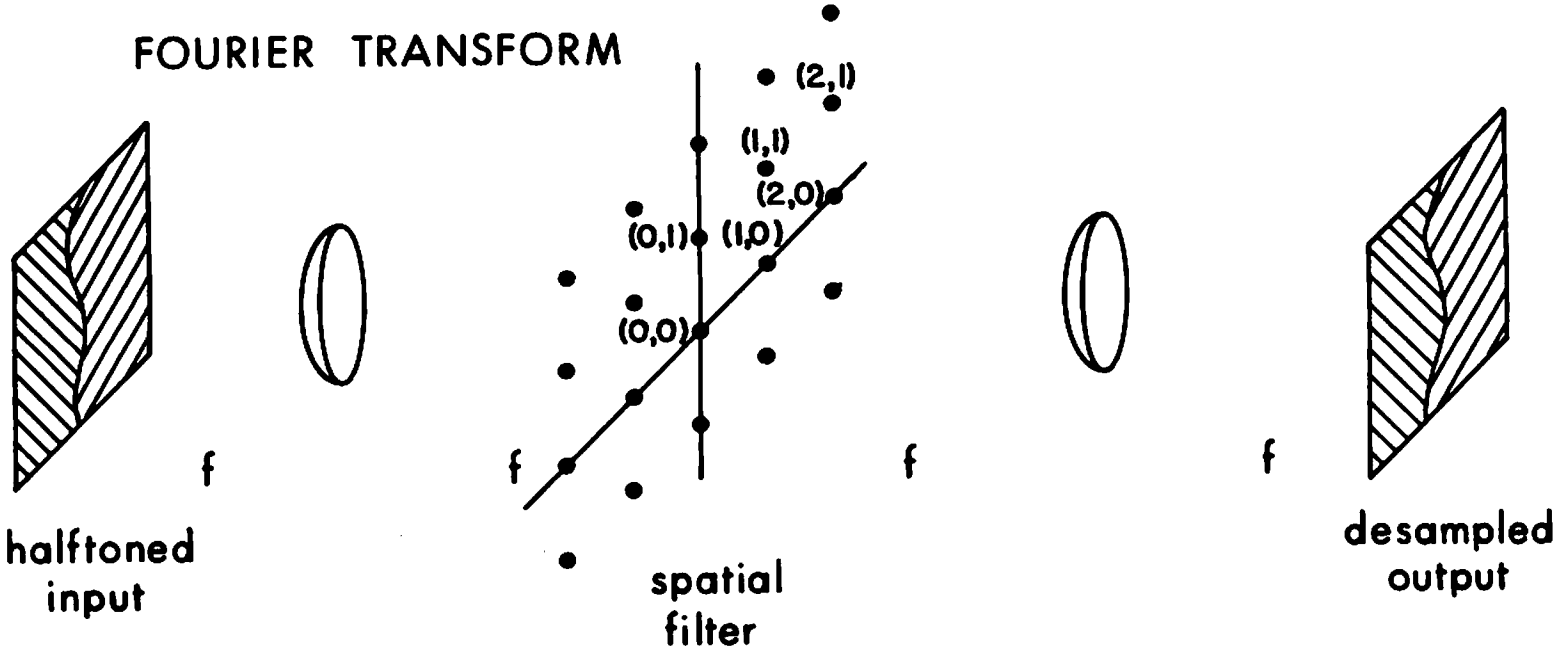

Figure 1-6. Coherent optical system used for optically processing the halftoned picture.

isophotes. Liu has also done some work with equidensitometry using halftone screens [1-17]. Some of the results of this dissertation have been summarized in several publications [1-18,19,20,21,22], where operations such as exponentiation, level slicing, notch filtering, and quantization have been demonstrated using the halftone process.

The following is an outline of the chapters of this dissertation and a summary of the specific research contributions in each.

Chapter 2 considers in detail the dependence of the system transfer function on the halftone screen and the diffraction order used. An ideal binary copy film is assumed throughout. It concludes with a computer synthesis algorithm for specifying the shape of a monotonic halftone screen required for a particular transfer function and specifies the diffraction order to use. Chapter 3 contains several specific examples of the use of this algorithm, including halftone screen profiles and transfer functions.

In chapter 4, the consequences of using a copy film which is not an ideal binary device are explored and a mathematical model to predict the system performance is developed. Numerous computer results showing the effects

of parameter variation are given using this model.

Chapter 5 considers non-monotonic halftone screens, an unusual variation on the normal type of monotonic halftone screen. Certain capabilities of this type of halftone screen for nonlinear processing are explored, and a synthesis algorithm for designing such halftone screens for a specific transfer function is presented, with examples.

Chapter 6 discusses a precompensation technique which allows non-ideal copy film to be used with minimum degradation of the ultimate transfer function. A technique for calculating compensated cell shapes is given, with examples. The use of a phase halftoned picture in the coherent optical system is also considered.

Chapter 7 discusses the procedure used for making several halftone screens, and presents the experimental results obtained. Finally, conclusions and recommendations for further research in this subject are contained in chapter 8.

CHAPTER 2

SYMMETRICAL AND NON-SYMMETRICAL MONOTONIC HALFTONE CELLS

A halftone screen consists of a one or two-dimensional periodic array of halftone cells. Commercially available screens for photoreproduction are usually two-dimensional, although the screens made for experimentally realizing particular transfer functions as described later are one-dimensional because they are somewhat easier to fabricate. For this reason, two-dimensional cells will not be considered in great detail. Another degree of freedom is that both symmetrical and non-symmetrical cells can be used. Briefly, a halftone screen is considered symmetrical and monotonic if each cell in the screen is an even function about its center and the density increases monotonically on either side of center. The screen is considered non-symmetrical but monotonic if the density increases monotonically from edge to edge of the cell but is not an even function about the center. Both types of cells are shown in Fig. 2-1, in which the fundamental period of the

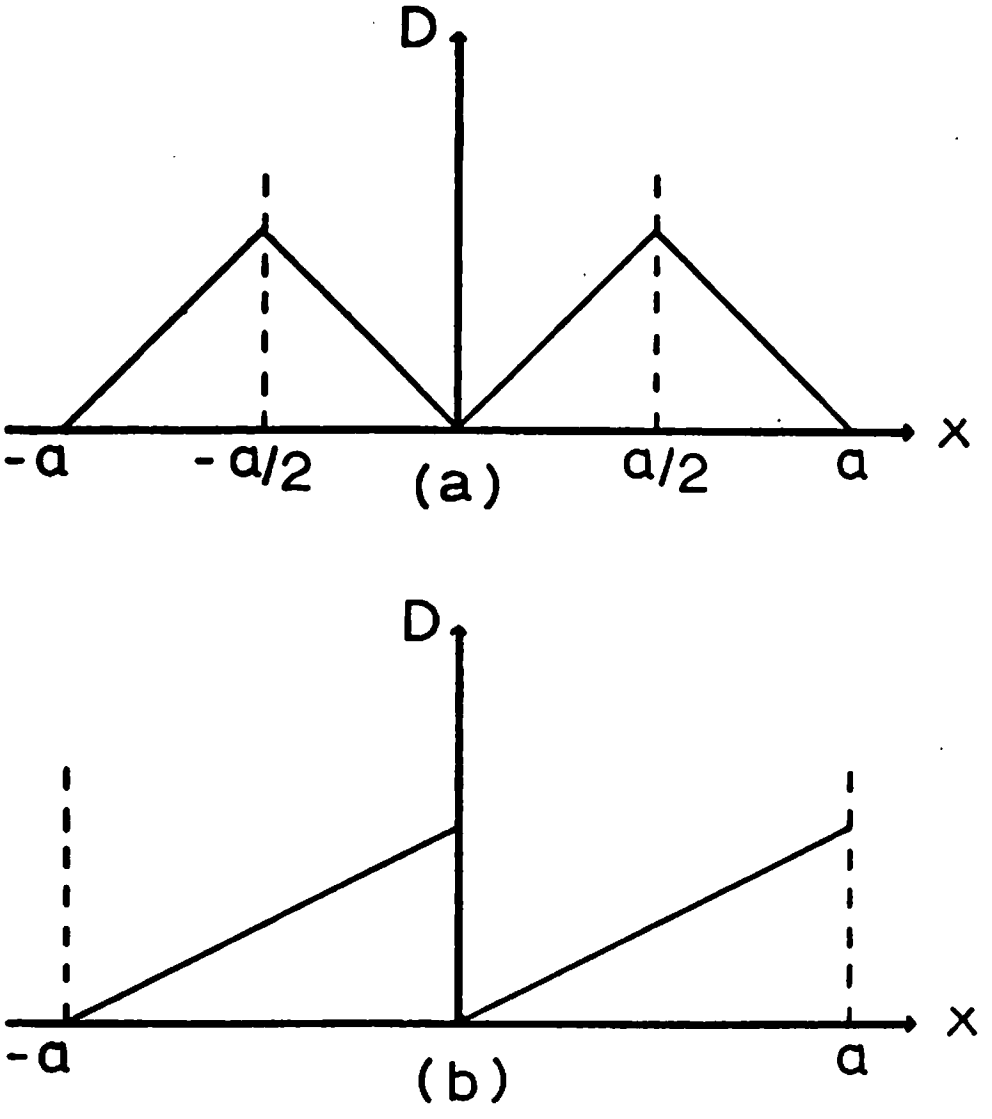

Figure 2-1. (a) Symmetrical halftone cell.
(b) Non-symmetric halftone cell.

repeated cells is denoted by a.

In using halftones for nonlinear transformations, the end product of the first processing operation is a binary halftoned picture. All of the analysis to follow assumes that the sampling theorem [2-1] is satisfied and the amplitude distribution present in the Fourier transform consists of discrete spectral islands, one of which can be selected for retransforming. If the sampling theorem is not satisfied, aliasing will occur and the situation becomes much more complicated. If the sampling theorem is satisfied, that is, if the screen frequency is at least twice as high as the highest spatial frequency present in the image being halftoned, this halftoned picture will be a pulse-width modulated negative of the original input. The halftoned picture will consist of dots, usually square, of varying size, or of bars of varying widths. It will be shown that the possible transfer functions are essentially the same for one-dimensional and two-dimensional screens. This minimum of twice the maximum image spatial frequency may be overly cautious, but it is quite difficult or impossible to analytically determine the minimum screen frequency actually required due to the nonlinear halftoning step [2-2].

2.1 Amplitude Output from Symmetrical Halftones with a One-Film Process

As a first step, an expression for the Fourier transform of an infinite array of opaque bars of width b spaced a distance a apart on a clear background is required. As will be shown in section 2.5, the bar width b is controlled by the halftone screen and is a function of the input intensity in the process. The array of bars analyzed here represents the pattern on the copy film following the halftoning step.

A single transparent bar of width b on an infinite opaque background can be represented as

$$v(x)=\text{rect}(x/b) \quad , \tag{2.1}$$

and an infinite one-dimensional array of such bars spaced a distance a apart on an opaque background can be represented as

$$\begin{aligned} u(x) &= v(x) * ((1/a) \cdot \text{comb}(x/a)) \\ &= \text{rect}(x/b) * ((1/a) \cdot \text{comb}(x/a)) \end{aligned} \tag{2.2}$$

where comb is defined by [2-3]

$$\mathrm{comb}(x)=\sum_{n=-\infty}^{\infty}\delta(x-n) \tag{2.3}$$

and * denotes convolution. Inverting the contrast to get opaque bars on a transparent background yields

$$\begin{aligned} t(x) &= 1-u(x) \\ &= 1-\mathrm{rect}(x/b)*((1/a)\cdot\mathrm{comb}(x/a)) \end{aligned} \tag{2.4}$$

as the film transmittance function.

Equation (2.4) represents the local pattern present on the halftoned picture, where the width b is some function of input intensity determined by the halftone preprocessing. The amplitude distribution represented by eq. (2.4) is optically Fourier transformed [2-4] by the system shown in Fig. 1-6 and a single diffraction order is selected by a pinhole spatial filter for retransforming to yield the final output. Ignoring focal length and wavelength factors for simplicity, the Fourier transform of eq. (2.4) is given by

$$\mathcal{F}\{t(x)\}=\delta(f_x)-b\cdot\mathrm{sinc}(bf_x)\cdot\mathrm{comb}(af_x) \tag{2.5}$$

where $\mathcal{F}\{\cdot\}$ denotes the Fourier transform operation. The separation into distinct diffraction orders is more easily

seen if the comb function in eq. (2.5) is replaced by a sum of delta functions as indicated in eq. (2.3). Equation (2.5) is equivalent to

$$\mathcal{F}\{t(x)\} = \delta(f_x) - (1/a)\cdot\sum_{n=-\infty}^{\infty} \delta(f_x - n/a)\cdot b\cdot \mathrm{sinc}(bf_x) \quad . \qquad (2.6)$$

Replacing f_x in the sinc function with the values specified by the delta function yields

$$\mathcal{F}\{t(x)\} = \delta(f_x) - \sum_{n=-\infty}^{\infty} \delta(f_x - n/a)\cdot(b/a)\cdot \mathrm{sinc}(bn/a) \qquad (2.7)$$

as the Fourier transform of the input pattern specified by eq. (2.4). All image information is clustered in spectral islands positioned at $f_x = 0, +1/a, -1/a, +2/a, -2/a, \ldots$ in the Fourier transform plane, as shown in Fig. 1-6 for the two-dimensional situation. A complete description of the amplitude present in this plane is rather complicated and unnecessary, since it is assumed that the islands are completely separate. In normal use, a single diffraction order (spectral island) is passed by an aperture of suitable size and retransformed to yield the output. If the Nyquist criterion is satisfied in the original halftoning process a single spectral island can be selected, and no subject detail will be lost by this band pass operation.

The two distinct cases of interest are the zero and non-zero order selections. Selecting only the n=0 term of eq. (2.7) yields

$$\mathcal{F}\{t(x)\}_{n=0} = \delta(f_x) \cdot (1-b/a) \qquad (2.8)$$

as the amplitude in the zero order diffraction component. Selecting any term for which n≠0 gives

$$\mathcal{F}\{t(x)\}_{n\neq 0} = -\delta(f_x - n/a) \cdot (b/a) \cdot \mathrm{sinc}(bn/a) \qquad (2.9)$$

as the amplitude present in the nth diffraction order. The order passed is retransformed to yield the output amplitude. Retransforming eq. (2.8) yields

$$\mathcal{F}\{\mathcal{F}\{t(x)\}_{n=0}\} = 1-(b/a) \qquad (2.10)$$

and retransforming eq. (2.9) gives

$$\begin{aligned}\mathcal{F}\{\mathcal{F}\{t(x)\}_{n\neq 0}\} &= -(b/a) \cdot \mathrm{sinc}(bn/a) \cdot \exp(-j2\pi nx/a) \\ &= -(1/n\pi) \cdot \sin(\pi bn/a) \cdot \exp(-j2\pi nx/a) \qquad (2.11)\end{aligned}$$

for the local complex amplitude in the image plane. The operation of the two lenses is modeled as two successive Fourier transforms. This is the same as a Fourier

transform followed by an inverse Fourier transform except for a coordinate inversion, which is immaterial here.

The same sampling considerations and technique can be used to analyze two-dimensional patterns. A single transparent square with side b on an opaque background is represented as

$$v(x,y)=\mathrm{rect}(x/b)\cdot\mathrm{rect}(y/b) \quad , \tag{2.12}$$

and a two-dimensional array of such squares with a center to center spacing a is written as

$$\begin{aligned} u(x,y) &= v(x,y) * ((1/a^2)\cdot\mathrm{comb}(x/a)\cdot\mathrm{comb}(y/a)) \\ &= \mathrm{rect}(x/b)\cdot\mathrm{rect}(y/b) * \\ &\quad ((1/a^2)\cdot\mathrm{comb}(x/a)\cdot\mathrm{comb}(y/a)) \quad . \end{aligned} \tag{2.13}$$

Inverting the contrast yields

$$\begin{aligned} t(x,y) &= 1-u(x,y) \\ &= 1-\mathrm{rect}(x/b)\cdot\mathrm{rect}(y/b) * \\ &\quad ((1/a^2)\cdot\mathrm{comb}(x/a)\cdot\mathrm{comb}(y/a)) \quad , \end{aligned} \tag{2.14}$$

and Fourier transforming eq. (2.14) gives

$$\mathcal{F}\{t(x,y)\} = \delta(f_x,f_y) - b^2 \cdot \mathrm{sinc}(bf_x) \cdot \mathrm{sinc}(bf_y) \cdot \mathrm{comb}(af_x) \cdot \mathrm{comb}(af_y) \qquad (2.15)$$

as the amplitude in the transform plane. Rewriting the comb functions as a summation of delta functions making use of eq. (2.3) gives

$$\mathcal{F}\{t(x,y)\} = \delta(f_x,f_y) - (1/a^2) \cdot \sum_{n=-\infty}^{\infty} \cdot \sum_{m=-\infty}^{\infty} \delta(f_x - n/a) \cdot \delta(f_y - m/a) \cdot b^2 \cdot \mathrm{sinc}(bf_x) \cdot \mathrm{sinc}(bf_y) \qquad (2.16)$$

where the m and n specify two-dimensional diffraction orders. Putting in actual values for f_x and f_y yields as a final expression

$$\mathcal{F}\{t(x,y)\} = \delta(f_x,f_y) - (b^2/a^2) \cdot \sum_{n=-\infty}^{\infty} \sum_{m=-\infty}^{\infty} \delta(f_x - n/a) \cdot \delta(f_y - m/a) \cdot \mathrm{sinc}(bn/a) \cdot \mathrm{sinc}(bm/a) \quad . \qquad (2.17)$$

Once again, a single order is selected in the transform plane and retransformed to yield the output. The possibilities break up into three distinct cases: 1.) $m=n=0$, 2.) $m=0$ and $n\neq 0$ or $m\neq 0$ and $n=0$, or 3.) both m and n non-zero. In the second case, it is unimportant whether m or n is chosen to be zero. Examining the three cases

yields expressions from eq. (2.17) as follows

$$\mathcal{F}\{t(x,y)\}_{0,0} = \delta(f_x, f_y) \cdot (1 - b^2/a^2) \quad , \tag{2.18}$$

$$\begin{aligned}\mathcal{F}\{t(x,y)\}_{0,n} &= -\delta(f_x - n/a) \cdot \delta(f_y) \cdot (b^2/a^2) \cdot \mathrm{sinc}(bn/a) \\ &= -\delta(f_x - n/a) \cdot \delta(f_y) \cdot (b/\pi na) \cdot \sin(\pi bn/a) \quad , \end{aligned} \tag{2.19}$$

and

$$\begin{aligned}\mathcal{F}\{t(x,y)\}_{m,n} &= -\delta(f_x - n/a) \cdot \delta(f_y - m/a) \cdot (b^2/a^2) \cdot \\ &\qquad \mathrm{sinc}(bn/a) \cdot \mathrm{sinc}(bm/a) \\ &= -\delta(f_x - n/a) \cdot \delta(f_y - m/a) \cdot (1/\pi^2 mn) \cdot \\ &\qquad \sin(\pi bn/a) \cdot \sin(\pi bm/a) \quad . \end{aligned} \tag{2.20}$$

The final output amplitude is obtained by retransforming eq. (2.18), (2.19), or (2.20) to give

$$\mathcal{F}\{\mathcal{F}\{t(x,y)\}_{0,0}\} = 1 - b^2/a^2 \quad , \tag{2.21}$$

$$\begin{aligned}\mathcal{F}\{\mathcal{F}\{t(x,y)\}_{0,n}\} &= -(b/\pi na) \cdot \sin(\pi bn/a) \cdot \\ &\qquad \exp(-j2\pi nx/a) \quad , \end{aligned} \tag{2.22}$$

and

$$\mathcal{F}\{\mathcal{F}\{t(x,y)\}_{m,n}\} = -(1/\pi^2 mn)\cdot \sin(\pi bn/a)\cdot \sin(\pi bm/a)\cdot$$

$$\exp(-j2\pi(nx+my)/a) \quad , \qquad (2.23)$$

respectively.

The output amplitude for non-zero orders in one and two dimensions are similar functionally, but the differences deserve some comment. Equation (2.11) for the one-dimensional output has evenly spaced zeros, as does eq. (2.22) for the two-dimensional case, but does not have the b/a multiplicative factor. Equation (2.23) will have unevenly spaced zeros if $m \neq n$, and it also lacks the b/a factor.

2.2 Amplitude Output from Non-Symmetrical Halftones with a One-Film Process

If a halftone screen is constructed on some device which makes each cell by plotting a finite number of points or lines depending on whether the cell is two-dimensional or one-dimensional, a non-symmetrical cell has twice the possible number of points to cover a specified density range. For example, if a cell for use in the zero order has to range in density continuously

from density=Ø to density=1 and has twenty lines per cell, a symmetric cell has only ten lines from density=Ø at the center to density=1 at the edge. A non-symmetrical cell has twenty lines in this density range, therefore the step approximation to the desired function takes smaller steps in density, and will be a closer approximation to the function.

The effects of using a non-symmetrical halftone cell must be analyzed. The analysis proceeds in a fashion similar to that beginning at eq. (2.1), and only one-dimensional cells are considered for simplicity. Beginning with eq. (2.1),

$$v(x)=\text{rect}(x/b)$$

is a representation of a transparent bar of width b on an opaque background. An infinite one-dimensional array of such bars, spaced a distance a apart on an opaque background with one edge fixed in position can be represented by

$$\begin{aligned} u(x) &= v(x) * ((1/a) \cdot \text{comb}((x-b/2)/a)) \\ &= \text{rect}(x/b) * ((1/a) \cdot \text{comb}((x-b/2)/a)) \quad . \end{aligned} \tag{2.24}$$

Inverting the contrast yields

$$t(x)=1-u(x)$$

$$=1-\text{rect}(x/b)*((1/a)\cdot\text{comb}((x-b/2)/a)) \quad , \qquad (2.25)$$

and Fourier transforming this transmittance yields

$$\mathcal{F}\{t(x)\}=\delta(f_x)-b\cdot\text{sinc}(bf_x)\cdot\text{comb}(af_x)\cdot \exp(-j\pi bf_x) \qquad (2.26)$$

as the amplitude distribution present in the Fourier transform plane. Replacing the comb function by a summation of delta functions yields

$$\mathcal{F}\{t(x)\}=\delta(f_x)-\sum_{n=-\infty}^{\infty}\delta(f_x-n/a)\cdot(b/a)\cdot\text{sinc}(bf_x)\cdot \exp(-j\pi bf_x) \quad . \qquad (2.27)$$

Replacing f_x by the values selected by the delta function yields

$$\mathcal{F}\{t(x)\}=\delta(f_x)-\sum_{n=-\infty}^{\infty}\delta(f_x-n/a)\cdot(b/a)\cdot\text{sinc}(bn/a)\cdot \exp(-j\pi bn/a) \quad , \qquad (2.28)$$

which represents spectral islands in the transform plane. These islands will be distinct and separable if the sampling criteria are satisfied.

The specific cases of interest are n=0 and n≠0. With n=0 eq. (2.28) becomes

$$\mathcal{F}\{t(x)\}_{n=0} = \delta(f_x)\cdot(1-b/a) \quad , \tag{2.29}$$

an expression identical to eq. (2.8) for symmetrical cells. Therefore, since they yield equivalent output, non-symmetrical cells are to be preferred for the zero order because they can be made more precisely. For n≠0, eq. (2.28) becomes

$$\mathcal{F}\{t(x)\}_{n\neq 0} = -\delta(f_x - n/a)\cdot(b/a)\cdot\mathrm{sinc}(bn/a)\cdot \exp(-j\pi bn/a) \quad . \tag{2.30}$$

Note that eq. (2.30) contains a nonconstant phase factor which was not present in eq. (2.9).

The output amplitude is given by the Fourier transform of eq. (2.29) or (2.30),

$$\mathcal{F}\{\mathcal{F}\{t(x)\}_{n=0}\} = (1-b/a) \tag{2.31}$$

or

$$\mathcal{F}\{\mathcal{F}\{t(x)\}_{n\neq 0}\} = -(b/a)\cdot\mathrm{sinc}(bn/a)\cdot \exp(-j\pi bn/a)\cdot\exp(-j2\pi nx/a)$$

$$= -(1/n\pi) \cdot \sin(\pi bn/a) \cdot$$

$$\exp(-j\pi(b+2x)n/a) \quad . \qquad (2.32)$$

If intensity is detected at this step, as with photographic film, the additional phase factor in eq. (2.32) will not matter and eq. (2.32) becomes equivalent to eq. (2.12).

2.3 Amplitude Output from Symmetrical Halftones with a Two-Film Process

The procedure involved in the two-film process is to take the halftoned picture and contact print it onto a second piece of copy film. The result is a contrast reversed halftoned picture.

The motivation for considering this case is twofold. Real photographic films do not behave as they have been ideally modeled in chapter 1. The film gamma or saturation density could be low, rather than infinite. Using a two-film process allows the effective gamma of the process to be higher than the gamma of either individual film, assuming both gammas are larger than one. Intuitively, it seems that a higher combined gamma should be superior to either of the lower individual gammas, and this idea is considered in more detail in chapter 4. The

second motivation is the sign of the slope of the zero order characteristic. Examination of eq. (2.10), the n=0 case, indicates that the output amplitude is a monotonically decreasing function of the bar width b.

It will now be shown that by going to a two-film process, a monotonically increasing function of b, where b is the bar width on the first film, can be realized in the zero order. The analysis proceeds as before, beginning with eq. (2.1). In this case, the derivation is identical until eq. (2.3).

To begin, the expression for t(x) must be modified to yield

$$t(x)=u(x)$$
$$=\text{rect}(x/b)*((1/a)\cdot\text{comb}(x/a)) \qquad (2.33)$$

as the amplitude distribution at the input plane of the optical system. The amplitude distribution in the transform plane is given by

$$\mathcal{F}\{t(x)\}=b\cdot\text{sinc}(bf_x)\cdot\text{comb}(af_x) \quad , \qquad (2.34)$$

the Fourier transform of eq. (2.33). Replacing the comb function with a summation of delta functions yields

$$\mathcal{F}\{t(x)\}=(1/a)\cdot\sum_{n=-\infty}^{\infty}\delta(f_x-n/a)\cdot b\cdot\mathrm{sinc}(bf_x) \quad , \qquad (2.35)$$

and putting in the actual values for f_x gives

$$\mathcal{F}\{t(x)\}=(1/a)\cdot\sum_{n=-\infty}^{\infty}\delta(f_x-n/a)\cdot b\cdot\mathrm{sinc}(bn/a) \qquad (2.36)$$

as the general expression for the amplitude distribution in the Fourier transform plane. Again, the two cases of interest are $n=0$ and $n\neq 0$. For $n=0$, eq. (2.36) becomes

$$\mathcal{F}\{t(x)\}_{n=0}=(b/a)\cdot\delta(f_x) \qquad (2.37)$$

and for $n\neq 0$, eq. (2.36) becomes

$$\begin{aligned}\mathcal{F}\{t(x)\}_{n\neq 0}&=(b/a)\cdot\mathrm{sinc}(bn/a)\cdot\delta(f_x-n/a)\\&=(1/\pi n)\cdot\sin(\pi bn/a)\cdot\delta(f_x-n/a) \quad . \qquad (2.38)\end{aligned}$$

The final output amplitude is obtained by Fourier transforming eq. (2.37) and (2.38) to yield

$$\mathcal{F}\{\mathcal{F}\{t(x)\}_{n=0}\}=b/a \qquad (2.39)$$

and

$$\mathcal{F}\{\mathcal{F}\{t(x)\}_{n\neq 0}\} = (1/\pi n)\cdot \sin(\pi bn/a)\cdot \exp(-j\pi bn/a) \qquad (2.40)$$

as the amplitude distribution present in the output plane for the zero and nth order respectively. Observe that eq. (2.39) is monotonically increasing in b, as opposed to eq. (2.10) which is monotonically decreasing.

2.4 Output Intensity

If the system output is detected by photographic film or other intensity detector, the modulus of the output amplitudes previously obtained must be squared. From eq. (2.10) and (2.11), the intensity output for the one-dimensional one-film process with a symmetrical halftone cell is

$$I_{out}(b) = \left|\mathcal{F}\{\mathcal{F}\{t(x)\}_{n=0}\}\right|^2 = (1-b/a)^2 \qquad (2.41)$$

for the zero order, and

$$\begin{aligned} I_{out}(b) &= \left|\mathcal{F}\{\mathcal{F}\{t(x)\}_{n\neq 0}\}\right|^2 \\ &= \left|(-1/n\pi)\cdot \sin(\pi bn/a)\cdot \exp(-j2\pi nx/a)\right|^2 \\ &= (1/n\pi)^2 \cdot \sin^2(\pi bn/a) \end{aligned} \qquad (2.42)$$

for the nth order. From eq. (2.21), (2.22), or (2.23) the

intensity output for the two-dimensional one-film process with a symmetrical halftone cell is

$$I_{out}(b) = \left| \mathcal{F}\{\mathcal{F}\{t(x)\}_{0,0}\} \right|^2 = (1-b^2/a^2)^2 \quad , \tag{2.43}$$

$$I_{out}(b) = \left| \mathcal{F}\{\mathcal{F}\{t(x)\}_{0,n}\} \right|^2 = \left| (-b/n\pi a) \cdot \sin(\pi bn/a) \cdot \exp(-j2\pi nx/a) \right|^2 = b^2/(n\pi a)^2 \cdot \sin^2(\pi bn/a) \quad , \tag{2.44}$$

and

$$I_{out}(b) = \left| \mathcal{F}\{\mathcal{F}\{t(x)\}_{m,n}\} \right|^2 = \left| (-1/\pi^2 mn) \cdot \sin(\pi bn/a) \cdot \sin(\pi bm/a) \cdot \exp(-j2\pi(nx+my)/a) \right|^2 = (1/\pi^2 mn)^2 \cdot \sin^2(\pi bn/a) \cdot \sin^2(\pi bm/a) \quad , \tag{2.45}$$

respectively. From eq. (2.31) or (2.32), the intensity output for the one-dimensional non-symmetrical halftone cell with the one-film process is

$$I_{out}(b) = \left| \mathcal{F}\{\mathcal{F}\{t(x)\}_{n=0}\} \right|^2 = (1-b/a)^2 \tag{2.46}$$

for the zero order, and

$$I_{out}(b) = \left| \mathcal{F}\{\mathcal{F}\{t(x)\}_{n\neq 0}\} \right|^2$$
$$= \left| (-1/n\pi) \cdot \sin(\pi bn/a) \cdot \exp(-j\pi(b+2x)n/a) \right|^2$$
$$= (1/n\pi)^2 \cdot \sin^2(\pi bn/a) \qquad (2.47)$$

for the nth order. From eq. (2.39) or (2.40) the intensity output for the one-dimensional two-film process with a symmetrical halftone cell is

$$I_{out}(b) = \left| \mathcal{F}\{\mathcal{F}\{t(x)\}_{n=0}\} \right|^2$$
$$= (b/a)^2 \qquad (2.48)$$

for the zero order, and

$$I_{out}(b) = \left| \mathcal{F}\{\mathcal{F}\{t(x)\}_{n\neq 0}\} \right|^2$$
$$= \left| (1/n\pi) \cdot \sin(\pi bn/a) \cdot \exp(-j\pi bn/a) \right|^2$$
$$= (1/n\pi)^2 \cdot \sin^2(\pi bn/a) \qquad (2.49)$$

for the nth order.

Certain features of output intensity behavior should be noted from eq. (2.41) to (2.49).

1. The zero order (n=0) I_{out} is the same monotonically decreasing function of b for the symmetrical and non-symmetrical one-film process, and is a

monotonically increasing function of b for the two-film process. This has been shown for one dimension and could be shown for two dimensions.

2. The non-zero order ($n \neq 0$) one-dimensional I_{out} expressions, eq. (2.42), (2.47), and (2.49), are all the same. This means that the same symmetric cell shape can be used for either the one-film or two-film process, and yield identical results. The non-symmetric version of the same cell will yield equivalent output intensity.

3. The two-dimensional characteristics are not identical to their one-dimensional counterparts, though they are similar. In particular, eq. (2.44) has a multiplicative b^2/a^2 factor which makes it depart from a strict $\sin^2$ relation.

2.5 Bar Width Dependence on Input Intensity

Equations (2.41) to (2.49) relate the intensity at the output plane of a two lens Fourier transform system to the width b of opaque bars or dots spaced a distance a apart on a transparent background in the system input plane. It is the function of the halftone screen to provide a mapping between local input intensity and resulting local bar or dot size on the halftoned picture.

This mapping will be examined more closely for the one-dimensional halftone, and can be analyzed similarly with two-dimensional halftones.

For this analysis of the ideal situation, the copy film used to make the halftoned picture is assumed to have an infinite gamma, and a given threshold intensity I'. The threshold is defined so that an illumination level below I' will not result in any film exposure. Illumination equal to or larger than I' will completely expose the film, resulting in an opaque region after development. Let

$f(x)$ = The density of the halftone cell, one period of the halftone screen, as a function of position. X ranges from 0 to a/2 for symmetric cells and 0 to a for non-symmetric cells.

I'_{in} = Input intensity

$I_t(x)$ = Intensity transmitted locally by the halftone cell.

The halftone cell can be regarded as a spatially varying attenuator, and the intensity transmitted by the cell is represented as the product of I'_{in} and the local intensity transmittance. Therefore,

$$I_t(x) = I'_{in} \cdot 10^{-f(x)} . \qquad (2.50)$$

If $I_t(x) < I'$ the film will not expose and the developed film will be clear at that value of x. If $I_t(x) \geq I'$ the film exposes and the developed film will be opaque at that value of x. Therefore, for all x such that

$$I_t(x) \geq I' \tag{2.51}$$

the film will become opaque. This process and the resulting copy film are shown in Fig. 1-3 and 1-5.

Assume for now that f(x) is a monotonically increasing function on (0,a/2) for symmetrical cells, or on (0,a) for non-symmetrical cells. The halftone screen is assumed to be made up of such functions repeating with a period of a. Using such a screen, bars a distance a apart will be formed whose width is dependent on I'_{in} and f(x). This dependence is found from eq. (2.50) and (2.51). Combining them gives

$$I'_{in}/I' \geq 10^{f(x)} \tag{2.52}$$

as the condition for film exposure. Taking the logarithm of eq. (2.52) yields

$$\log_{10}(I'_{in}/I') \geq f(x) \quad , \tag{2.53}$$

and taking the inverse function of eq. (2.53) yields

$$x \leq f^{-1}(\log_{10} I_{in}) \qquad (2.54)$$

$$\text{where} \qquad I_{in} = I'_{in} / I' \quad . \qquad (2.55)$$

The bar resulting from a symmetrical halftone cell is centered at zero and is twice the width obtained from eq. (2.54), for f defined on (0,a/2). For non-symmetrical halftone cells the width is given directly by eq. (2.54), with f defined on (0,a) and one edge is fixed at zero relative position.

2.6 Transfer Functions and Cell Profile Description

Equations (2.41) to (2.49) describe I_{out} as a function of bar width b, which is in turn a function of I_{in}. These relationships can be consolidated to yield I_{out} as a function of I_{in}, $I_{out} = h(I_{in})$, and also $f^{-1}(x)$ as a function of $h(I_{in})$. The one-dimensional case is somewhat simpler than the two-dimensional case, and is the one which will be considered here. The two-dimensional case could be handled similarly.

It was noted previously that some of the equations (2.41) to (2.49) are identical. For the one-dimensional

case, there are only three different expressions to consider. These are eq. (2.41) for the zero order one-film process, eq. (2.48) for the zero order two-film process, and eq. (2.42), (2.47), or (2.49) for the non-zero order one-film or two-film process. Only symmetrical cells will be treated, with the understanding that the result obtained need only be multiplied by 2 to give the non-symmetrical result. For symmetrical cells, the bar width b is given by

$$b=2f^{-1}(\log_{10} I_{in}) \quad . \tag{2.56}$$

Using this value for b in eq. (2.41) yields

$$I_{out}=h(I_{in})=(1-2f^{-1}(\log_{10} I_{in})/a)^2 \tag{2.57}$$

as the transfer function expression. Taking the square root of both sides of eq. (2.57) gives

$$\sqrt{h(I_{in})}=1-2f^{-1}(\log_{10} I_{in})/a \tag{2.58}$$

and after some algebra, eq. (2.58) becomes

$$f^{-1}(\log_{10} I_{in})=(a/2)\cdot(1-\sqrt{h(I_{in})}) \quad , \tag{2.59}$$

an expression for the halftone cell profile in terms of the desired transfer function. I_{in} must never be less than 1, or a portion of the desired transfer function will be truncated to zero. The expression for $h(I_{in})$ should be rescaled if necessary to make this so. The logarithm represents cell density ranging from 0 for $I_{in}=1$ to some maximum corresponding to the maximum normalized input intensity. Equation (2.59) is in the form

$$f^{-1}(D)=x \tag{2.60}$$

where D is cell density and x is the position in the halftone cell.

The other two cases, the zero order two-film case, and the non-zero order case, can be treated in a similar manner. Substituting eq. (2.56) into eq. (2.48) yields

$$I_{out}=h(I_{in})=(2f^{-1}(\log_{10} I_{in})/a)^2 \tag{2.61}$$

as the transfer function expression. Taking the square root of both sides of eq. (2.61) gives

$$\sqrt{h(I_{in})}=2f^{-1}(\log_{10} I_{in})/a \quad , \tag{2.62}$$

or equivalently,

$$f^{-1}(\log_{10} I_{in}) = (a/2) \cdot \sqrt{h(I_{in})} \quad , \qquad (2.63)$$

an expression for halftone cell profile in terms of desired transfer function, for the zero order two-film process. Substituting eq. (2.56) into eq. (2.42), an nth order expression, yields

$$I_{out} = h(I_{in}) = (1/n\pi)^2 \cdot \sin^2((\pi n/a) \cdot 2f^{-1}(\log_{10} I_{in})) \qquad (2.64)$$

as the transfer function expression. Taking the square root gives

$$n\pi \sqrt{h(I_{in})} = \sin((\pi n/a) \cdot 2f^{-1}(\log_{10} I_{in})) \quad ,$$

or equivalently,

$$f^{-1}(\log_{10} I_{in}) = (a/2n\pi) \cdot \sin^{-1}(n\pi \sqrt{h(I_{in})}) \quad , \qquad (2.65)$$

the halftone cell profile description for any of the three nth order processes.

If the expressions are desired for non-symmetrical cells, the cell position predicted from eq. (2.59), (2.63), or (2.65) should be doubled. Similar expressions could be obtained for two-dimensional halftones.

2.7 Halftone Cell Design Technique

Given a desired intensity transfer function, eqs. (2.59), (2.63), and (2.65) provide an exact technique for halftone cell design to achieve the function. The procedure breaks down into several distinct steps, which are outlined in the following synthesis algorithm for monotonic halftone cell design:

1. Determine the minimum diffraction order, n, to use by counting the number of sign changes q in the slope of the desired transfer function, h. The order required is given by $n \geq (q+1)/2$, where n is an integer. There are three exceptions to this rule:

   a. The zero order one-film process has a negative slope for h everywhere. This means that a monotonically increasing function can not be synthesized with a zero order one-film process. The first order, or the two-film process in the zero order must be used.

   b. The zero order two-film process has a positive slope for h everywhere. A monotonically decreasing function has to be synthesized in the first order or with the one-film process in the zero order.

c. If the h function has $q \geq 1$ and has a negative initial slope, q must be increased by one.

This sign change counting rule and the exceptions are indicated for up to four sign changes in Table 2-1. The table can easily be extended to more than four sign changes. An additional consideration is that n should be chosen as small as possible, given q, for maximum diffraction efficiency.

2. Normalize h so the maximum value is equal to the maximum possible for the diffraction order used, for all possible I_{in}. If $n=0$, $h \leq 1$. If $n \neq 0$, $h \leq 1/n^2\pi^2$.

3. Select eq. (2.59), (2.63), or (2.65), whichever is appropriate to the process and diffraction order being used. Substitute the desired h into the expression.

4. All three of these expressions are in the form shown in eq. (2.60). To calculate the cell shape, either solve analytically for $f(x)=D$, or solve by numerically running over the possible values of I_{in}. For n=1 or more, whenever the slope of h changes sign, the cell size must abruptly increase such that the output remains constant, while jumping to a region of eq. (2.64) of opposite slope.

T A B L E 2 - 1

ALLOWABLE NUMBER OF SLOPE CHANGES IN THE TRANSFER FUNCTION FOR VARIOUS DIFFRACTION ORDERS USING THE ONE-FILM PROCESS

number of sign changes in $h(I_{in})$	initial slope	minimum order required
0	-	0
0	+	1
1	-	2
1	+	1
2	-	2
2	+	2
3	-	3
3	+	2
4	-	3
4	+	3

This procedure has been reduced to a computer program which automatically does all the calculations once a desired transfer function is specified. The following chapter has numerous examples of cell shapes calculated for specific transfer functions using this procedure.

CHAPTER 3

MONOTONIC HALFTONE CELL DESIGN EXAMPLES

In this chapter, halftone cell shapes for various transfer functions are calculated. The graphs of cell shapes are all computer calculated by the cell design synthesis procedure described in section 2.7.

3.1 Logarithmic Response

In many signal processing situations, noise or disturbances are frequently multiplicative. Examples include non-uniform illumination and multiplication of two transmittance functions. One useful method of handling multiplicative noise is to use a homomorphic filter [3-1,2]. This type of filter performs a logarithmic transformation on the signal to convert the multiplicative noise to an additive form which can be eliminated more easily. The additive noise filtering is followed by an exponential transformation which restores the signal to its previous form. Either monotonically increasing or decreasing logarithmic functions can be made. The two

general functions are

$$I_{out}=h(I_{in})=1-k\cdot\log_{10}(I_{in}) \qquad (3.1)$$

where $k\cdot\log_{10}(I_{in}) \leq 1$ for all I_{in}, and

$$I_{out}=h(I_{in})=k\cdot\log_{10}(I_{in}) \qquad (3.2)$$

A transfer function of the form of eq. (3.1) is monotonically decreasing and can be achieved with the one-film process in the zero order. Equation (3.2) is monotonically increasing and requires the two-film process with the zero diffraction order.

To illustrate the synthesis procedure of section 2.7 in detail, the synthesis algorithm will be followed for both of these functions, assuming two desired decades of input range. Starting with eq. (3.1), a suitable choice of k is .5 yielding

$$h(I_{in})=1-.5\cdot\log_{10}(I_{in}) \qquad (3.3)$$

where $1 \leq I_{in} \leq 100$. Equation (3.3) is then correctly normalized so that $0 \leq I_{out} \leq 1$.

The appropriate $h(I_{in})$ expression is eq. (2.59). Substituting this transfer function into eq. (2.59) yields

$$f^{-1}(\log_{10} I_{in}) = (a/2)\cdot(1-\sqrt{1-.5\cdot\log_{10}(I_{in})}) \qquad (3.4)$$

for the expression which must be solved to obtain the halftone cell shape.

Equation (3.2) is also normalized by setting k=.5 yielding

$$h(I_{in}) = .5\cdot\log_{10}(I_{in}) \qquad (3.5)$$

where $1 \le I_{in} \le 100$. The appropriate expression for the two-film process is eq. (2.63). Combining eq. (3.5) with eq. (2.63) yields

$$f^{-1}(\log_{10} I_{in}) = (a/2)\cdot\sqrt{.5\log_{10}(I_{in})} \qquad (3.6)$$

as the expression to be solved for the cell shape.

In keeping with the philosophy that zero order operations are best done with non-symmetrical cells, eq. (3.4) and (3.6) should be modified by replacing a/2 with a to give

$$f^{-1}(\log_{10} I_{in}) = a \cdot (1 - \sqrt{1 - .5 \cdot \log_{10}(I_{in})}) \qquad (3.7)$$

and,

$$f^{-1}(\log_{10} I_{in}) = a \cdot \sqrt{.5 \cdot \log_{10}(I_{in})} \quad . \qquad (3.8)$$

Both of these equations are in the form of eq. (2.60).

Graphs of these transfer functions and the halftone cells which will produce them are shown in Fig. 3-1 and 3-2. The monotonically decreasing logarithm was tried experimentally, and the results are presented in section 7.4.2.

3.2 Exponential Response

The exponential transformation is of interest as the final step in a homomorphic filter. In common with the logarithmic response, either monotonically increasing or decreasing functions can be made. The general functions are

$$I_{out} = h(I_{in}) = 10^{1-I_{in}} \qquad (3.9)$$

or

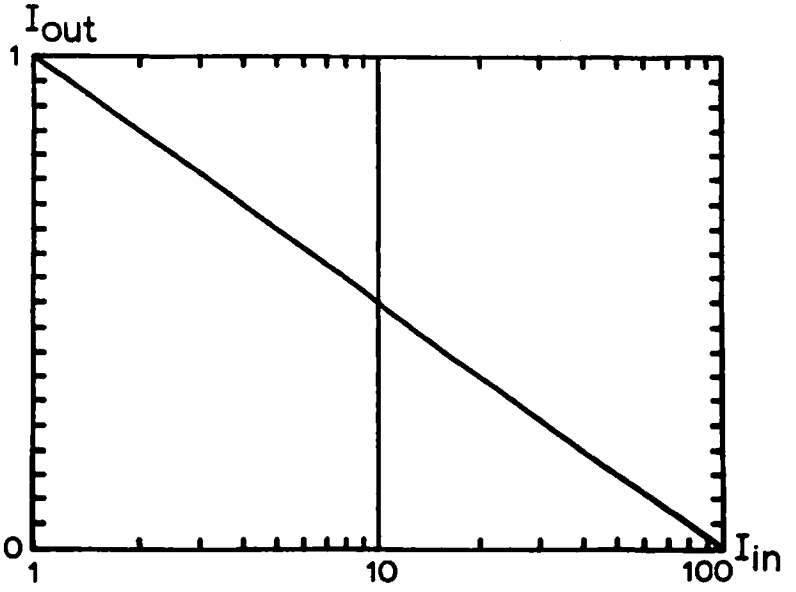

(a)

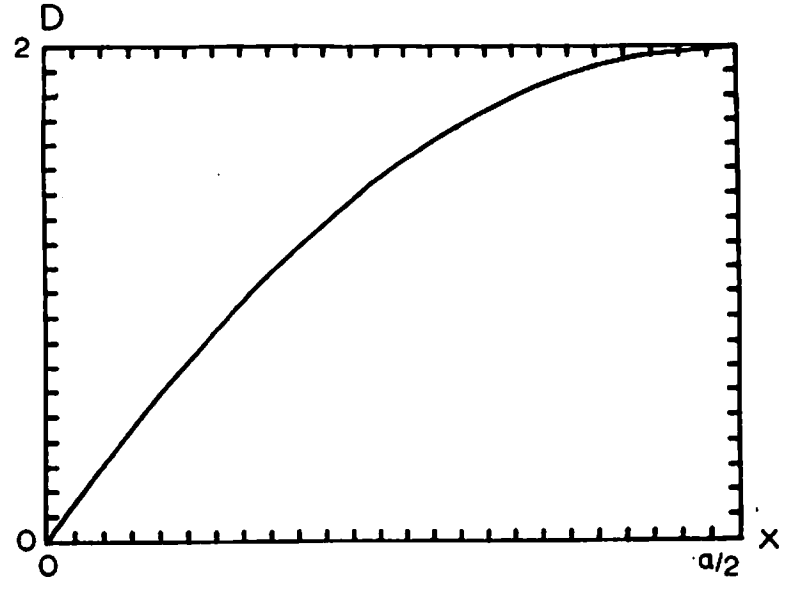

(b)

Figure 3-1. (a) Decreasing logarithm transfer function.
(b) Corresponding halftone cell shape.

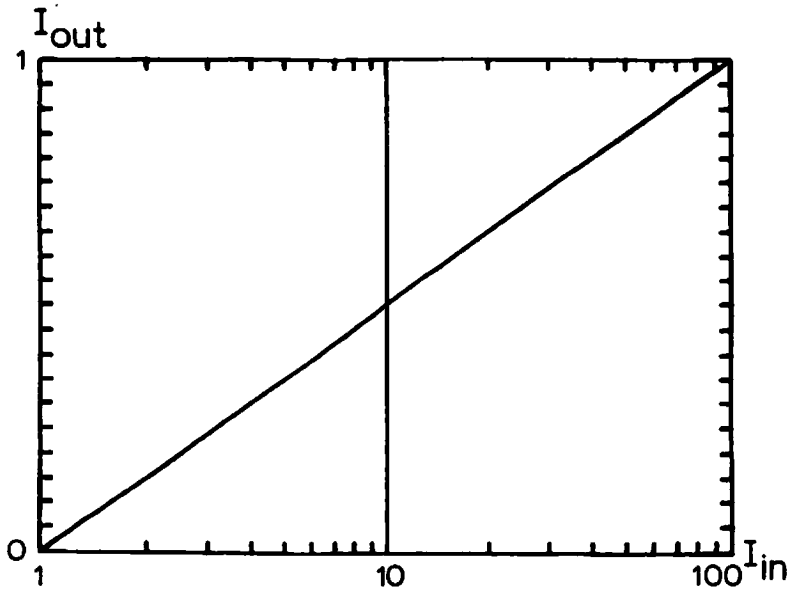

(a)

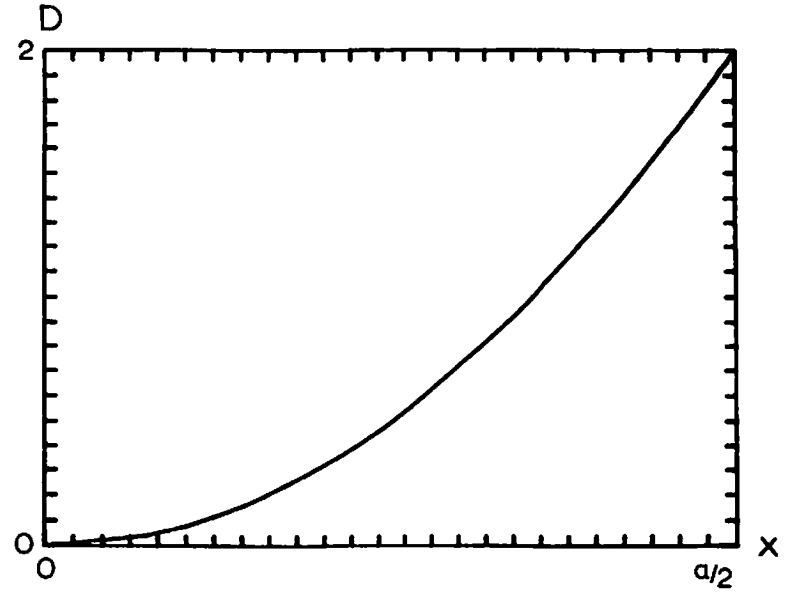

(b)

Figure 3-2. (a) Increasing logarithm transfer function.
(b) Corresponding halftone cell shape.

$$I_{out} = h(I_{in}) = k \cdot 10^{I_{in}-1} \quad , \qquad (3.10)$$

where $I_{in} \leq 1 - \log_{10} k$. A transfer function represented by eq. (3.9) can be achieved with the one-film process in the zero order. A function of the form in eq. (3.10) requires the two-film process and the zero order.

A three decade decreasing exponential can be represented by eq. (3.9) simply by restricting I_{in} to range between 1 and 4. The appropriate $h(I_{in})$ expression is eq. (2.59). Combining eq. (3.9) and (2.59) yields

$$f^{-1}(\log_{10} I_{in}) = (a/2) \cdot (1 - \sqrt{10^{1-I_{in}}}) \qquad (3.11)$$

as the expression to be solved for the halftone cell shape.

The transfer function for a three decade monotonically increasing exponential can be represented by eq. (3.10) by setting k=.001 to yield

$$h(I_{in}) = .001 \cdot 10^{I_{in}-1} \quad . \qquad (3.12)$$

Combining eq. (2.63) and eq. (3.12) yields

$$f^{-1}(\log_{10} I_{in}) = (a/2)\cdot\sqrt{.001\cdot 10^{I_{in}-1}} \quad , \qquad (3.13)$$

the expression to be solved for the increasing exponential halftone cell shape.

Equations (3.11) and (3.13) both describe symmetrical cells. The corresponding expressions for non-symmetrical cells are

$$f^{-1}(\log_{10} I_{in}) = a\cdot(1-\sqrt{10^{1-I_{in}}}) \qquad (3.14)$$

and,

$$f^{-1}(\log_{10} I_{in}) = a\cdot\sqrt{.001\cdot 10^{I_{in}-1}} \qquad (3.15)$$

respectively.

Graphs of the exponential transfer functions and the required cells are shown in Fig. 3-3 and 3-4. Experimental results with specially synthesized halftone screens are presented in section 7.4.3.

3.3 Level Slice

The level slice characteristic is useful for doing equidensity contour slicing on images and for histogram

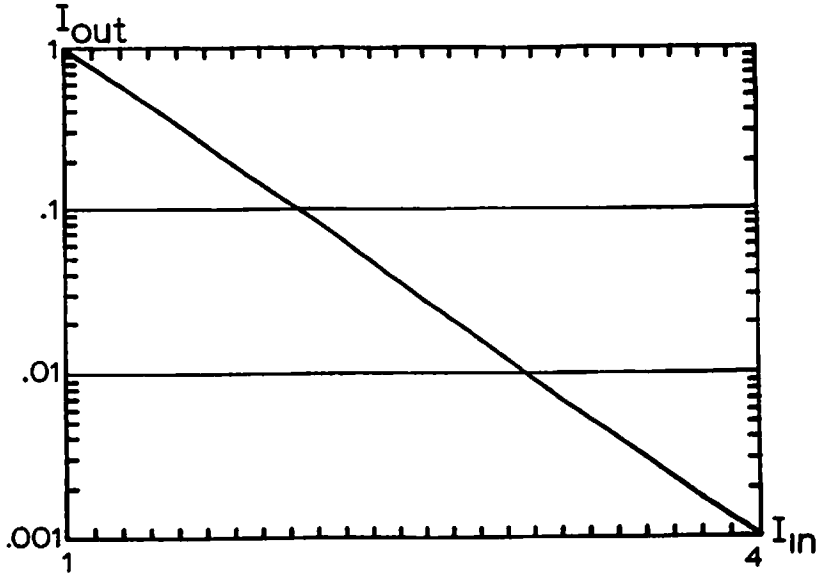

(a)

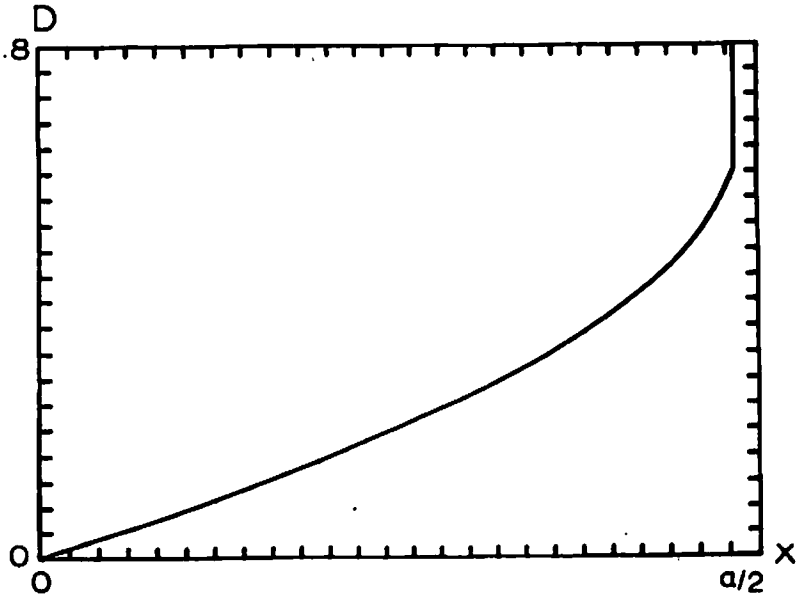

(b)

Figure 3-3. (a) Decreasing exponential transfer function.
(b) Corresponding halftone cell shape.

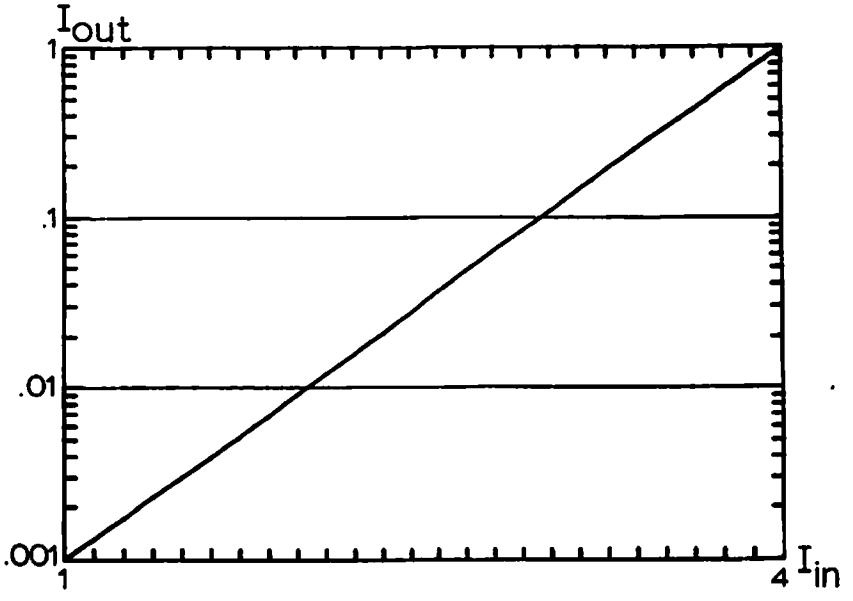

(a)

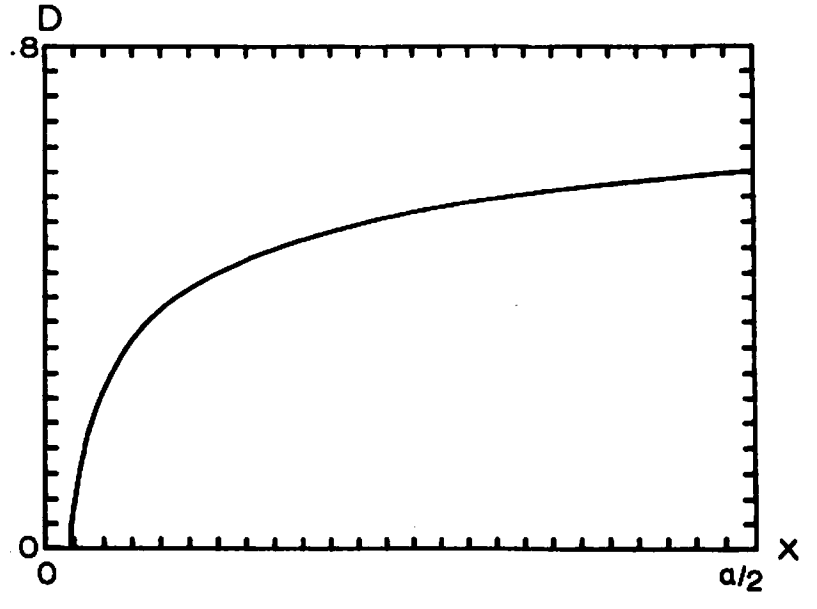

(b)

Figure 3-4. (a) Increasing exponential transfer function.
(b) Corresponding halftone cell shape.

calculations [3-3]. The desired function is

$$I_{out} = h(I_{in}) = \begin{cases} 0 & I_{in} < I_1 \\ k & I_1 \le I_{in} < I_2 \\ 0 & I_2 \le I_{in} \end{cases} . \qquad (3.16)$$

This function has only one sign change, so the first order can be used. The normalization condition is satisfied by setting $k=1/\pi^2$, and the appropriate $h(I_{in})$ expression is eq. (2.65). With n set equal to one for the first order eq. (2.65) becomes

$$f^{-1}(\log_{10} I_{in}) = (a/2\pi)\cdot \sin^{-1}(\pi\sqrt{h(I_{in})}) \quad , \qquad (3.17)$$

which is the equation to be solved for the halftone cell shape. For the first range, $I_{in} < I_1$, this becomes

$$f^{-1}(\log_{10} I_{in}) = (a/2\pi)\cdot \sin^{-1}(0) \quad . \qquad (3.18)$$

The $\sin^{-1}(0)$ could be either 0 or π. Because the value of $f^{-1}(\log_{10} I_{in})$ is required to be a monotonically increasing function, 0 should be selected. Therefore, for $I_{in} < I_1$, the bar width on the copy film must be 0, which means there can be no regions on the halftone screen which have densities less than $\log_{10} I_1$.

For the second range, $I_1 \leq I_{in} < I_2$, eq. (3.17) becomes

$$f^{-1}(\log_{10} I_{in}) = (a/2\pi) \cdot \sin^{-1}(\pi\sqrt{1/\pi^2})$$
$$= (a/2\pi) \cdot \sin^{-1}(1)$$
$$= a/4 \qquad (3.19)$$

where a/4 is chosen as the smallest available solution. This range corresponds to a 50% duty cycle square wave with transmission alternating between 0 and 1.

For the third range, $I_2 \leq I_{in}$, the expression is identical to eq. (3.18). In this case, select $\sin^{-1}(0) = \pi$ to yield

$$f^{-1}(\log_{10} I_{in}) = a/2 \qquad (3.20)$$

as the smallest possible solution. This corresponds to opaque bars equal in width to their separation, that is, a completely opaque film. The screen must therefore be everywhere less dense than $\log_{10} I_2$.

The transfer function and calculated cell shape for a level slice are shown in Fig. 3-5. Experimental results for this function are presented in section 7.4.1.

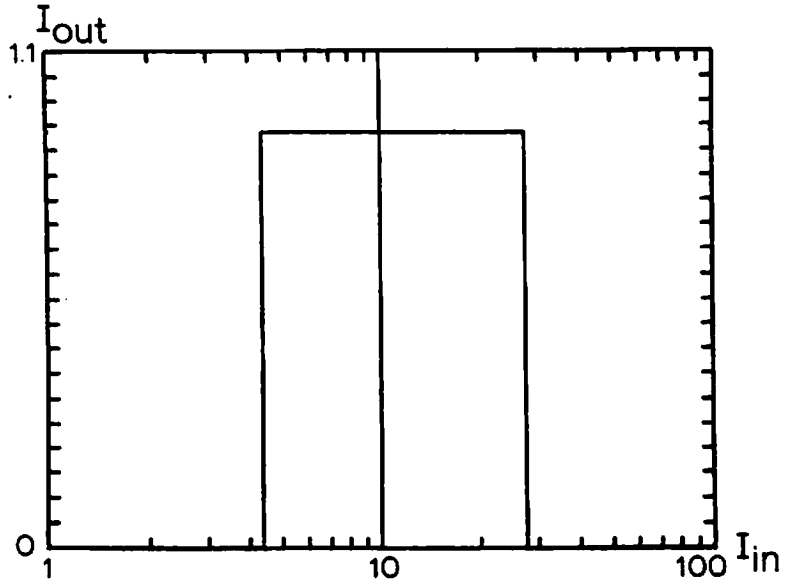

(a)

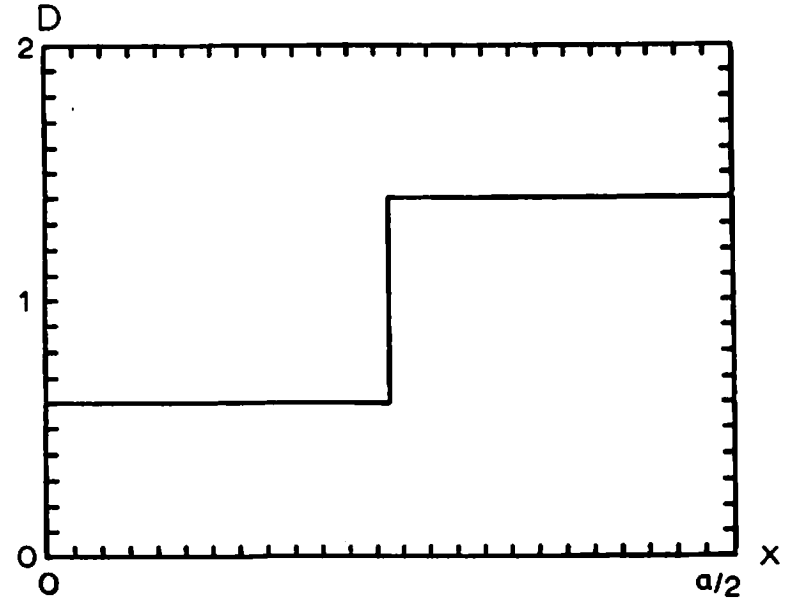

(b)

Figure 3-5. (a) Level slice transfer function.
(b) Corresponding halftone cell shape.

3.4 Second Order Example

Consider a function such as

$$I_{out} = h(I_{in}) = \begin{cases} \emptyset & I_{in} < I_1 \\ 1.\emptyset & I_1 \leq I_{in} < I_2 \\ .25 & I_2 \leq I_{in} < I_3 \\ .5 & I_3 \leq I_{in} < I_4 \\ \emptyset & I_4 \leq I_{in} \end{cases} . \qquad (3.21)$$

This function has three changes of sign in the slope, so the second order is required. The normalization condition requires that $h(I_{in}) \leq 1/4\pi^2$. The appropriate $h(I_{in})$ expression is eq. (2.65), which becomes

$$f^{-1}(\log_{10} I_{in}) = (a/4\pi) \cdot \sin^{-1}(2\pi \sqrt{h(I_{in})}) \qquad (3.22)$$

when n is set equal to 2. For $I_{in} < I_1$, eq. (3.22) becomes

$$f^{-1}(\log_{10} I_{in}) = (a/4\pi) \cdot \sin^{-1}(\emptyset) = \emptyset \qquad (3.23)$$

where the zero solution was chosen because it is the minimum cell size choice possible. For $I_1 \leq I_{in} < I_2$ eq. (3.22) becomes

$$f^{-1}(\log_{10} I_{in}) = (a/4\pi) \cdot \sin^{-1}(1) = a/8 \quad . \qquad (3.24)$$

The a/8 solution is the smallest possible choice in this case. For $I_2 \leq I_{in} < I_3$,

$$f^{-1}(\log_{10} I_{in}) = (a/4\pi) \cdot \sin^{-1}(.5)$$
$$= a/24 \text{ or } 5a/24 \quad . \qquad (3.25)$$

For the halftone cell to be physically realizable, the choice made must be no smaller than some previous value. For this reason, choose 5a/24. For $I_3 \leq I_{in} < I_4$,

$$f^{-1}(\log_{10} I_{in}) = (a/4\pi) \cdot \sin^{-1}(1/\sqrt{2}) \quad . \qquad (3.26)$$

The smallest angle which has $1/\sqrt{2}$ as its arcsin and which will also result in a position in the cell at least as large as the preceeding position is $5\pi/4$. Using this value gives

$$f^{-1}(\log_{10} I_{in}) = 5a/16 \qquad (3.27)$$

as the desired solution. For $I_4 \leq I_{in}$,

$$f^{-1}(\log_{10} I_{in}) = (a/4\pi)\cdot \sin^{-1}(\emptyset)$$
$$= a/2 \qquad (3.28)$$

where $\sin^{-1}(\emptyset)$ has been chosen to equal 2 .

This transfer function and resulting cell shape are shown in Fig. 3-6.

3.5 Edge Tailored Bandpass

Consider a function

$$I_{out} = h(I_{in}) = \begin{cases} \emptyset & I_{in} < I_1 \\ g(I_{in}) & I_1 \le I_{in} < I_2 \\ k & I_2 \le I_{in} < I_3 \\ r(I_{in}) & I_3 \le I_{in} < I_4 \\ \emptyset & I_4 \le I_{in} \end{cases} . \qquad (3.29)$$

Assume that $g(I_1)=\emptyset$, $g(I_2)=k$, and that g is monotonically increasing between I_1 and I_2. Also assume that $r(I_3)=k$, $r(I_4)=\emptyset$, and r is monotonically decreasing between I_3 and I_4. The first order should be used because there is only one change of sign in the slope of h, and the normalization is satisfied by setting $k=1/\pi^2$. Equation (2.65), with n=1 is the appropriate $h(I_{in})$ expression.

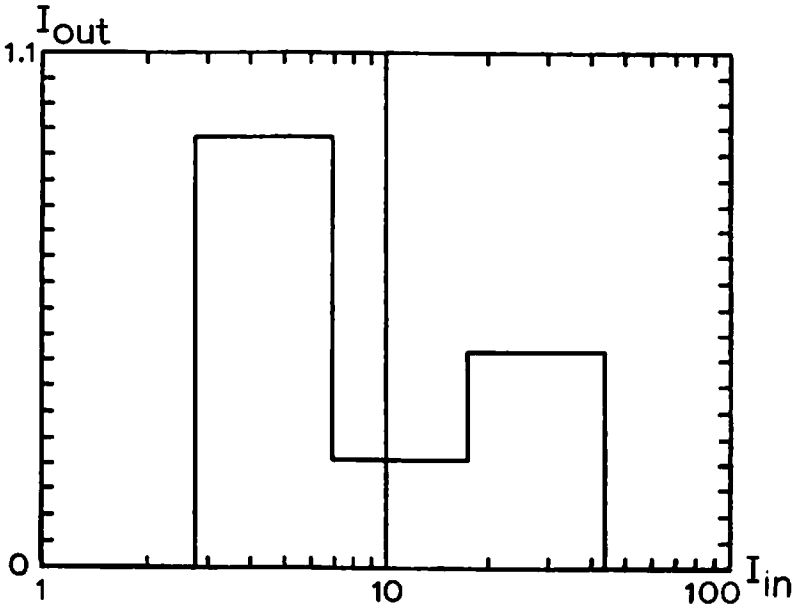

(a)

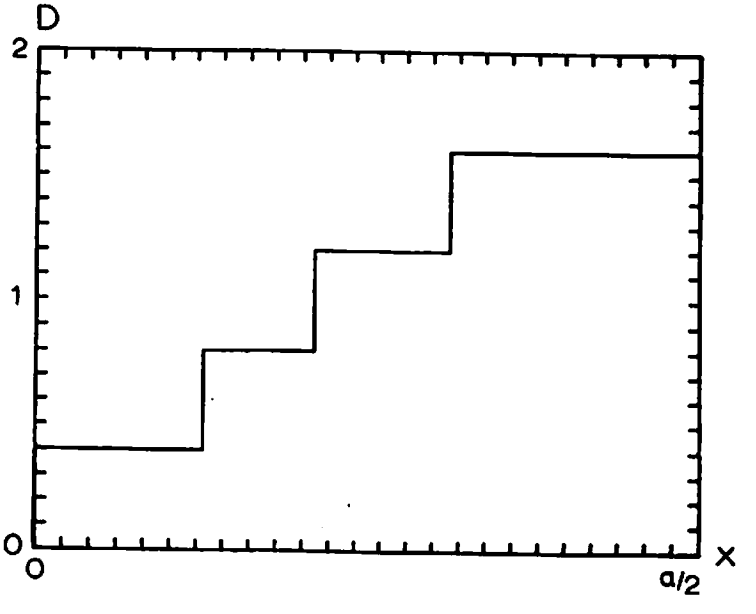

(b)

Figure 3-6. (a) Transfer function for second order example. (b) Corresponding halftone cell shape.

For $I_{in} \leq I_1$, eq. (2.65) becomes

$$f^{-1}(\log_{10} I_{in}) = (a/2\pi) \cdot \sin^{-1}(\emptyset) = \emptyset \qquad (3.30)$$

where $\emptyset$ is chosen as the smallest possible solution. For $I_1 \leq I_{in} < I_2$

$$f^{-1}(\log_{10} I_{in}) = (a/2\pi) \cdot \sin^{-1}(\pi\sqrt{g(I_{in})}) \quad . \qquad (3.31)$$

For $I_2 \leq I_{in} < I_3$,

$$f^{-1}(\log_{10} I_{in}) = (a/2\pi) \cdot \sin^{-1}(1) = a/4 \quad . \qquad (3.32)$$

For $I_3 \leq I_{in} < I_4$,

$$f^{-1}(\log_{10} I_{in}) = (a/2\pi) \cdot \sin^{-1}(\pi\sqrt{h(I_{in})}) \quad . \qquad (3.33)$$

For $I_4 \leq I_{in}$,

$$f^{-1}(\log_{10} I_{in}) = (a/2\pi) \cdot \sin^{-1}(\emptyset) = a/2 \quad . \qquad (3.34)$$

When solved for f, eqs. (3.30) to (3.34) yield the desired halftone cell. Each equation defines the cell in a specific range of densities.

A possible transfer function of this type and the resulting cell shape are shown in Fig. 3-7. A transfer function similar to this was tried experimentally and is presented in section 7.4.4.

3.6 Non-Symmetric Cell Design

The examples shown in the figures have all been symmetric halftone cells. The corresponding non-symmetric cell can be obtained in all cases by rescaling the x axis to range from Ø to a. The output intensity will be the same as for the corresponding symmetric cell.

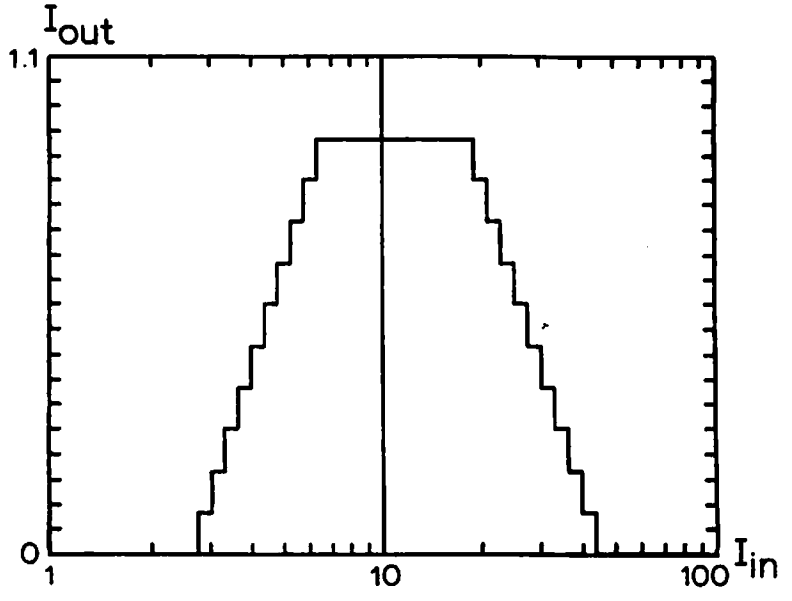

(a)

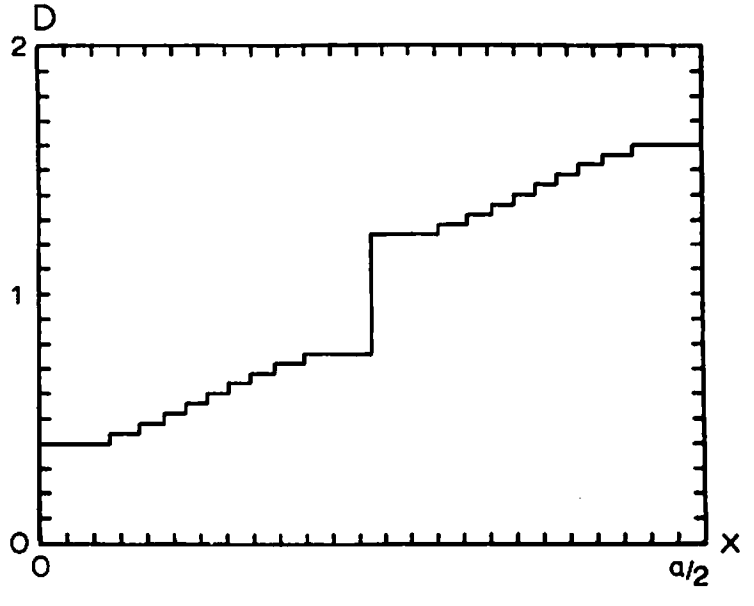

(b)

Figure 3-7. (a) Edge tailored bandpass transfer function.
(b) Corresponding halftone cell shape.

CHAPTER 4

NON-IDEAL FILM ANALYSIS

The analysis and examples of chapters 2 and 3 assume that the copy film used to make the halftoned picture has a binary response (infinite gamma and infinite saturation density). If this is not so, the original assumption that the halftoned picture consists of opaque bars of varying widths is incorrect. The purpose of this chapter is to analyze what happens to the transfer function when the film gamma and saturation density are finite. These effects are separately considered for the one-film and the two-film processes.

As an introduction, the problem will be examined qualitatively. For simplicity, only symmetric cells will be considered, although the analysis for non-symmetric cells is similar. Consider a cell of some shape as shown in Fig. 4-1. Given a copy film with an infinite gamma, the cell shown in Fig. 4-1, and an input intensity equal to $10^{D_1} \cdot I'$, the bar width should be b_1. If the gamma is not infinite, the bar width will differ from b_1. For this

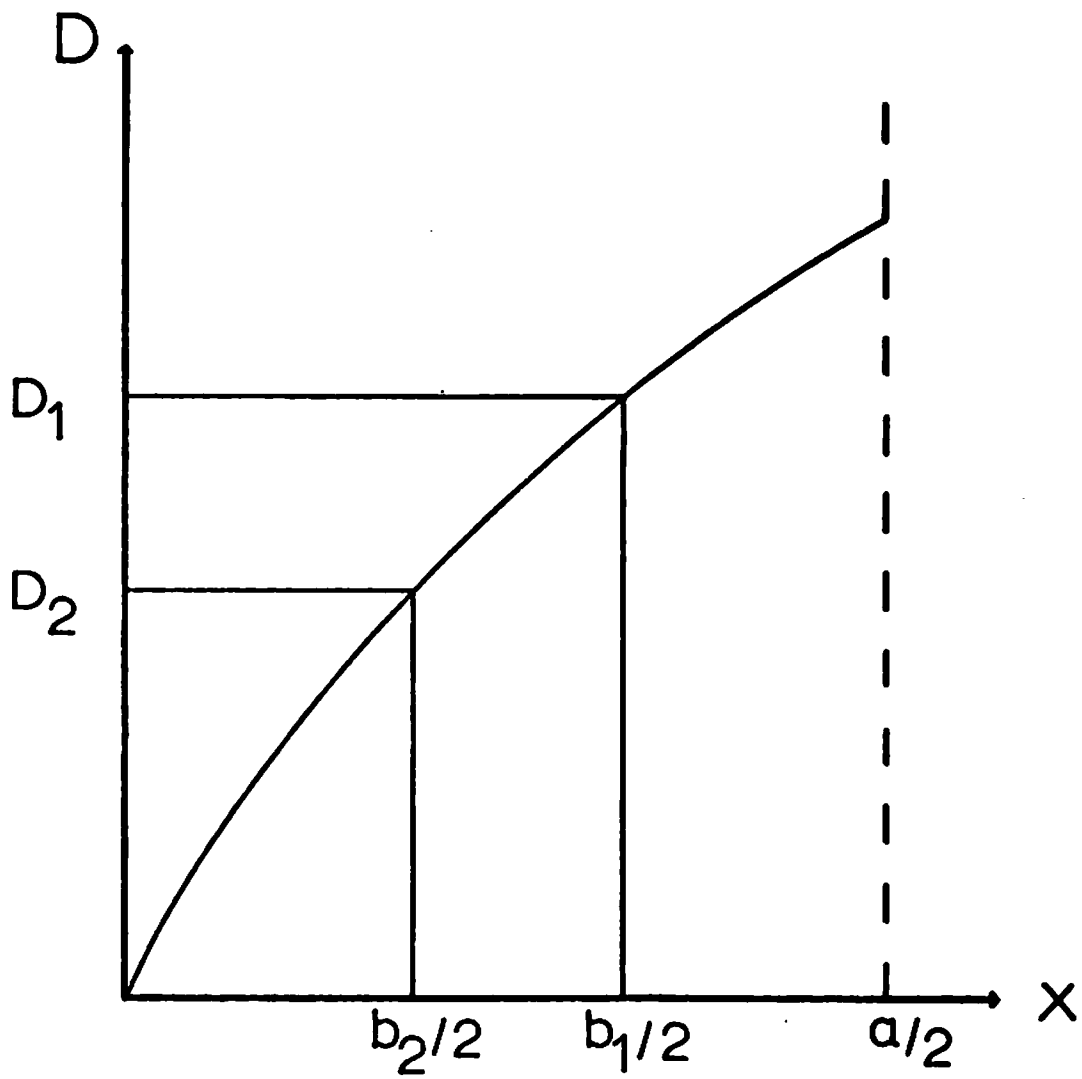

Figure 4-1. Typical symmetric halftone cell with two different bar widths indicated.

analysis, assume that the film threshold, I′, stays fixed. The only effect of varying the gamma is to introduce a grey scale range into the film response, as indicated in Fig. 4-2. The saturation density D_{sat} and film gamma γ are the two fundamental variables considered in determining the film effects.

4.1 One-Film Process

Assuming a copy film with finite gamma, the halftone bars on the copy film resulting from a cell as shown in Fig. 4-1 can be analyzed. The assumption that I′ is fixed means that for a width b the density on the copy film will be non-zero. Since the gamma is finite, not all of the bar will have density D_{sat}. If D is selected so that $\gamma(D_1-D_2)=D_{sat}$, a center section of the bar of width b_2 will have density D_{sat} and the bar edges will be varying densities rather than abrupt. The resulting bar shape is shown in Fig. 4-3. It is clear that the Fourier transform of a periodic array of such bars will be different than the Fourier transform of an array of rect functions. It is this difference, and its dependence on D_{sat} and γ which must be investigated.

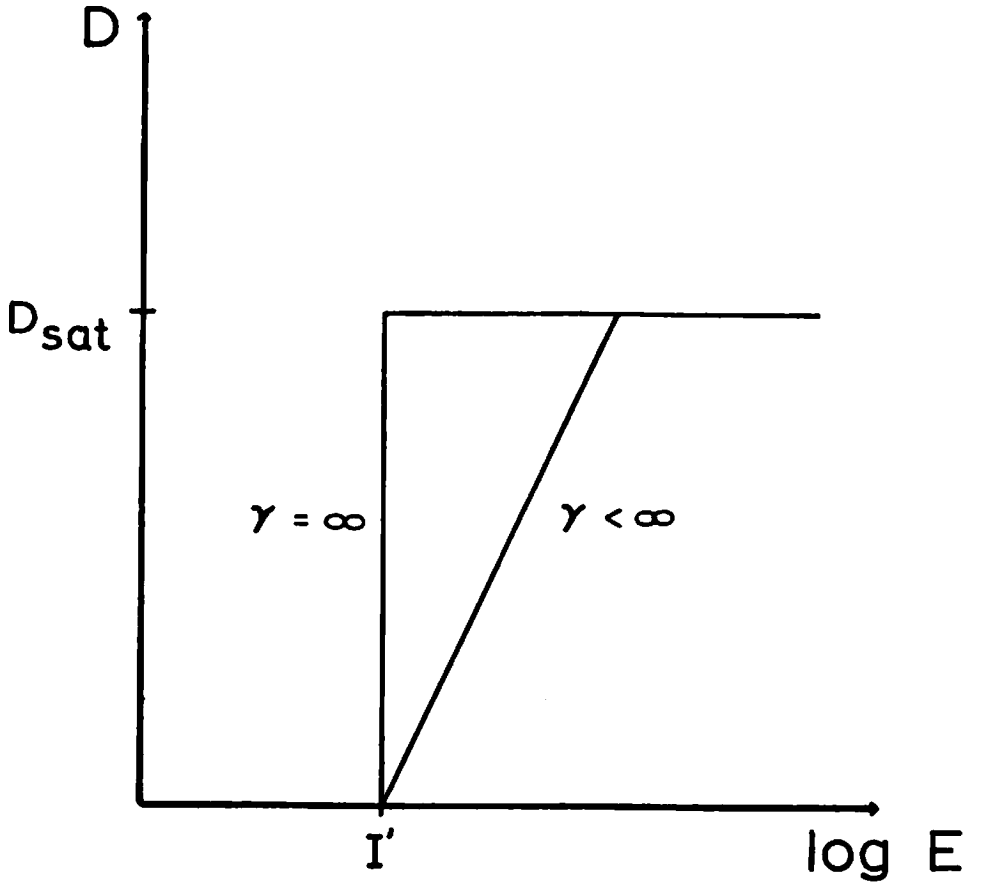

Figure 4-2. Assumed film response.

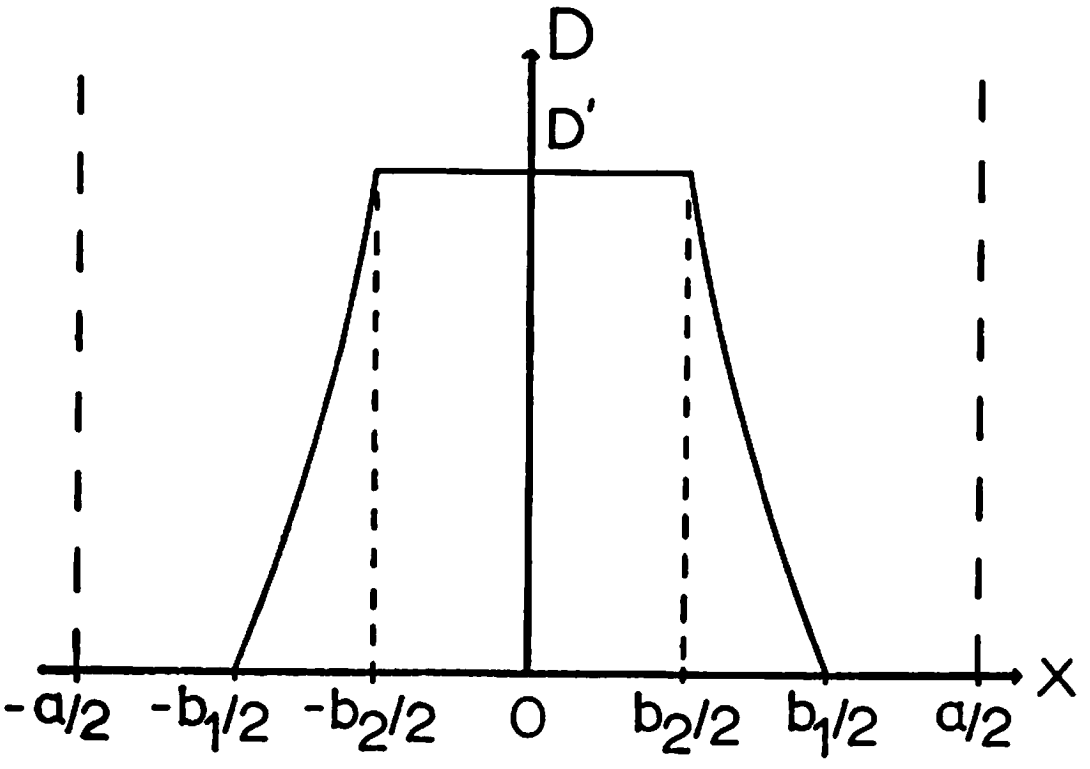

Figure 4-3. Density profile of a typical bar on non-ideal copy film.

4.1.1 Amplitude Output

The quantity of interest here is the complex amplitude transmittance of the bar structure shown in Fig. 4-4. The transmittance bar is simply another representation of the density bar shown in Fig. 4-3. The transmittance bars as shown in Fig. 4-4 will be the subject of the analysis.

The shape of the sloping sides depends on the shape of the halftone cell. In this model, the bar as sketched in Fig. 4-3 is represented as a stack of k trapezoids of height ΔD, where $\Delta D \cdot k = D_{sat}$. Figure 4-5 illustrates this procedure. Each trapezoid will have a top of width $2f^{-1}(D_1 - i\Delta D)$ and a bottom of width $2f^{-1}(D_1 - (i-1)\Delta D)$, where i runs from 1 to k. The trapezoids are a piecewise linear approximation of the continuous curve. The f^{-1} function used here is the same function of halftone cell shape as was used in the previous chapters. Next, consider what this implies as a representation for an amplitude transmittance such as shown in Fig. 4-4. The total amplitude transmittance of a bar such as shown in Fig. 4-4 can be represented as

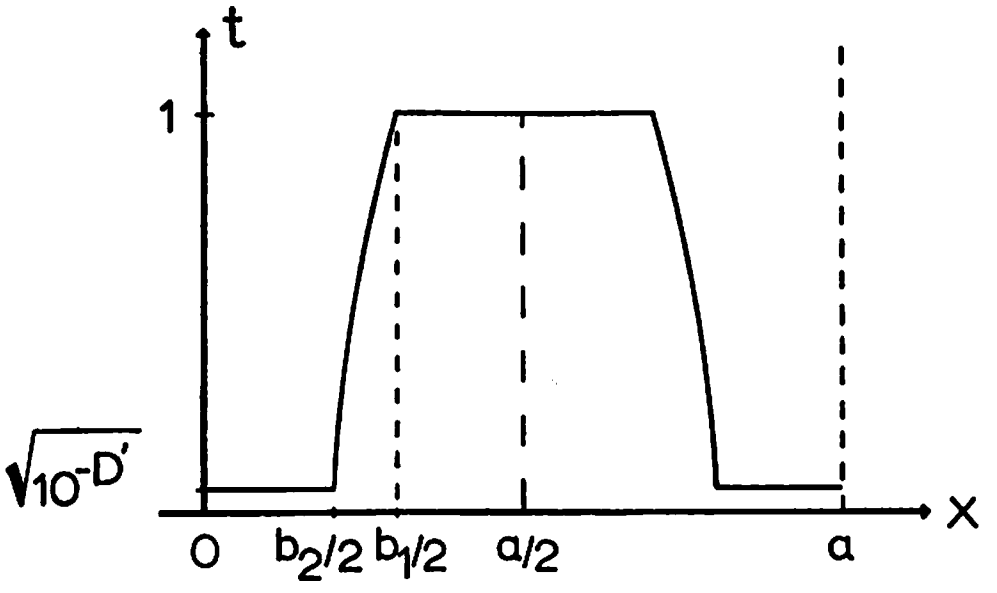

Figure 4-4. Amplitude transmission profile of the bar shown in Fig. 4-3.

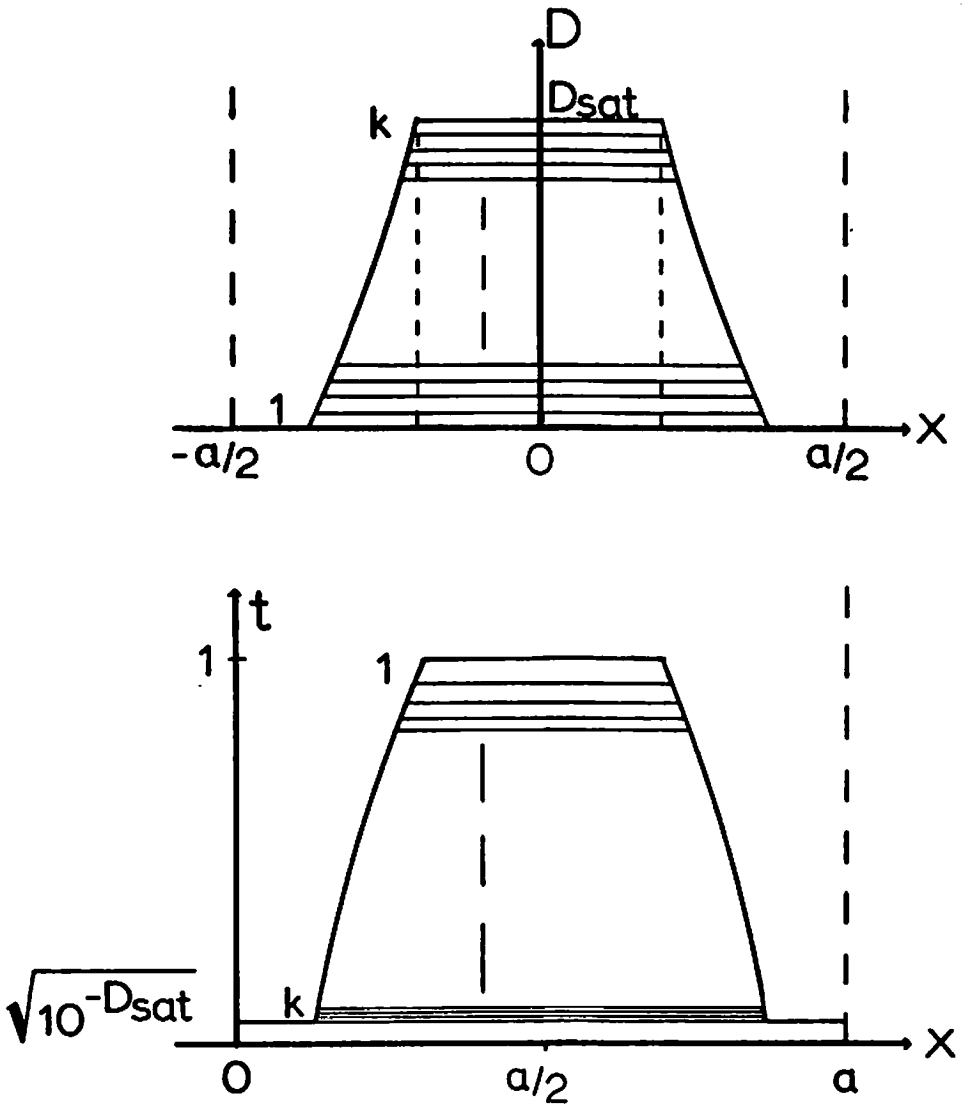

Figure 4-5. Trapezoid approximation technique. Density and transmittance representations of the same bar are shown. Although both functions represent one cycle of a periodic function, the density is drawn symmetrically about x=0 and the corresponding transmittance is drawn symmetrically about x=a/2.

$$v(x,D_{sat},D_1,\gamma)=\sqrt{10^{-D'}}+\sum_{i=1}^{k} q(i,D_{sat},D_1,\gamma)\cdot trap(i,D_{sat},D_1,\gamma) \qquad (4.1)$$

where $D'=D_{sat}$ or $\gamma\cdot D_1$, whichever is smaller

$=\gamma k\Delta D$

$$q(\cdot)=q(i,D_{sat},D_1,\gamma)=\sqrt{10^{-\gamma(i-1)\Delta D}}-\sqrt{10^{-\gamma i\Delta D}}$$

$trap(\cdot)=trap(i,D_{sat},D_1,\gamma)$=A trapezoid function with top width $a-2f^{-1}(D_1-(i-1)\Delta D)$ and bottom width $a-2f^{-1}(D_1-i\Delta D)$

The x dependence of v is contained in the f^{-1} functions of the trapezoid representation, and the $q(\cdot)$ function is the weight applied to the ith trapezoid. The $(\cdot)$ notation is used to avoid carrying several arguments through the analysis.

The fixed height steps in density from Fig. 4-3 have become monotonically decreasing height steps in amplitude transmittance. Note also that the base width of a trapezoid of a particular density corresponds to the top width of the associated trapezoid of amplitude transmittance.

A linear array of bars of the form of eq. (4.1) can be written as

$$t(\cdot)=t(x,D_{sat},D_1,\gamma)=\sqrt{10^{-D'}}+\left(\sum_{i=1}^{k} g(\cdot)\cdot trap(\cdot)\right)* ((1/a)\cdot comb(x/a)) \quad , \qquad (4.2)$$

where a is the fundamental screen period as before. The advantage of using a sum of trapezoids is that the continuous Fourier transform of each elementary trapezoid can be described analytically. In the limit of a large number of trapezoids, the sum of the individual transforms of the trapezoids is a good description of the continuous transform of the entire bar. The next step is to Fourier transform eq. (4.2). A Fourier series representation for an array of trapezoids, such as shown in Fig. 4-6 is given by [4-1]

$$a_n=(A(T_0+T_1)/a)\cdot sinc(nT_1/a)\cdot sinc(n(T_0+T_1)/a) \qquad (4.3)$$

$$DC=a_0$$

where $sinc(x)=sin(\pi x)/\pi x$. The a_n terms are the coefficients of the cosine terms of the double sided Fourier series expansion.

The dimensions of the trapezoid for the case being

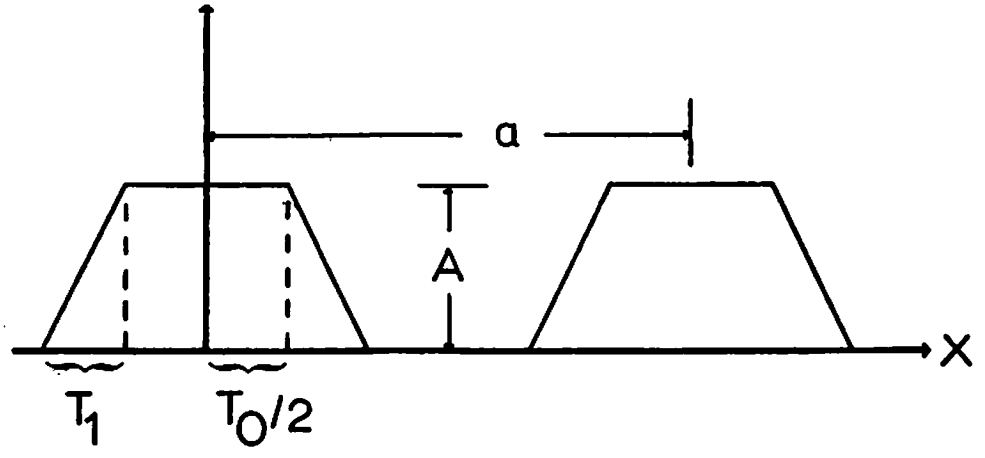

Figure 4-6. Trapezoids for series representation.

considered are

$$T_0(\cdot)=T_0(i,D_{sat},D_1,\gamma)=a-2f^{-1}(D_1-(i-1)\Delta D) \quad , \qquad (4.4)$$

$$\begin{aligned} T_1(\cdot)=T_1(i,D_{sat},D_1,\gamma)&=(a-2f^{-1}(D_1-i\Delta D)- \\ &\quad a+2f^{-1}(D_1-(i-1)\Delta D))/2 \\ &=f^{-1}(D_1-(i-1)\Delta D)-f^{-1}(D_1-i\Delta D) \quad , \end{aligned} \qquad (4.5)$$

and

$$A(i,D_{sat},D_1,\gamma)=g(\cdot) \quad . \qquad (4.6)$$

Using the formulation from eq. (4.3), the Fourier transform of eq. (4.2) can be written as

$$\begin{aligned} \mathcal{F}\{t(\cdot)\}=\sqrt{10^{-D'}}\ \delta(f_x)+\sum_{i=1}^{k} g(\cdot)\cdot\sum_{n=-\infty}^{\infty}((T_0(\cdot)+T_1(\cdot))/a)\cdot \\ \operatorname{sinc}(nT_1(\cdot)/a)\cdot\operatorname{sinc}(n(T_0(\cdot)+T_1(\cdot))/a)\cdot \\ \delta(f_x-n/a) \quad , \end{aligned} \qquad (4.7)$$

where the two special cases of interest are the zero and non-zero orders.

The zero order expression

$$\mathcal{F}\{t(\cdot)\}_{n=0} = \sqrt{10^{-D'}}\ \delta(f_x) + \sum_{i=1}^{k} g(\cdot)\cdot ((T_0(\cdot)+T_1(\cdot))/a)\cdot \delta(f_x) \tag{4.8}$$

is obtained by selecting the n=0 term of eq. (4.7). The non-zero order expression

$$\mathcal{F}\{t(\cdot)\}_{n\neq 0} = [\sum_{i=1}^{k} g(\cdot)\cdot((T_0(\cdot)+T_1(\cdot))/a)\cdot \operatorname{sinc}(nT_1(\cdot)/a)\cdot\operatorname{sinc}(n(T_0(\cdot)+T_1(\cdot))/a)]\cdot \delta(f_x - n/a) \tag{4.9}$$

is given by selecting n≠0 in eq. (4.7).

The output amplitude will be given by Fourier transforming eq. (4.8) or (4.9) to yield

$$\mathcal{F}\{\mathcal{F}\{t(\cdot)\}_{n=0}\} = [\sqrt{10^{-D'}} + \sum_{i=1}^{k} g(\cdot)\cdot (T_0(\cdot)+T_1(\cdot))/a] \tag{4.10}$$

and

$$\mathcal{F}\{\mathcal{F}\{t(\cdot)\}_{n\neq 0}\} = [\sum_{i=1}^{k} g(\cdot)\cdot((T_0(\cdot)+T_1(\cdot))/a)\cdot \operatorname{sinc}(nT_1(\cdot)/a)\cdot\operatorname{sinc}(n(T_0(\cdot)+T_1(\cdot))/a)]\cdot \exp(-j2\pi xn/a)$$

$$\mathcal{F}\{\mathcal{F}\{t(\cdot)\}_{n\neq 0}\}=[\sum_{i=1}^{k} q(\cdot)\cdot \mathrm{sinc}(nT_1(\cdot)/a)\cdot(1/n\pi)\cdot$$
$$\sin(n\pi(T_0(\cdot)+T_1(\cdot))/a)]\cdot$$
$$\exp(-j2\pi xn/a) \qquad (4.11)$$

respectively.

4.1.2 The Ideal Limit

If the ideal film assumptions are made, namely that $\gamma=\infty$, $D_{sat}\rightarrow\infty$, and $D_1>0$, it should be possible to reduce eq. (4.8) and (4.9) to eq. (2.8) and (2.9) respectively. This means simply that the trapezoid representation should be a somewhat more complicated but equally valid representation of the ideal case, given the previously mentioned film assumptions.

Considering the zero order expression, eqs. (4.4), (4.5) and the expression for $q(\cdot)$ from eq. (4.1) are rewritten to yield

$$T_0(\cdot)=a-2f^{-1}(D_1-(i-1)D'/\gamma k) \quad , \qquad (4.12)$$

$$T_1(\cdot)=f^{-1}(D_1-(i-1)D'/\gamma k)-f^{-1}(D_1-iD'/\gamma k) \quad , \qquad (4.13)$$

and

$$q(\cdot)=\sqrt{10^{-(i-1)D'/k}}-\sqrt{10^{-iD'/k}} \quad , \qquad (4.14)$$

where in each case ΔD has been replaced by $D'/\gamma k$. Substituting these into eq. (4.8) yields

$$\mathfrak{F}\{t(\cdot)\}_{\substack{n=0\\ \gamma=\infty}}=[\sqrt{10^{-D'}}+\sum_{i=1}^{k}(\sqrt{10^{-(i-1)D'/k}}-\sqrt{10^{-iD'/k}}\,)\cdot (a-f^{-1}(D_1-(i-1)D'/\gamma k)-f^{-1}(D_1-iD'/\gamma k))/a]\cdot \delta(f_x) \qquad (4.15)$$

as a rewritten zero order expression. Equation (4.15) reduces to

$$\mathfrak{F}\{t(\cdot)\}_{n\neq 0}=[\sqrt{10^{-D'}}+\sum_{i=1}^{k}(\sqrt{10^{-(i-1)D'/k}}-\sqrt{10^{-iD'/k}}\,)\cdot (a-2f^{-1}(D_1))/a]\cdot \delta(f_x) \qquad (4.16)$$

by setting $\gamma=\infty$. As D_{sat} becomes arbitrarily large,

$$\sqrt{10^{-D'}} \rightarrow 0$$

$$\sqrt{10^{-(i-1)D'/k}}-\sqrt{10^{-iD'/k}} = 1 \quad \text{for } i=1$$

$$= 0 \quad \text{for } 2 \leq i \leq k \quad , \qquad (4.17)$$

that is, for $\gamma=\infty$ and large D_{sat}, the DC term and all terms above the first become negligible. Therefore, eq. (4.16) becomes

$$\mathcal{F}\{t(\cdot)\}_{\substack{n=0 \\ \gamma=\infty \\ D_{sat}\to\infty}} = ((a-2f^{-1}(D_1))/a)\cdot \delta(f_x) \quad . \qquad (4.18)$$

Noting that $f^{-1}(D_1)=b_1/2$, eq. (4.18) becomes

$$\mathcal{F}\{t(\cdot)\}_{\substack{n=0 \\ \gamma=\infty \\ D_{sat}\to\infty}} = (1-b_1/a)\cdot \delta(f_x) \quad , \qquad (4.19)$$

which is identical to eq. (2.8). Therefore the trapezoidal approximation agrees with the ideal film analysis in the zero diffraction order.

Now consider eq. (4.9), the non-zero order expression, with the same ideal film assumptions. It should reduce to eq. (2.9), the corresponding ideal film expression. As a first step, rewrite it somewhat to yield

$$\mathcal{F}\{t(\cdot)\}_{n\neq 0} = \sum_{i=1}^{k} g(\cdot)\cdot \mathrm{sinc}(nT_1(\cdot)/a)\cdot \sin(n\pi(T_0(\cdot)+T_1(\cdot))/a)\cdot (1/n\pi)\cdot \delta(f_x-n/a) \quad . \qquad (4.20)$$

Combining eq. (4.12), (4.13), and (4.14) with eq. (4.20) yields

$$\mathcal{F}\{t(\cdot)\}_{n\neq 0} = \sum_{i=1}^{k} \left(\sqrt{10^{-(i-1)D'/k}} - \sqrt{10^{-iD'/k}} \right) \cdot$$
$$\operatorname{sinc}(n(f^{-1}(D_1-(i-1)D'/\gamma k)-f^{-1}(D_1-iD'/\gamma k))/a) \cdot$$
$$\sin(n\pi(a-f^{-1}(D_1-(i-1)D'/\gamma k)-f^{-1}(D_1-iD'/\gamma k))/a) \cdot$$
$$(1/n\pi) \cdot \delta(f_x-n/a) \qquad (4.21)$$

as the expanded expression for the amplitude present in a non-zero diffraction order in the Fourier transform plane. Setting $\gamma=\infty$ in eq. (4.21) gives

$$\mathcal{F}\{t(\cdot)\}_{\substack{n\neq 0 \\ \gamma=\infty}} = \sum_{i=1}^{k} \left(\sqrt{10^{-(i-1)D'/k}} - \sqrt{10^{-iD'/k}} \right) \cdot$$
$$\sin(n\pi(a-2f^{-1}(D_1))/a) \cdot$$
$$(1/n\pi) \cdot \delta(f_x-n/a) \quad . \qquad (4.22)$$

Using eq. (4.17), for limiting values of D_{sat} the summation of eq. (4.22) reduces to

$$\mathcal{F}\{t(\cdot)\}_{\substack{n\neq 0 \\ \gamma=\infty \\ D_{sat}\to\infty}} = (1/n\pi) \cdot \sin(n\pi(a-2f^{-1}(D_1))/a) \cdot$$
$$\delta(f_x-n/a)$$

$$= (1/n\pi) \cdot \sin(n\pi(1-b_1/a)) \cdot \delta(f_x - n/a) \qquad (4.23)$$

which contains only the first term of the summation. Noting that $\sin(n\pi(1-b_1/a)) = -\cos(n\pi) \cdot \sin(n\pi b_1/a)$, eq. (4.23) can be rewritten as

$$\mathcal{F}\{t(\cdot)\}_{\substack{n\neq 0 \\ \gamma=\infty \\ D_{sat}\to\infty}} = \pm(1/n\pi) \cdot \sin(\pi b_1 n/a) \cdot \delta(f_x - n/a)$$

$$= \pm(b_1/a) \cdot \mathrm{sinc}(b_1 n/a) \cdot \delta(f_x - n/a) \qquad (4.24)$$

which is equivalent to eq. (2.9) describing the ideal case, except for the sign alternation.

The sign changes are accounted for by noting that in the analysis leading to eq. (4.24), the transmissive bar was centered at x=a/2 rather than at x=∅ as assumed by eq. (4.3). Equation (4.24) and eq. (2.9) can be reconciled by shifting the input pattern, eq. (4.2), by one-half period. This shift produces a phase shift equal to $\exp(-j\pi n)$ in the Fourier transform. The product of $(-\cos(n\pi))$ and $\exp(-j\pi n)$ is always equal to -1, demonstrating that eq. (4.24) is identical to eq. (2.9), as desired.

As shown here, the trapezoid representation reduces

to the ideal case when the ideal film assumptions are made. Thus, the trapezoidal model will perform satisfactorily over all possible values of the film parameters, including the ideal values.

4.1.3 Output Intensities

The output intensities

$$I_{\substack{out \\ n=0}} = h_0(\cdot) = h_0(D_1, D_{sat}, \gamma) = \left| \sqrt{10^{-D'}} + \sum_{i=1}^{k} g(\cdot) \cdot (T_0(\cdot) + T_1(\cdot))/a \right|^2 \tag{4.25}$$

and

$$I_{\substack{out \\ n\neq 0}} = h_n(\cdot) = h_n(D_1, D_{sat}, \gamma) = \left| [\sum_{i=1}^{k} g(\cdot) \ \mathrm{sinc}(nT_1(\cdot)/a) \cdot (1/n\pi) \cdot \sin(n\pi(T_0(\cdot) + T_1(\cdot))/a)] \cdot \exp(-j2\pi x n/a) \right|^2 \tag{4.26}$$

are given by the modulus squared of eq. (4.10) and (4.11). Writing these out with $T_0(\cdot)$, $T_1(\cdot)$, and the weighting function $g(\cdot)$ expanded yields

$$I_{\substack{out\\ n=0}} = h_0(\cdot)$$

$$= \left[\sqrt{10^{-D'}} + \sum_{i=1}^{k} \left(\sqrt{10^{-(i-1)D'/k}} - \sqrt{10^{-iD'/k}} \right) \cdot \left(a - f^{-1}(D_1 - (i-1)D'/\gamma k) - f^{-1}(D_1 - iD'/\gamma k) \right)/a \right]^2 \quad (4.27)$$

and

$$I_{\substack{out\\ n\neq 0}} = h_n(\cdot)$$

$$= \left[\sum_{i=1}^{k} \left(\sqrt{10^{-(i-1)D'/k}} - \sqrt{10^{-iD'/k}} \right) \cdot (1/n\pi) \cdot \operatorname{sinc}\left(n\left(f^{-1}(D_1 - (i-1)D'/\gamma k) - f^{-1}(D_1 - iD'/\gamma k) \right)/a \right) \cdot \sin\left(n\pi\left(a - f^{-1}(D_1 - (i-1)D'/\gamma k) - f^{-1}(D_1 - iD'/\gamma k) \right)/a \right) \right]^2 \quad (4.28)$$

as the final expanded transfer function relationships.

Since $D_1 = \log_{10} I_{in}$, eq. (4.27) and (4.28) are functions which are fundamentally functions of I_{in}, D_{sat}, and γ. They can be used to calculate anticipated transfer functions given specified non-ideal film characteristics. A pair of general computer routines have been written using eq. (4.27) and (4.28) which calculate and plot transfer functions degraded by finite gamma and D_{sat}. The following examples were calculated with them.

4.1.4 Discussion

Some examples of one-film transfer functions degraded by non-ideal film characteristics are shown in figures 4-7 to 4-12. Figures 4-7 and 4-8 are decreasing logarithm transfer functions. Note that these are semi-logarithmic plots, so the ideal response is a straight line. Figures 4-9 to 4-12 are level slice transfer functions.

Figure 4-7 a and b shows the effect of varying the film gamma while holding the saturation density at a high value. Figure 4-7 is typical of the response of a smooth transfer function to low film gammas. The effect of lowering the gamma is to make the bar edges on the copy film more curved than they would be for a higher gamma. Note that as the gamma becomes very large the expected transfer function is very nearly the ideal film transfer function.

Figure 4-8a shows the effect of holding the film gamma low and varying the saturation density. Figure 4-8b shows the effect of holding the film gamma high and varying the saturation density. This figure illustrates the effect of low saturation density in the one-film process. Increasing the saturation density decreases the transmission of areas on the halftoned picture which would ideally be opaque, and causes the expected transfer

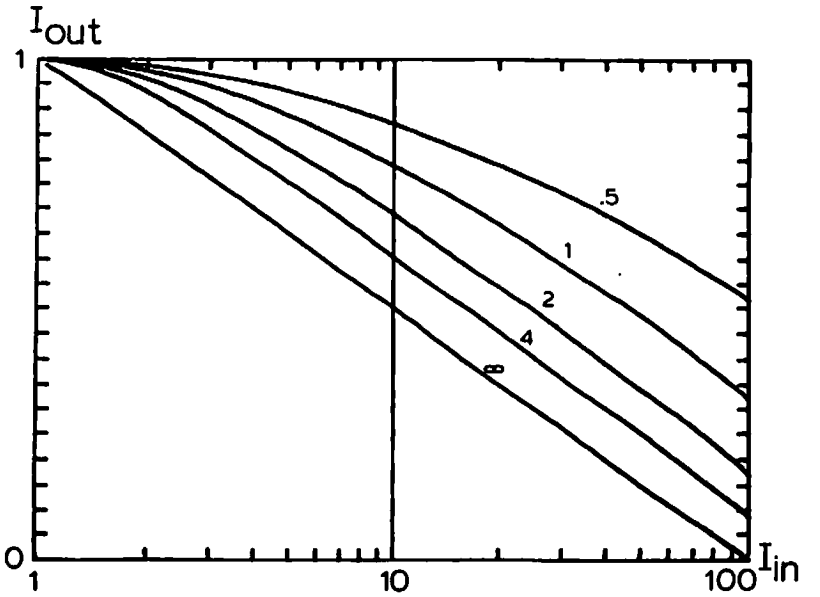

(a)

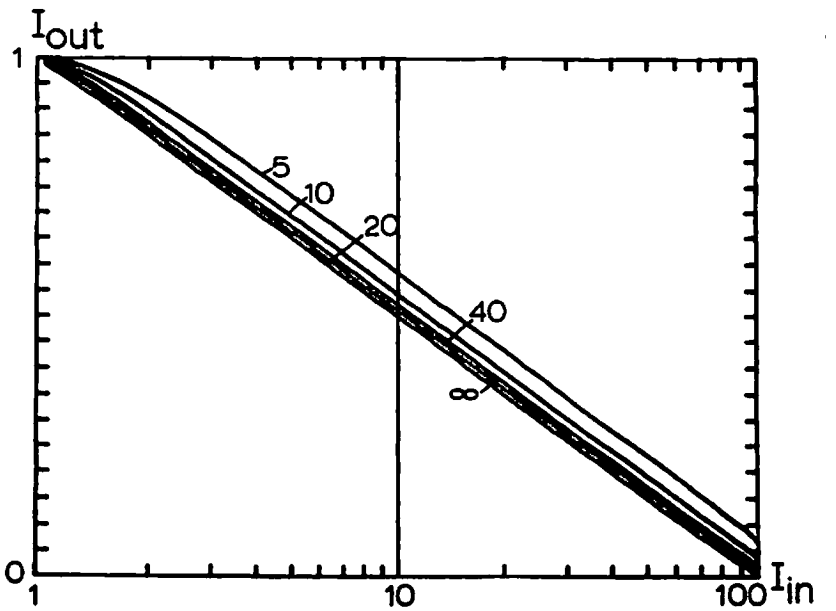

(b)

Figure 4-7. One-film logarithm transfer functions. $D_{sat} = 10$
(a) $\gamma = .5, 1, 2, 4$
(b) $\gamma = 5, 10, 20, 40$

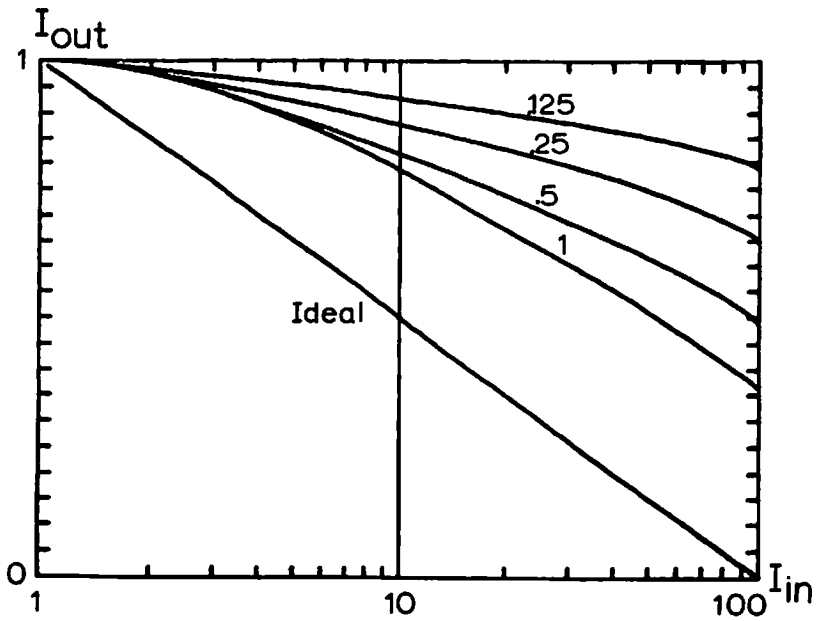

(a)

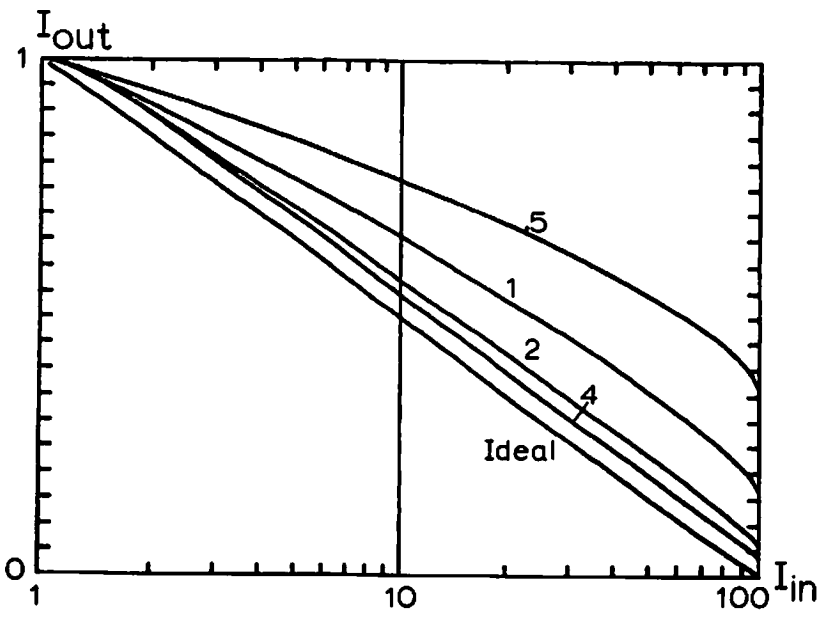

(b)

Figure 4-8. One-film logarithm transfer functions.
(a) $\gamma = 1$, $D_{sat} = .125, .25, .5, 1$
(b) $\gamma = 10$, $D_{sat} = .5, 1, 2, 4$

function to be closer to the ideal function.

In the following four figures, and all later plots of transfer functions involving any abrupt jumps, both the ideal and calculated transfer functions are computed at a discrete number of points by computer evaluation. Although this leads to the discrete jumps shown in some of the calculated transfer functions, in the limit of a continuous representation for the calculated function, the curve would be smooth. It is the general shape which should be noted.

Figure 4-9 shows the effect of holding the saturation density high with two values of gamma. Certain irregularities in the step size in the rising and falling edge are noticeable. In a continuous curve, these would be bends or kinks in what should be a smooth curve. The step size does not change smoothly, and on the trailing edge of Fig. 4-9a it is not even monotonic. This is due to choosing k, the number of trapezoids too small for the low gammas used. In this case the approximation of the bar by a stack of 50 trapezoids is not good enough. The same curves are shown in Fig. 4-10 with a 500 trapezoid approximation. The improved smoothness in the slope and step size variation in the curve is clearly visible. Larger values of gamma do not require the value of k to be

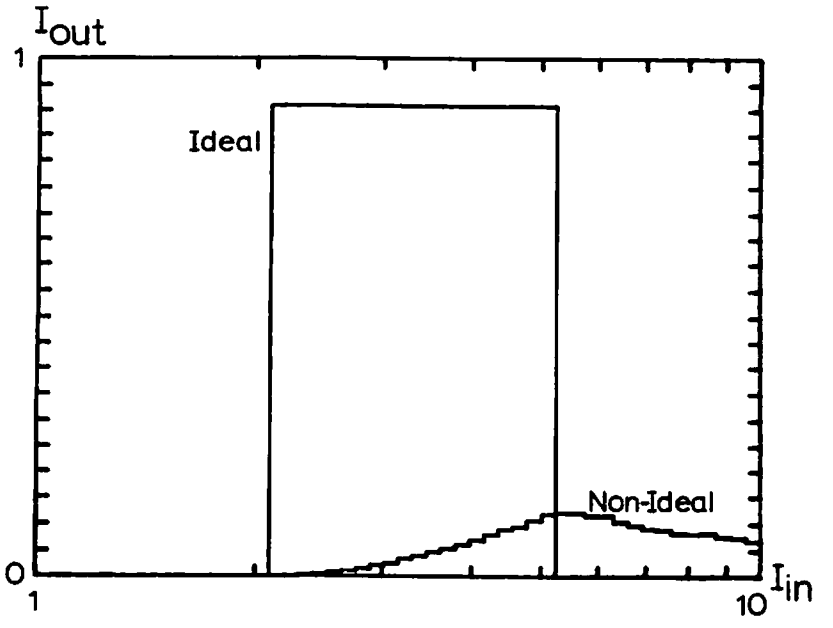

(a)

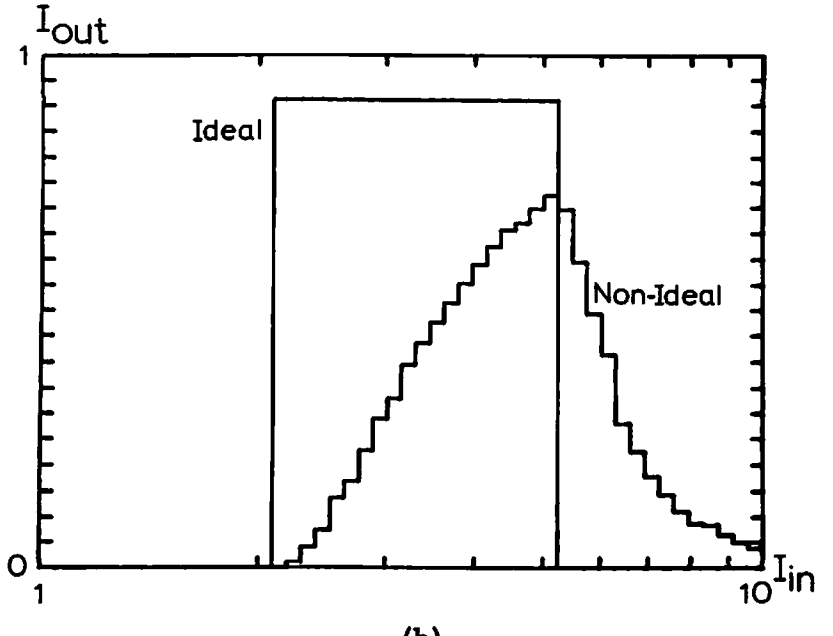

(b)

Figure 4-9. One-film level slice. $D_{sat} = 10$, $k = 50$
(a) $\gamma = 1$
(b) $\gamma = 5$

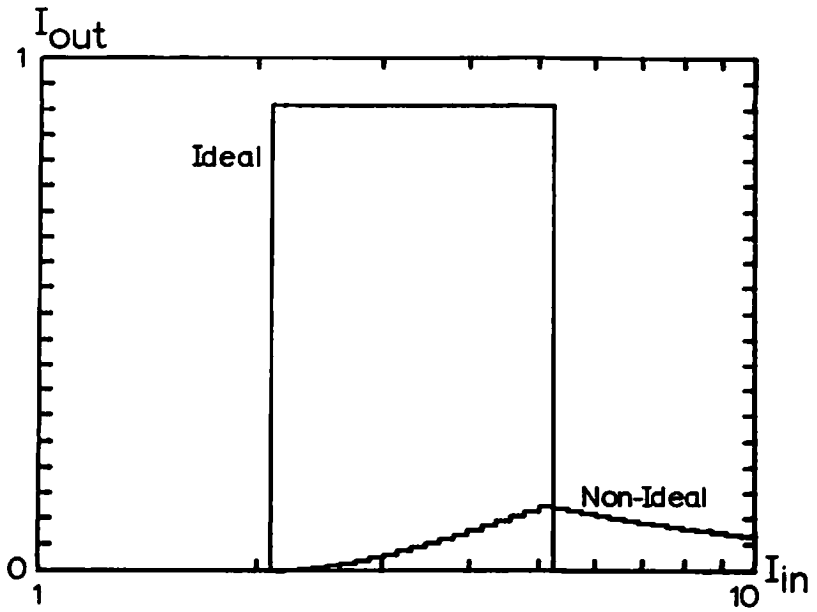

(a)

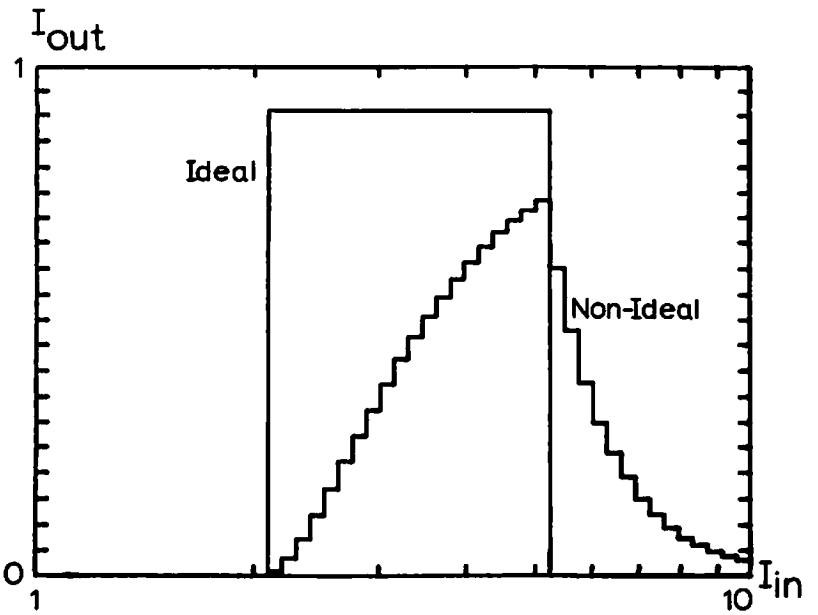

(b)

Figure 4-10. One-film level slice. D_{sat}= 10, k = 500
(a) $\gamma = 1$
(b) $\gamma = 5$

as large for accurate modeling. Because of the low film gamma in this example, areas which should be opaque will be transmissive to some degree, causing the type of transfer function shown.

Figure 4-11 shows a high saturation density with two high values of gamma. As the gamma becomes larger, the expected curve more nearly approaches the ideal curve, because the bar edges are becoming sharper. Figure 4-12 shows an extremely high gamma with two values of saturation density. The effect of lowering the saturation density is seen to be to decrease the output intensity, while leaving the shape of the rising and falling edges unaffected. This occurs because the bar edges are abrupt, but areas which should be opaque are transmissive to some degree.

4.2 Two-Film Process

The two-film process is of value in two situations: 1.) to change the sign of the transfer function slope when using the zero order and 2.) to achieve a higher effective film gamma. With the two-film process, a different gamma equal to the product of the individual gammas can be achieved. Thus if both individual gammas are larger than one, the product will more closely approach the ideal

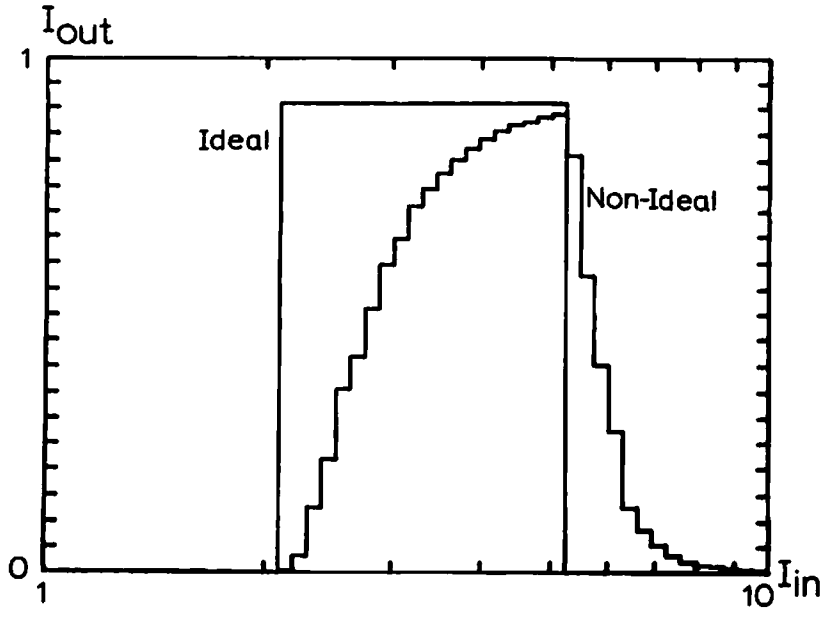

(a)

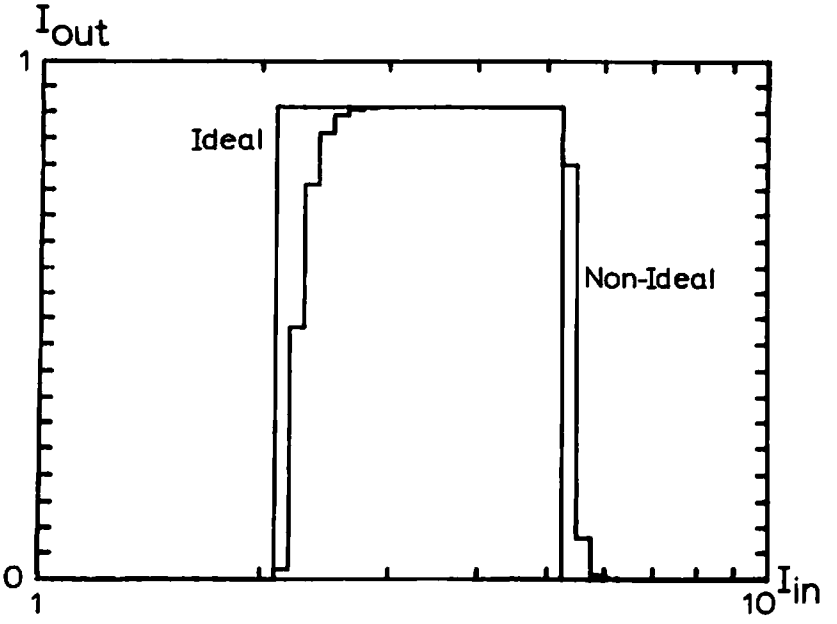

(b)

Figure 4-11. One-film level slice. D_{sat} = 10, k = 50
(a) γ = 10
(b) γ = 50

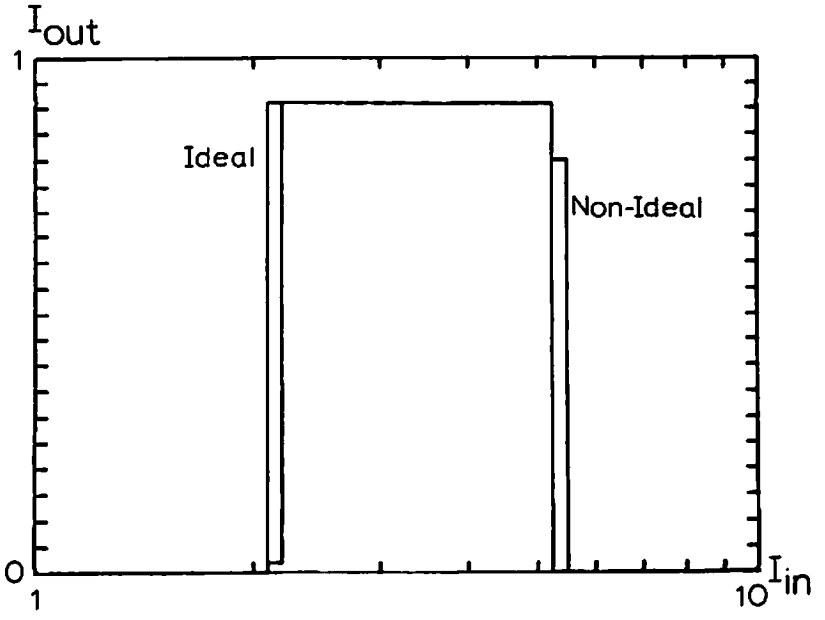

(a)

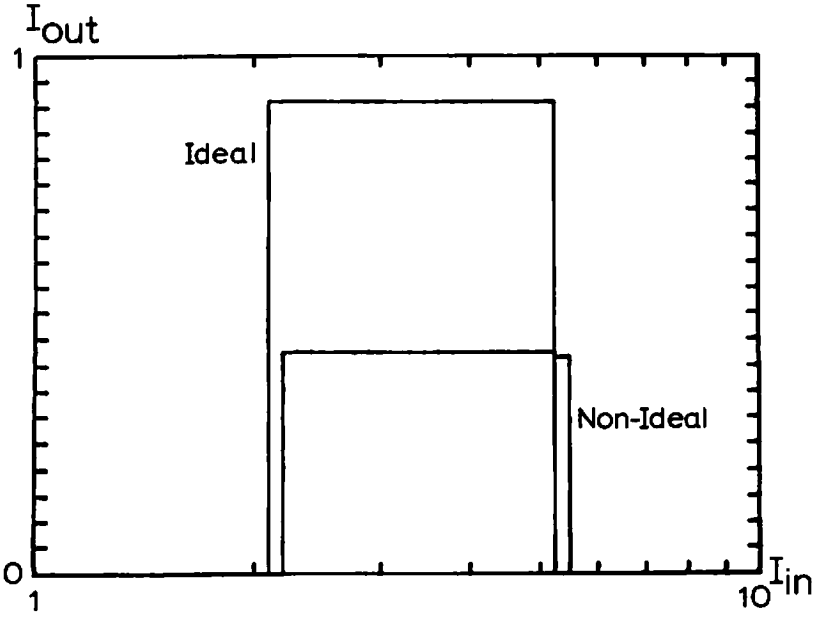

(b)

Figure 4-12. One-film level slice $\gamma = 500$, $k = 50$
(a) $D_{sat} = 10$
(b) $D_{sat} = 1$

infinite gamma.

The production of the first halftoned picture, film 1, proceeds exactly as described in chapter 1 or section 7.3, resulting in a bar pattern consisting of individual bars as shown in Fig. 4-3. The halftoned picture resulting from this process is copied onto another piece of film, film 2. The variables present in this second step are γ_2 , D_{sat2} , and the illumination, I_{copy}, used in the copying step. This copying step is illustrated in Fig. 4-13. Film 1 is assumed to have a specified gamma and D_{sat1} , yielding a bar profile sketched in Fig. 4-3. Depending on I_{copy}, it may not be possible to expose film 2 through a saturated region of film 1. Regions of film 1 whose density are greater than

$$D_{max}=\log_{10}(I_{copy}/I_2') \qquad (4.29)$$

where I_2'=the threshold illumination level for film 2, will yield zero exposure and hence unity transmission on film 2. Figure 4-13 is an accurate representation of the copying step whenever $D_{sat2} > D_{max}\cdot\gamma_2$. This will be true in practically all normal situations, since D_{max} is usually chosen rather small. If $D_{sat2} \leq D_{max}\cdot\gamma_2$, the corner of the bar on film 2 will not occur at $b_1/2$ as shown, but rather at a point between $b_3/2$ and $b_1/2$ whose

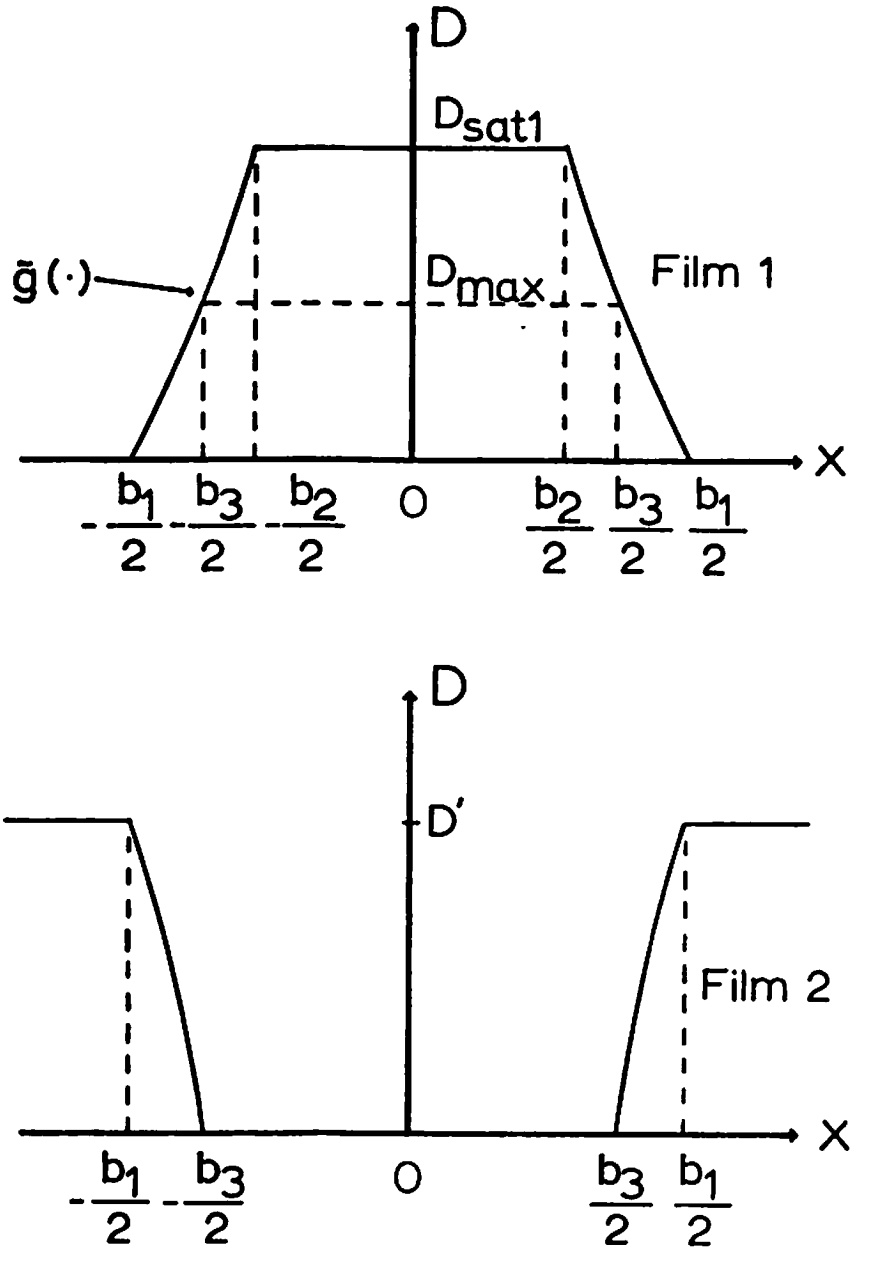

Figure 4-13. Film 1 to film 2 mapping.

precise location depends on $\tilde{q}(\cdot)$, γ_2, D_{max}, and D_{sat2}. The case of $D_{sat2} \leq D_{max} \cdot \gamma_2$ is implicitly included in the following analysis. The density on film 2 can be represented also as an amplitude transmittance as shown in Fig. 4-14. The qualitative effect of the second film is a steepening of the edges on the transmissive bar. Analysis of a bar pattern with bars as shown in Fig. 4-14 proceeds much as for the one-film process.

4.2.1 Amplitude Output

It will first be necessary to obtain the functional dependence of the bar shape in terms of the screen parameters. The $\tilde{q}(\cdot)$ shown in Fig. 4-13 is this function.

$$\begin{aligned} \tilde{q}(\cdot)=\tilde{q}(x,D_1,\gamma_1) &= \gamma_1(D_1-f(x)) \\ &= D_{sat1} \quad \text{if } \gamma_1(D_1-f(x)) \geq D_{sat1} \\ &= 0 \quad \text{if } \gamma_1(D_1-f(x)) \leq 0 \end{aligned} \tag{4.30}$$

where once again the $(\cdot)$ notation is used to avoid carrying a list of arguments through the calculations. It has been assumed that the fog level on the film is zero.

Proceeding in parallel with the one-film case, the amplitude transmittance of Fig. 4-14 can be represented as

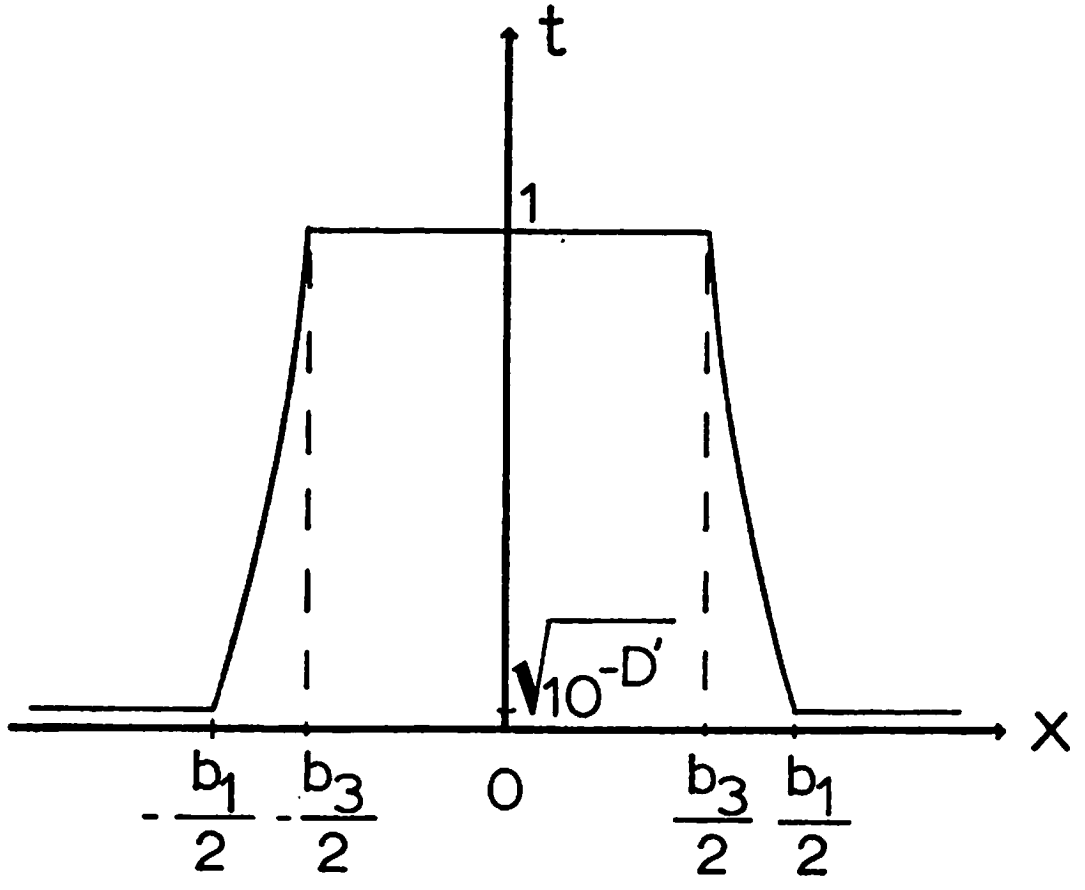

Figure 4-14. Transmission profile of bar on film 2.

$$v(x,D_{sat2},D_{max},D_1,\gamma_1,\gamma_2)=\sqrt{10^{-D'}}+\sum_{i=1}^{k}h(\cdot)\cdot trap(\cdot) \qquad (4.31)$$

$$\text{where } h(\cdot)=h(i,D_{sat2},D_{max},\gamma_2)=\sqrt{10^{-\gamma_2(i-1)\Delta D}}-\sqrt{10^{-\gamma_2 i\Delta D}}\ , \qquad (4.32)$$

$$\Delta D=D'/\gamma_2 k\ ,$$

$D'=D_{sat2}$ or $D_{max}\cdot\gamma_2$, whichever is smaller,

and

$$trap(\cdot)=trap(i,D_{sat2},D_{max},D_1,\gamma_1,\gamma_2)$$

=A trapezoid function with top width $2\tilde{g}^{-1}((D'/\gamma_2-(i-1)\Delta D),D_1,\gamma_1)$ and bottom width $2\tilde{g}^{-1}((D'/\gamma_2-i\Delta D),D_1,\gamma_1)$.

The x dependence is implicitly contained in the trap function.

Using the representation for a trapezoid given in Fig. 4-6 and eq. (4.3), the dimensions become

$$\tilde{T}_0(\cdot)=\tilde{T}_0(i,D_{sat2},D_{max},D_1,\gamma_1,\gamma_2)$$
$$=2\tilde{g}^{-1}((D'/\gamma_2-(i-1)\Delta D),D_1,\gamma_1) \qquad (4.33)$$

for the length of the top of the trapezoid,

$$\tilde{T}_1(\cdot)=\tilde{T}_1(i,D_{sat2},D_{max},D_1,\gamma_1,\gamma_2)$$
$$=\tilde{g}^{-1}((D'/\gamma_2-i\Delta D),D_1,\gamma_1)-$$
$$\tilde{g}^{-1}((D'/\gamma_2-(i-1)\Delta D),D_1,\gamma_1) \quad , \qquad (4.34)$$

which is one-half the difference of the bottom length and top length, and

$$A(i,D_{sat2},D_{max},\gamma_2)=h(\cdot)=h(i,D_{sat2},D_{max},\gamma_2) \quad , \qquad (4.35)$$

the height of the trapezoid. A linear array of bars in the form of eq. (4.31) can be represented as

$$t(\cdot)=t(x,D_{sat2},D_{max},D_1,\gamma_1,\gamma_2)=\sqrt{10^{-D'}}+$$
$$\left(\sum_{i=1}^{k}h(\cdot)\cdot trap(\cdot)\right)*((1/a)\cdot comb(x/a)) \qquad (4.36)$$

and Fourier transforming eq. (4.36) yields

$$\mathcal{F}\{t(\cdot)\} = \sqrt{10^{-D'}}\ \delta(f_x) + \sum_{i=1}^{k} h(\cdot)\cdot \sum_{n=-\infty}^{\infty} ((\tilde{T}_0(\cdot)+\tilde{T}_1(\cdot))/a)\cdot \mathrm{sinc}(n\tilde{T}_1(\cdot)/a)\cdot \mathrm{sinc}(n(\tilde{T}_0(\cdot)+\tilde{T}_1(\cdot))/a)\cdot \delta(f_x - n/a) \qquad (4.37)$$

as the general expression. The two cases of special interest are $n=0$ and $n\neq 0$. These are obtained by substituting into eq. (4.37) to obtain

$$\mathcal{F}\{t(\cdot)\}_{n=0} = [\sqrt{10^{-D'}} + \sum_{i=1}^{k} h(\cdot)\cdot (\tilde{T}_0(\cdot)+\tilde{T}_1(\cdot))/a]\cdot \delta(f_x) \qquad (4.38)$$

and

$$\mathcal{F}\{t(\cdot)\}_{n\neq 0} = [\sum_{i=1}^{k} h(\cdot)\cdot ((\tilde{T}_0(\cdot)+\tilde{T}_1(\cdot))/a)\cdot \mathrm{sinc}(n\tilde{T}_1(\cdot)/a)\cdot \mathrm{sinc}(n(\tilde{T}_0(\cdot)+\tilde{T}_1(\cdot))/a)]\cdot \delta(f_x - n/a) \quad . \qquad (4.39)$$

The output amplitude for $n=0$ and $n\neq 0$ is given by the Fourier transform of eq. (4.38) and (4.39) respectively.

$$\mathcal{F}\{\mathcal{F}\{t(\cdot)\}_{n=0}\} = \sqrt{10^{-D'}} + \sum_{i=1}^{k} h(\cdot)\cdot (\tilde{T}_0(\cdot)+\tilde{T}_1(\cdot))/a \qquad (4.40)$$

$$\mathcal{F}\{\mathcal{F}\{t(\cdot)\}_{n\neq 0}\}=[\sum_{i=1}^{k} h(\cdot)\cdot((\tilde{T}_0(\cdot)+\tilde{T}_1(\cdot))/a)\cdot \operatorname{sinc}(n\tilde{T}_1(\cdot)/a)\cdot \operatorname{sinc}(n(\tilde{T}_0(\cdot)+\tilde{T}_1(\cdot))/a)]\cdot \exp(-j2\pi nx/a) \qquad (4.41)$$

$\tilde{T}_0(\cdot)$ and $\tilde{T}_1(\cdot)$ contain $\tilde{g}^{-1}$ factors. It is necessary to get $\tilde{g}^{-1}$ in terms of f^{-1}. From eq. (4.30)

$$\tilde{g}(x,D_1,\gamma_1)=\gamma_1(D_1-f(x))$$

and if $\tilde{g}(x,D_1,\gamma_1)=\tilde{D}$ and $f(x)=\tilde{\tilde{D}}$,

$$\tilde{\tilde{D}}=D_1-\tilde{D}/\gamma_1 \qquad . \qquad (4.42)$$

Since $\tilde{g}^{-1}(\tilde{D},D_1,\gamma_1)=x=f^{-1}(\tilde{\tilde{D}})=f^{-1}(D_1-\tilde{D}/\gamma_1)$,

$$\tilde{g}^{-1}(\tilde{D},D_1,\gamma_1)=f^{-1}(D_1-\tilde{D}/\gamma_1) \qquad (4.43)$$

is the desired relationship between $\tilde{g}^{-1}$ and f^{-1}.

4.2.2 The Ideal Limit

Equations (4.38) and (4.39) should reduce to eq. (2.37) and (2.38) respectively if the ideal film assumptions are made. These assumptions are:

$$\gamma_1 = \gamma_2 = \infty$$

$$D_{sat2} \to \infty$$

$$D_{max} < D_{sat1}$$

First consider eq. (4.38), the zero order expression,

$$\mathcal{F}\{t(\cdot)\}_{n=0} = [\sqrt{10^{-D'}} + \sum_{i=1}^{k} h(\cdot) \cdot (\tilde{g}^{-1}((D'/\gamma_2 - (i-1)D'/\gamma_2 k), D_1, \gamma_1) + \tilde{g}^{-1}((D'/\gamma_2 - iD'/\gamma_2 k), D_1, \gamma_1))/a] \cdot \delta(f_x) \qquad (4.44)$$

where $\tilde{T}_0(\cdot)$ and $\tilde{T}_1(\cdot)$ have been expanded. Letting $\gamma_2 = \infty$ yields

$$\mathcal{F}\{t(\cdot)\}_{\substack{n=0 \\ \gamma_2=\infty}} = [\sqrt{10^{-D'}} + \sum_{i=1}^{k} h(\cdot) \cdot 2\tilde{g}^{-1}(0, D_1, \gamma_1)/a] \cdot \delta(f_x) \quad , \qquad (4.45)$$

and putting $\tilde{g}^{-1}$ in terms of f^{-1} gives

$$\mathcal{F}\{t(\cdot)\}_{\substack{n=0 \\ \gamma_2=\infty}} = [\sqrt{10^{-D'}} + \sum_{i=1}^{k} h(\cdot) \cdot 2f^{-1}(D_1)/a] \cdot \delta(f_x) \qquad (4.46)$$

as the amplitude present in the zero-order component in the Fourier transform plane with an infinite gamma for the second film. Equation (4.46) becomes

$$\mathcal{F}\{t(\cdot)\}_{\substack{n=0\\ \gamma_2=\infty}} = [\sqrt{10^{-D'}} + \sum_{i=1}^{k} (\sqrt{10^{-(i-1)D'/k}} - \sqrt{10^{-iD'/k}}) \cdot 2f^{-1}(D_1)/a] \cdot \delta(f_x) \qquad (4.47)$$

when actual values for $h(\cdot)$ are included. Now, letting $\gamma_1 = \infty$ and $D_{sat2} \to \infty$ only i=1 yields a non-zero contribution, and the DC term becomes zero. Equation (4.47) becomes

$$\mathcal{F}\{t(\cdot)\}_{\substack{n=0\\ \gamma_2=\infty\\ \gamma_1=\infty\\ D_{sat2}\to\infty}} = (2f^{-1}(D_1)/a) \cdot \delta(f_x) = (b_1/a) \cdot \delta(f_x) \qquad (4.48)$$

which is the same as eq. (2.37), as desired. Therefore the zero order expression from the trapezoidal approximation is consistent with the ideal case. Now consider the non-zero components. Begin by rewriting eq. (4.41) to yield

$$\mathcal{F}\{t(\cdot)\}_{n\neq 0} = [\sum_{i=1}^{k} h(\cdot)\cdot(1/n\pi)\cdot$$
$$\operatorname{sinc}(n(\tilde{g}^{-1}((D'/\gamma_2 - i\Delta D), D_1, \gamma_1)$$
$$-\tilde{g}^{-1}((D'/\gamma_2 - (i-1)\Delta D), D_1, \gamma_1))/a)\cdot$$
$$\sin(n\pi(\tilde{g}^{-1}((D'/\gamma_2 - (i-1)\Delta D), D_1, \gamma_1)$$
$$+\tilde{g}^{-1}((D'/\gamma_2 - i\Delta D), D_1, \gamma_1))/a)]\cdot$$
$$\delta(f_x - n/a) \qquad (4.49)$$

where $\tilde{T}_0(\cdot)$ and $\tilde{T}_1(\cdot)$ have been expanded. Using eq. (4.32), this becomes

$$\mathcal{F}\{t(\cdot)\}_{n\neq 0} = [\sum_{i=1}^{k} h(\cdot)\cdot(1/n\pi)\cdot$$
$$\operatorname{sinc}(n(\tilde{g}^{-1}((D'/\gamma_2 - iD'/\gamma_2 k), D_1, \gamma_1) -$$
$$\tilde{g}^{-1}((D'/\gamma_2 - (i-1)D'/\gamma_2 k), D_1, \gamma_1))/a)\cdot$$
$$\sin(n\pi(\tilde{g}^{-1}((D'/\gamma_2 - (i-1)D'/\gamma_2 k), D_1, \gamma_1)$$
$$+\tilde{g}^{-1}((D'/\gamma_2 - iD'/\gamma_2 k), D_1, \gamma_1))/a)]\cdot$$
$$\delta(f_x - n/a) \qquad (4.50)$$

where ΔD has been replaced with $D'/\gamma_2 k$. Letting $\gamma_2 = \infty$, eq. (4.50) reduces to

$$\mathcal{F}\{t(\cdot)\}_{\substack{n\neq 0\\ \gamma_2=\infty}} = [\sum_{i=1}^{k} h(\cdot)\cdot(1/n\pi)\cdot$$

$$\operatorname{sinc}(\emptyset)\cdot\sin(n\pi(\tilde{g}^{-1}(D',D_1,\gamma_1) + \tilde{g}^{-1}(D',D_1,\gamma_1))/a)]\cdot\delta(f_x-n/a) \qquad (4.51)$$

and putting $\tilde{g}^{-1}$ in terms of f^{-1} yields

$$\mathcal{F}\{t(\cdot)\}_{\substack{n\neq 0\\ \gamma_2=\infty}} = [\sum_{i=1}^{k} h(\cdot)\cdot(1/n\pi)\cdot$$

$$\sin(2\pi n f^{-1}(D_1 - D'/\gamma_1)/a)]\cdot\delta(f_x-n/a) \quad . \qquad (4.52)$$

Equation (4.52) is equivalent to

$$\mathcal{F}\{t(\cdot)\}_{\substack{n\neq 0\\ \gamma_2=\infty}} = [\sum_{i=1}^{k} (\sqrt{10^{-(i-1)D'/k}} - \sqrt{10^{-iD'/k}})\cdot$$

$$(1/n\pi)\cdot\sin(2n\pi f^{-1}(D_1 - D'/\gamma_1)/a)]\cdot\delta(f_x-n/a) \qquad (4.53)$$

where $h(\cdot)$ has been expanded. Letting $\gamma_1=\infty$ and $D_{sat2}\to\infty$, only the i=1 term yields any contribution, therefore eq. (4.53) simplifies to

$$\mathcal{F}\{t(\cdot)\}_{\substack{n\neq 0\\ \gamma_2=\infty\\ \gamma_1=\infty\\ D_{sat2}\to\infty}} = (1/n\pi)\cdot\sin(\pi n b_1/a)\cdot\delta(f_x-n/a) \qquad (4.54)$$

which is the same as eq. (2.38), the ideal two-film non-zero order expression, as desired. The trapezoid model for the two-film case is therefore consistent with the ideal analysis for both zero and non-zero diffraction orders.

4.2.3 Output Intensities

The output intensities are given by the modulus squared of eq. (4.40) and (4.41).

$$I_{\substack{out \\ n=0}} = h_0(\cdot) = h_0(D_1, D_{sat2}, D_{max}, \gamma_1, \gamma_2) = \left| \sqrt{10^{-D'}} + \sum_{i=1}^{k} h(\cdot) \cdot (\tilde{T}_0(\cdot) + \tilde{T}_1(\cdot))/a \right|^2 , \qquad (4.55)$$

and

$$I_{\substack{out \\ n\neq 0}} = h_n(\cdot) = h_n(D_1, D_{sat2}, D_{max}, \gamma_1, \gamma_2) = \left| \sum_{i=1}^{k} h(\cdot) \cdot (1/n\pi) \cdot \mathrm{sinc}(n\tilde{T}_1(\cdot)/a) \cdot \sin(n\pi(\tilde{T}_0(\cdot) + \tilde{T}_1(\cdot))/a) \cdot \exp(-j2\pi nx/a) \right|^2 \qquad (4.56)$$

respectively. Writing these out with the variables expressed in terms of the photographic parameters yields

$$I_{\substack{out\\ n\neq 0}} = h_n(\cdot) = [\sqrt{10^{-D'}} + \sum_{i=1}^{k} (\sqrt{10^{-(i-1)D'/k}} - \sqrt{10^{-iD'/k}}) \cdot$$
$$(\tilde{g}^{-1}((D'/\gamma_2 - (i-1)D'/\gamma_2 k), D_1, \gamma_1) +$$
$$\tilde{g}^{-1}((D'/\gamma_2 - iD'/\gamma_2 k), D_1, \gamma_1))/a]^2$$
$$= [\sqrt{10^{-D'}} + \sum_{i=1}^{k} (\sqrt{10^{-(i-1)D'/k}} - \sqrt{10^{-iD'/k}}) \cdot$$
$$(f^{-1}(D_1 - (D'/\gamma_2 - (i-1)D'/\gamma_2 k)/\gamma_1)$$
$$+ f^{-1}(D_1 - (D'/\gamma_2 - iD'/\gamma_2 k)/\gamma_1)/a)]^2 \qquad (4.57)$$

for the zero order expression and,

$$I_{\substack{out\\ n\neq 0}} = h_n(\cdot) = [\sum_{i=1}^{k} h(\cdot) \cdot (1/n\pi) \cdot$$
$$\text{sinc}(n(\tilde{g}^{-1}((D'/\gamma_2 - iD'/\gamma_2 k), D_1, \gamma_1)$$
$$- \tilde{g}^{-1}((D'/\gamma_2 - (i-1)D'/\gamma_2 k), D_1, \gamma_1))/a) \cdot$$
$$\sin(n\pi(\tilde{g}^{-1}((D'/\gamma_2 - (i-1)D'/\gamma_2 k), D_1, \gamma_1)$$
$$+ \tilde{g}^{-1}((D'/\gamma_2 - iD'/\gamma_2 k), D_1, \gamma_1))/a)]^2$$
$$= [\sum_{i=1}^{k} (\sqrt{10^{-(i-1)D'/k}} - \sqrt{10^{-iD'/k}}) \cdot (1/n\pi) \cdot$$
$$\text{sinc}(n(f^{-1}(D_1 - (D'/\gamma_2 - iD'/\gamma_2 k)/\gamma_1)$$
$$- f^{-1}(D_1 - (D'/\gamma_2 - (i-1)D'/\gamma_2 k)/\gamma_1))/a) \cdot$$
$$\sin(n\pi(f^{-1}(D_1 - (D'/\gamma_2 - (i-1)D'/\gamma_2 k)/\gamma_1)$$
$$+ f^{-1}(D_1 - (D'/\gamma_2 - iD'/\gamma_2 k)/\gamma_1))/a)]^2 \qquad (4.58)$$

for the non-zero order expression. Noting that

$D_1 = \log_{10} I_{in}$ and $D_{max} = \log_{10} (I_{copy}/I')$, it can be observed that eq. (4.57) and (4.58) are functions of I_{in}, I_{copy}, γ_1, γ_2, and D_{sat2} and can be used to calculate expected transfer functions given non-ideal film characteristics.

4.2.4 Discussion

Some transfer functions calculated using these expressions are shown in figures 4-15 to 4-21. The two-film monotonically increasing logarithm is considered in Fig. 4-15, 4-16, and 4-17. It could be considered as typical of the response of two-film smooth transfer functions to variations in the film parameters. Figures 4-18 to 4-21 are level slice transfer functions.

Figure 4-15 shows the effects of varying γ_1 while holding the other parameters fixed. It is indicative of the fact that the gamma of the first film only varies the shape of the edge of the bar on film 2, and consequently has only limited control over the resulting transfer function.

Figure 4-16 shows the effect of varying D_{max} while holding the other parameters fixed. It shows that increasing D_{max} causes the entire transfer function to shift toward larger values of I_{in}. This is especially

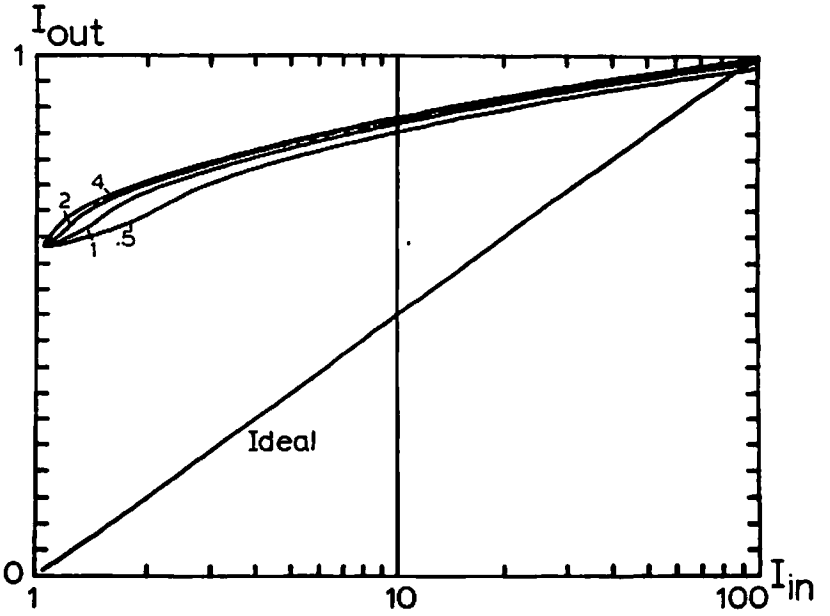

(a)

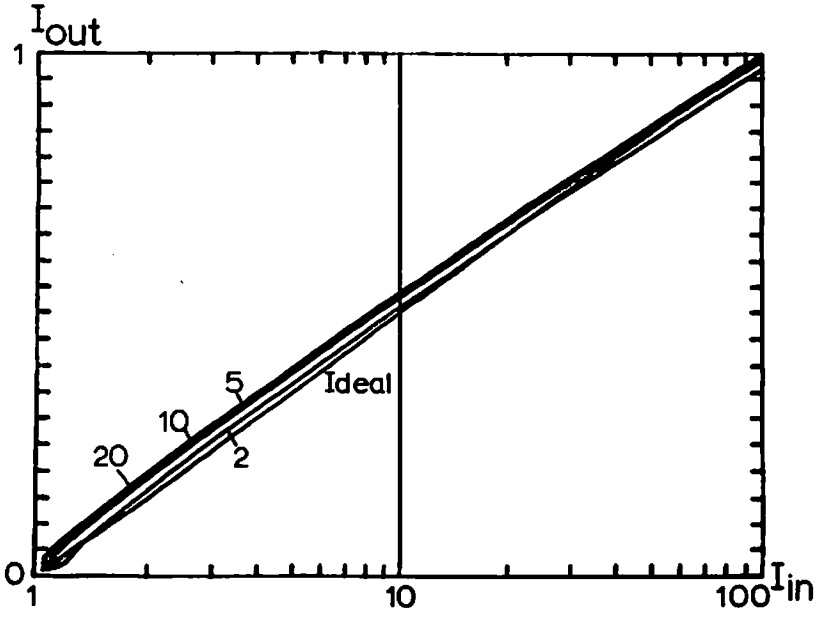

(b)

Figure 4-15. Two-film logarithm transfer function.
(a) $\gamma_2 = 1$, $D_{max} = 2$, $D_{sat2} = 1$, $\gamma_1 = .5, 1, 2, 4$
(b) $\gamma_2 = 10$, $D_{max} = 2$, $D_{sat2} = 10$, $\gamma_1 = 2, 5, 10, 20$

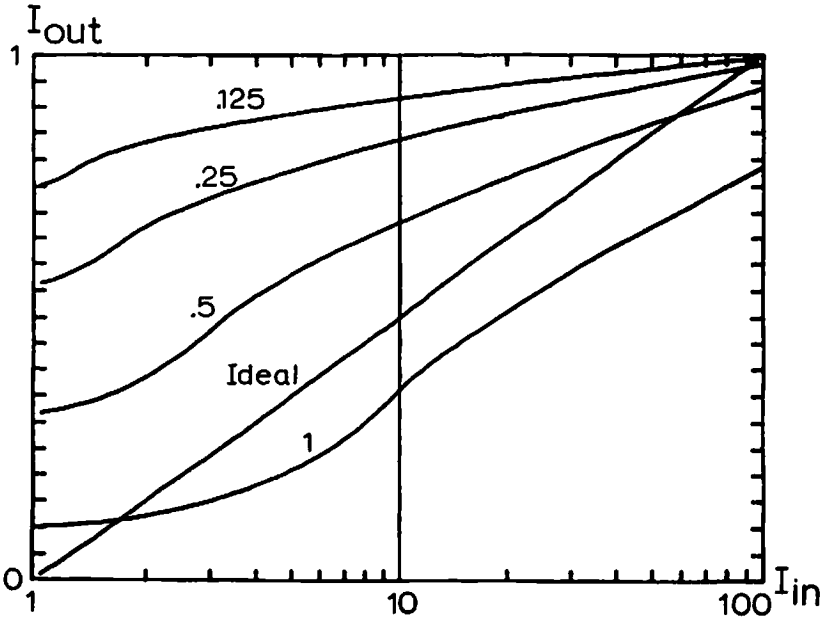

(a)

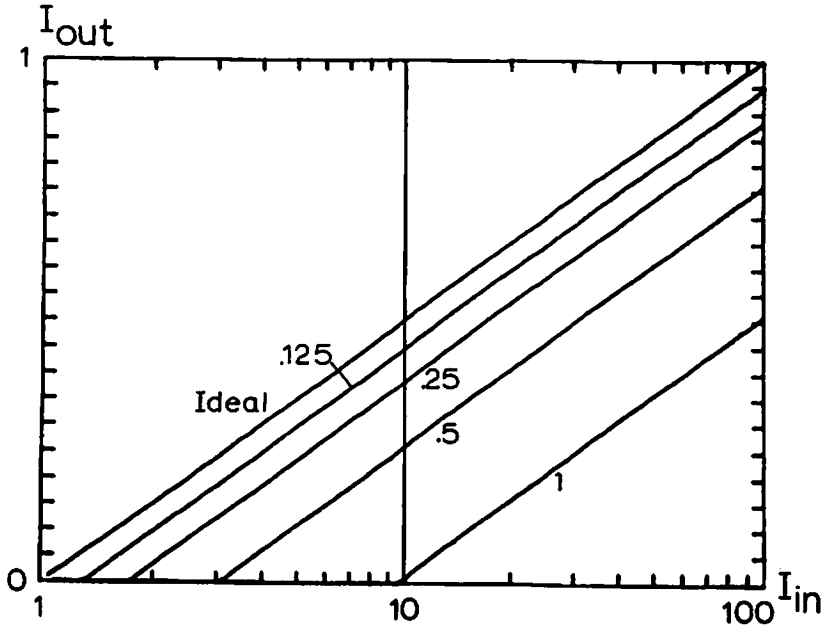

(b)

Figure 4-16. Two-film logarithm transfer function.
(a) $\gamma_1 = \gamma_2 = 1$, $D_{sat2} = 1$, $D_{max} = .125, .25, .5, 1$
(b) $\gamma_1 = 1$, $\gamma_2 = 50$, $D_{sat2} = 50$, $D_{max} = .125, .25, .5, 1$

clear in Fig. 4-16b.

Figure 4-17 shows the effect of varying only γ_2. Increasing this gamma causes a smaller region of the bar on film 1 to be used and therefore steepens the edge of the bar on film 2. Note that a higher gamma results in a closer approximation to the desired transfer function, though possibly shifted due to D_{max}.

Some of the possible variations in a two-film level slice are shown in Fig. 4-18 to 4-21. As Fig. 4-18 shows, with everything else fixed, increasing the gamma of film 2 results in increased I_{out}, as long as $D_{sat2} > D_{max} \cdot \gamma_2$. This occurs because the maximum density on the film increases and the diffraction efficiency improves. The shape of the transfer function also changes somewhat. Holding everything but D_{sat2} fixed again varies the diffraction efficiency, but has little effect on the transfer function edge shape. This case is shown in Fig. 4-19.

Varying only γ_1 is shown in Fig. 4-20. This has no effect on the diffraction efficiency, because γ_1 has no effect on the maximum density on film 2. It does have a pronounced effect on the shape of the transfer function. This is because increasing γ_1 results in greater contrast on film 2, which yields sharper edges on the transfer

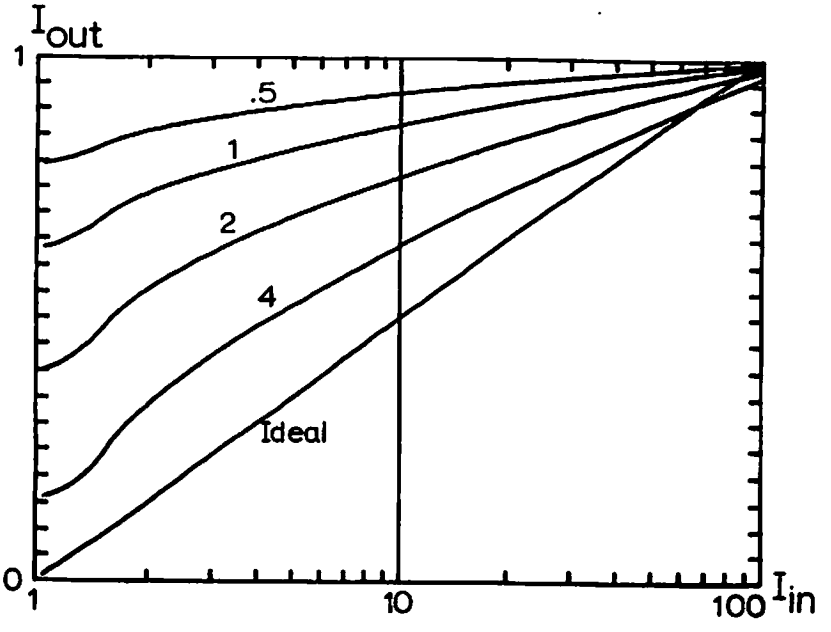

(a)

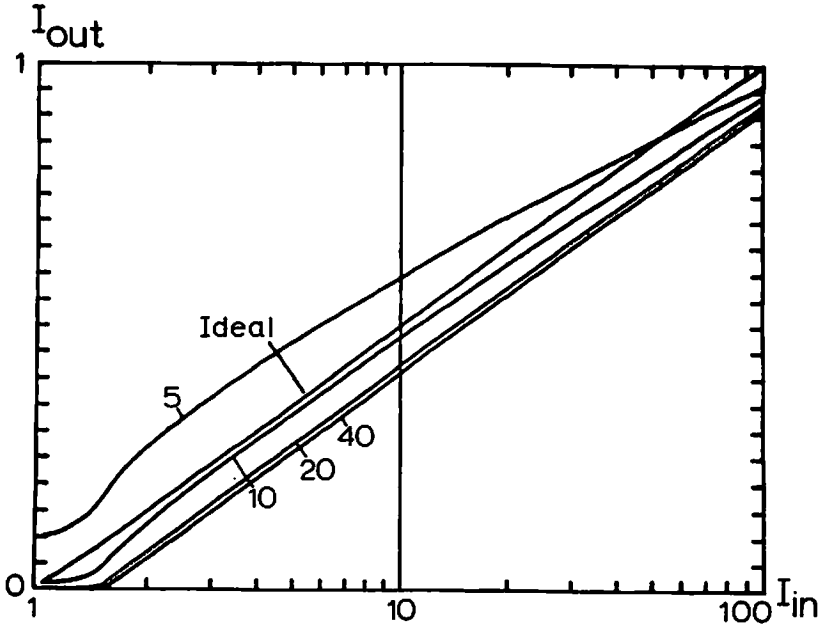

(b)

Figure 4-17. Two-film logarithm transfer function.
(a) $\gamma_1=1$, $D_{max}=.2$, $D_{sat2}=1$, $\gamma_2=.5, 1, 2, 4$
(b) $\gamma_1=1$, $D_{max}=.2$, $D_{sat2}=10$, $\gamma_2=5, 10, 20, 40$

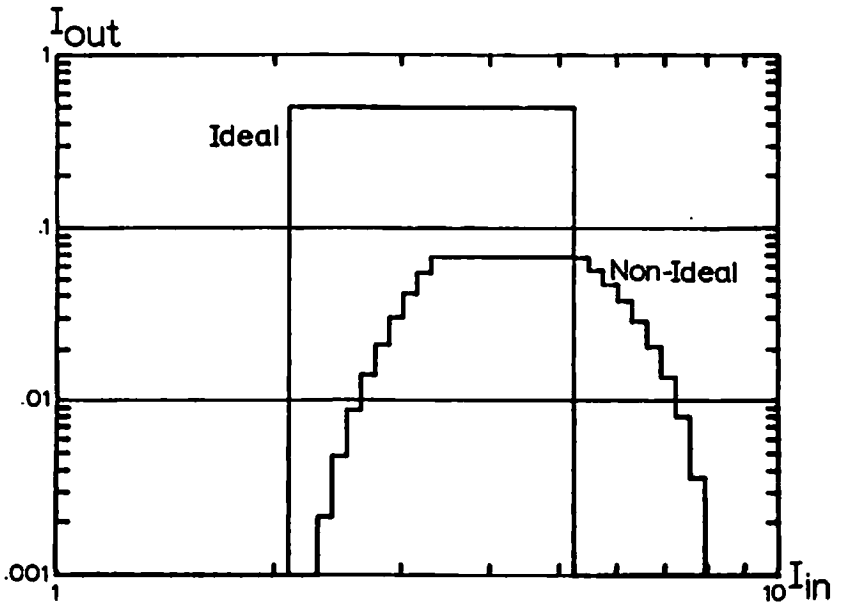

(a)

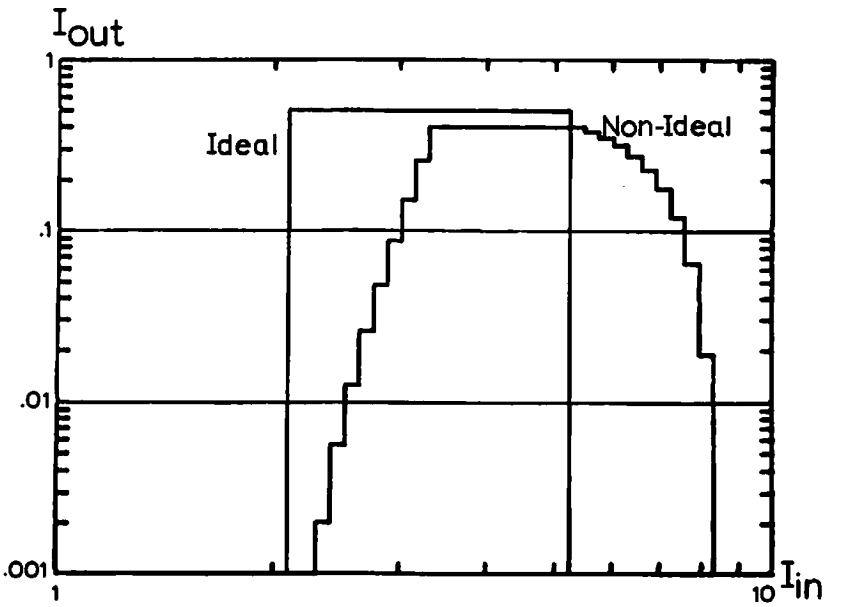

(b)

Figure 4-18. Two-film level slice. $\gamma_1 = 1, D_{max} = .2, D_{sat2} = 10$
(a) $\gamma_2 = 2$
(b) $\gamma_2 = 10$

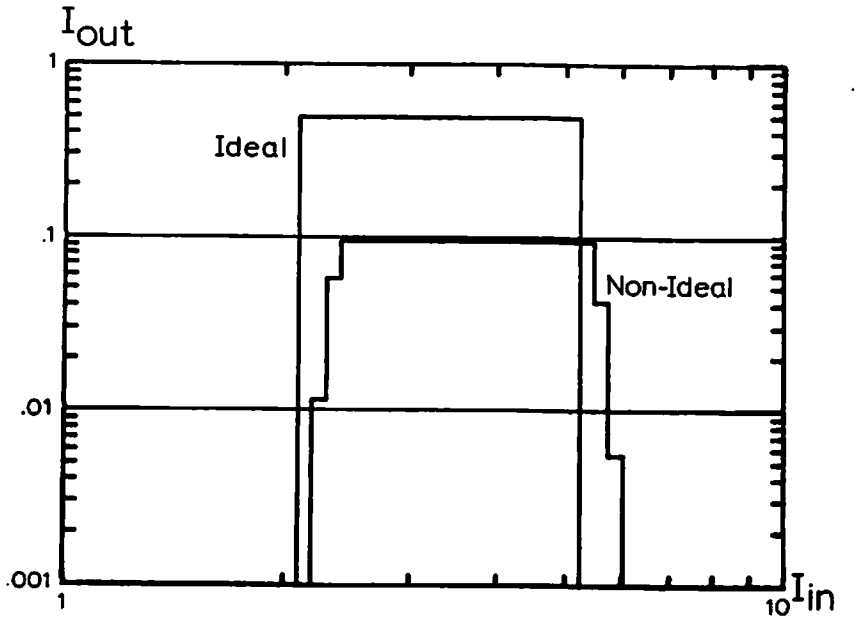

(a)

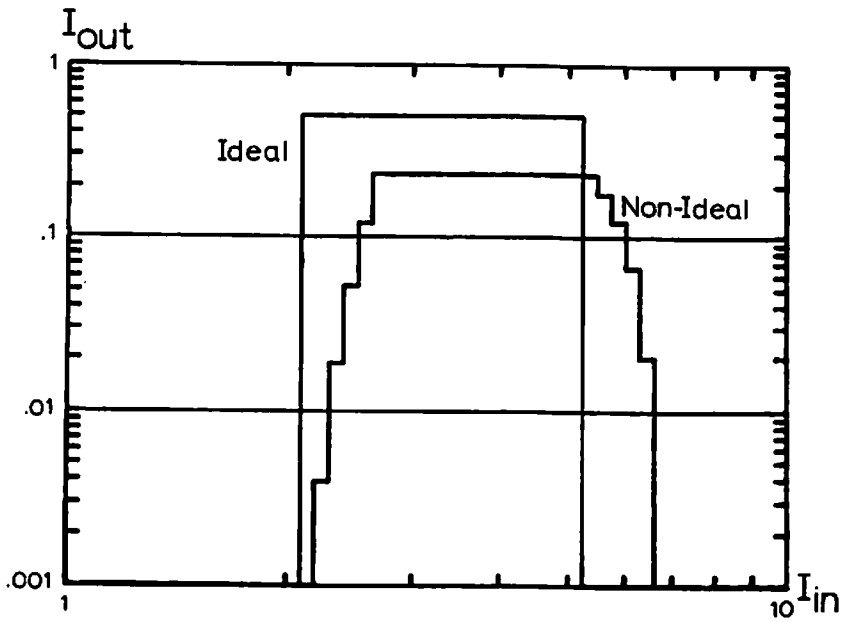

(b)

Figure 4-19. Two-film level slice. γ_1=1, γ_2= 10, D_{max}= .2
(a) D_{sat2}=.5
(b) D_{sat2}=1.0

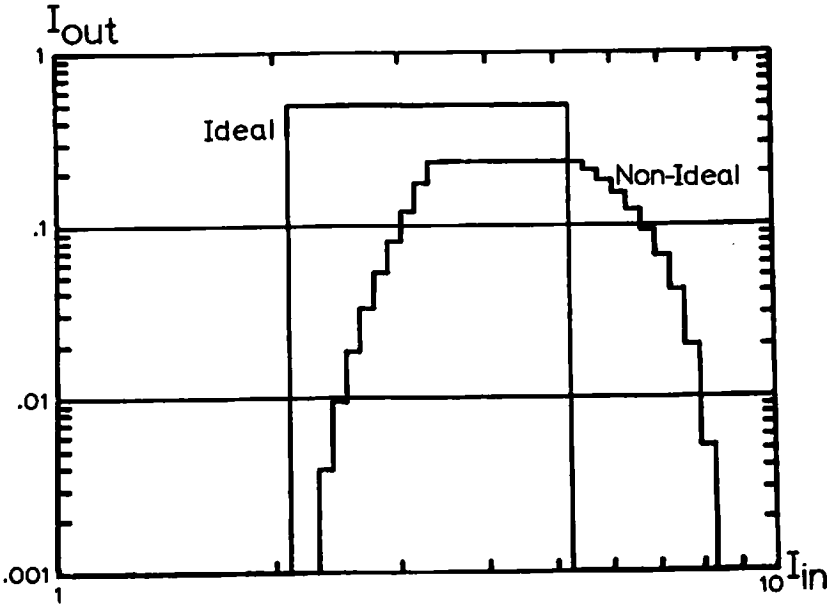

(a)

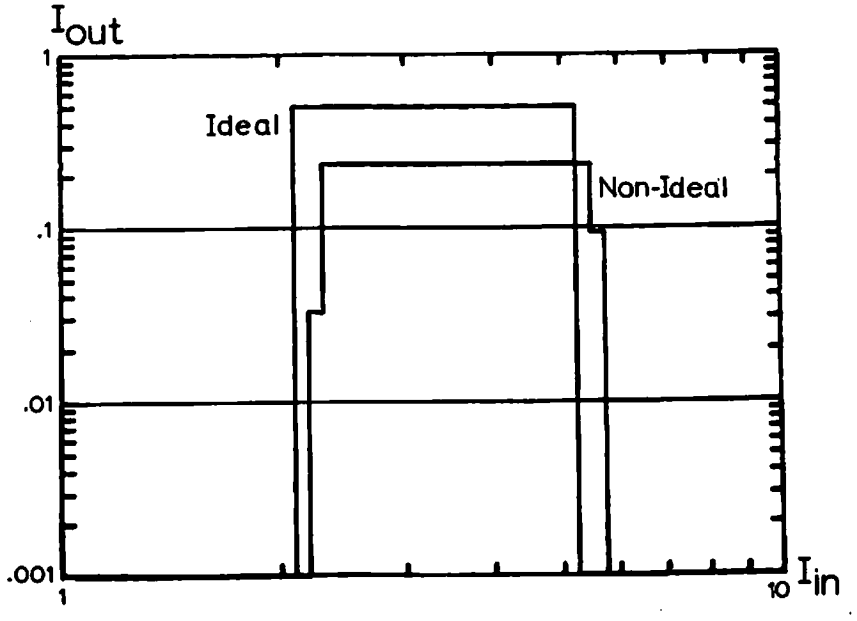

(b)

Figure 4-20. Two-film level slice. $\gamma_2 = 5$, $D_{max} = .2$, $D_{sat2} = 10$.
(a) $\gamma_1 = 1$
(b) $\gamma_1 = 5$

function.

Varying only D_{max} is shown in Fig. 4-21. Increasing D_{max} is seen to result in a shift of the transfer function to the left, and an increase in the diffraction efficiency as long as $D_{max} \cdot \gamma_2 < D_{sat2}$.

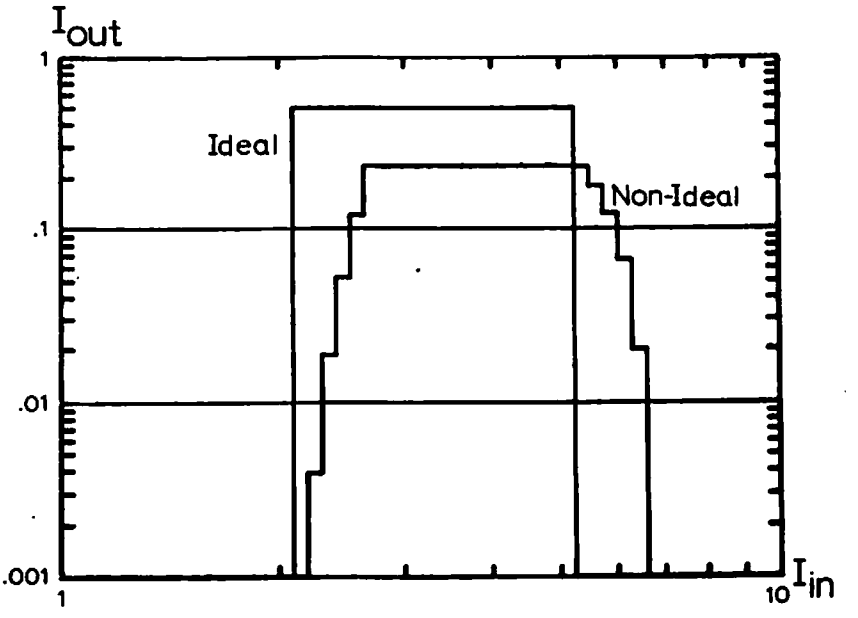

(a)

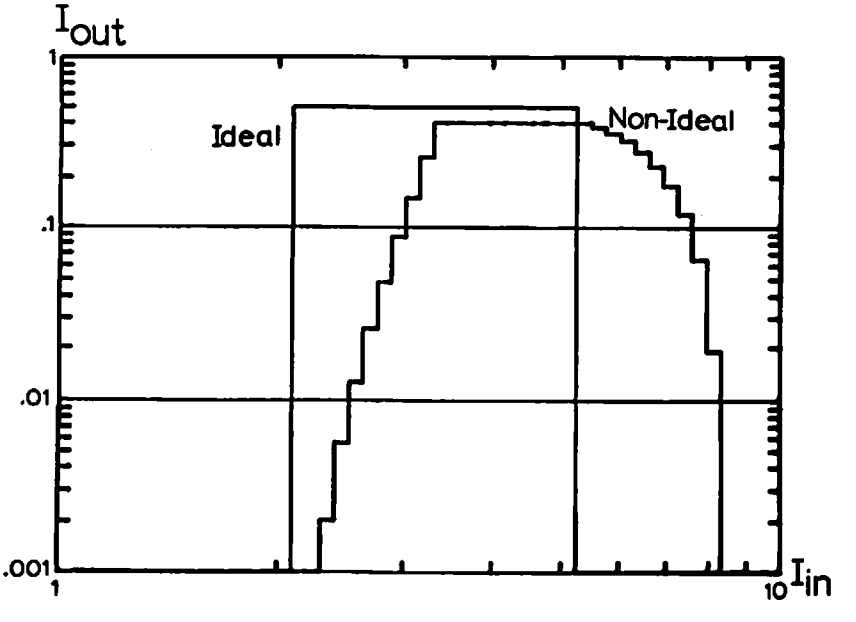

(b)

Figure 4-21. Two-film level slice. $\gamma_1 = 1$, $\gamma_2 = 10$, $D_{sat2} = 10$
(a) $D_{max} = .1$
(b) $D_{max} = .2$

CHAPTER 5

NON-MONOTONIC HALFTONE CELLS

The analysis of chapters 2 and 3 concerns monotonic halftone cells. In this chapter, the monotonicity requirement is relaxed and general non-monotonic halftone cells are introduced. The primary effect of a non-monotonic cell is to change the fundamental spatial frequency of the halftoned picture, in addition to varying the bar width. An advantage of non-monotonic halftone screens is that an arbitrary number of slope changes is possible in the first diffraction order.

5.1 Analysis

Consider a single cell region on the halftoned subject and represent the structure as a sum of small shifted rect functions,

$$u(x) = \sum_{k=1}^{\ell} I(k) \cdot \mathrm{rect}((x-ka/\ell+a/2\ell)/(a/\ell)) \qquad (5.1)$$

where ℓ is arbitrarily large and $I(k)=0$ or 1 depending on

whether that specific region is black or clear. Equation (5.1) represents each period of the halftoned picture as a sum of a large number of binary-valued shifted pulses, a form convenient for later computer analysis. A linear array of bars of the form given in eq. (5.1) can be represented as

$$t(x)=u(x)*((1/a)\cdot comb(x/a))$$
$$=[\sum_{k=1}^{\ell} I(k)\cdot rect((x-ka/\ell+a/2\ell)/(a/\ell))]*((1/a)\cdot comb(x/a)) \quad . \qquad (5.2)$$

Inverting the contrast to get black bars on a clear background gives

$$t(x)=1-(1/a)\cdot([\sum_{k=1}^{\ell} I(k)\cdot rect((x-ka/\ell+a/2\ell)/(a/\ell))]*comb(x/a)) \qquad (5.3)$$

as the amplitude distribution present in the input plane. Fourier transforming eq. (5.3) yields

$$\mathcal{F}\{t(x)\} = \delta(f_x) - [(1/\ell) \cdot (\sum_{k=1}^{\ell} I(k) \cdot \mathrm{sinc}(af_x/\ell) \cdot \exp(-j2\pi f_x(ka/\ell)) \cdot a \cdot \mathrm{comb}(af_x))] \cdot \exp(+j\pi f_x(a/\ell)) \quad (5.4)$$

as the transform plane amplitude distribution. Equation (5.4) is equivalent to

$$\mathcal{F}\{t(x)\} = \delta(f_x) - \sum_{n=-\infty}^{\infty} \delta(f_x - n/a) \cdot [(1/\ell) \cdot \sum_{k=1}^{\ell} I(k) \cdot \mathrm{sinc}(af_x/\ell) \cdot \exp(-j2\pi f_x(ka/\ell))] \cdot \exp(+j\pi f_x a/\ell) \quad (5.5)$$

where the comb function is relaced with a sum of delta functions as indicated in eq. (2.3). Substituting actual values of f_x into eq. (5.5) yields

$$\mathcal{F}\{t(x)\} = \delta(f_x) - \sum_{n=-\infty}^{\infty} \delta(f_x - n/a) \cdot [(1/\ell) \cdot \sum_{k=1}^{\ell} I(k) \cdot \mathrm{sinc}(n/\ell) \cdot \exp(-j2\pi nk/\ell)] \cdot \exp(+j\pi n/\ell) \quad (5.6)$$

as the final expression for the amplitude distribution in the transform plane. If ℓ is allowed to become very large with respect to n, the sinc term and the $\exp(+j\pi n/\ell)$ factor are approximately 1, and eq. (5.6) becomes

$$\mathcal{F}\{t(x)\} = \delta(f_x) - \sum_{n=-\infty}^{\infty} \delta(f_x - n/a) \cdot (1/\ell) \cdot \sum_{k=1}^{\ell} I(k) \cdot \exp(-j2\pi mk/\ell) \quad . \tag{5.7}$$

Equation (5.7) is the approximate expression which will be considered further. The cases of interest are $n=0$ and $n\neq 0$. Substituting these values into eq. (5.7) yields

$$\mathcal{F}\{t(x)\}_{n=0} = [1-(1/\ell) \cdot \sum_{k=1}^{\ell} I(k)] \cdot \delta(f_x) \tag{5.8}$$

as the zero order amplitude distribution, and

$$\mathcal{F}\{t(x)\}_{n\neq 0} = -\delta(f_x - n/a) \cdot (1/\ell) \cdot \sum_{k=1}^{\ell} I(k) \cdot \exp(-j2\pi kn/\ell) \tag{5.9}$$

as the nth order amplitude distribution in the Fourier transform plane.

Equation (5.8) is simply a variation on eq. (2.7) and is not particularly interesting, because the same basic type of response can be obtained from a monotonic cell. Equation (5.9) is more interesting, because it is the nth spectral component of the discrete Fourier transform of $I(k)$, scaled by the $1/\ell$ factor.

Fourier transforming eq. (5.9) yields

$$\mathcal{F}\{\mathcal{F}\{t(x)\}_{n\neq 0}\} = -(1/\ell)\cdot\sum_{k=1}^{\ell} I(k)\cdot\exp(-j2\pi kn/\ell) \quad , \qquad (5.10)$$

the amplitude distribution in the output plane from a non-zero order. The output intensity from the nth order is given by the modulus squared of eq. (5.10)

$$I_{\substack{out \\ n\neq 0}} = \left|-(1/\ell)\cdot\sum_{k=1}^{\ell} I(k)\cdot\exp(-j2\pi kn/\ell)\right|^2 \quad . \qquad (5.11)$$

A geometrical way of looking at eq. (5.11) is to consider it as a vector sum in the complex plane of ℓ vectors, some of which may have zero length. The angle of each vector is given by the exponential, and the length is 0 or $1/\ell$. An experimental example of screen synthesis and output calculation using this geometrical vector sum procedure is given in section 7.4.6.

Two things to note are that the monotonic cells are a subset of the non-monotonic cells, that is, the bar resulting from a monotonic cell can also be represented by eq. (5.1), and that if ℓ is sufficiently large, an arbitrary number of slope changes are possible in the transfer function by using only the first diffraction order.

5.2 Synthesis Algorithm

Designing a non-monotonic cell to perform a specific transfer function involves determining the relationship between I_{in} and I(k) which will yield the desired function. Equation (5.11) can be rewritten as

$$I_{\substack{out \\ n\neq 0}} = h(I_{in}) = \left| -(1/\ell) \cdot \sum_{k=1}^{\ell} I(k, I_{in}) \cdot \exp(-j2\pi kn/\ell) \right|^2 \qquad (5.12)$$

taking into account the implicit dependence of I(k) on the input intensity.

The cell design problem is one of deciding what function $I(k, I_{in})$ should be used such that the nth spectral component of its discrete Fourier transform will be the desired transfer function. This problem does not, in general, have a unique solution.

As a possible solution to this problem an algorithm has been developed which does not explicitly calculate any Fourier transforms. This algorithm is an approximation which becomes arbitrarily close to the exact solution as the number of vectors is increased. The algorithm iteratively performs the vector additions as suggested by the formulation. Only the first diffraction order is

used. A block diagram of the algorithm is shown in Fig. 5-1. Synthesis begins by dividing the available vectors into two groups: those whose angle given by the exponential falls between 0 and π, and those whose angle falls between π and 2π. On the halftoned picture, these two groups physically correspond to bar structures with widths in the ranges 0 to a/2 and a/2 to a respectively. The vectors are all the same length, which is chosen arbitrarily at the beginning. The desired transfer function is represented by an array of numbers. In the figures which follow, it is specified by 50 values over a one decade range. The number of values and the range can be changed as desired.

The algorithm begins by examining the first transfer function value, and adds vectors from the first group starting at 0 using adjacent vectors one at a time until the square of the length of the sum vector exceeds the desired value. The algorithm then examines the next transfer function value. If it is larger than the previous value, more vectors are added from the first group until the square of the length of the sum vector is again large enough. If the next value is smaller than the previous value, vectors from the second group, starting at π are added to the existing collection. The vectors from the second group cancel vectors from the first group and

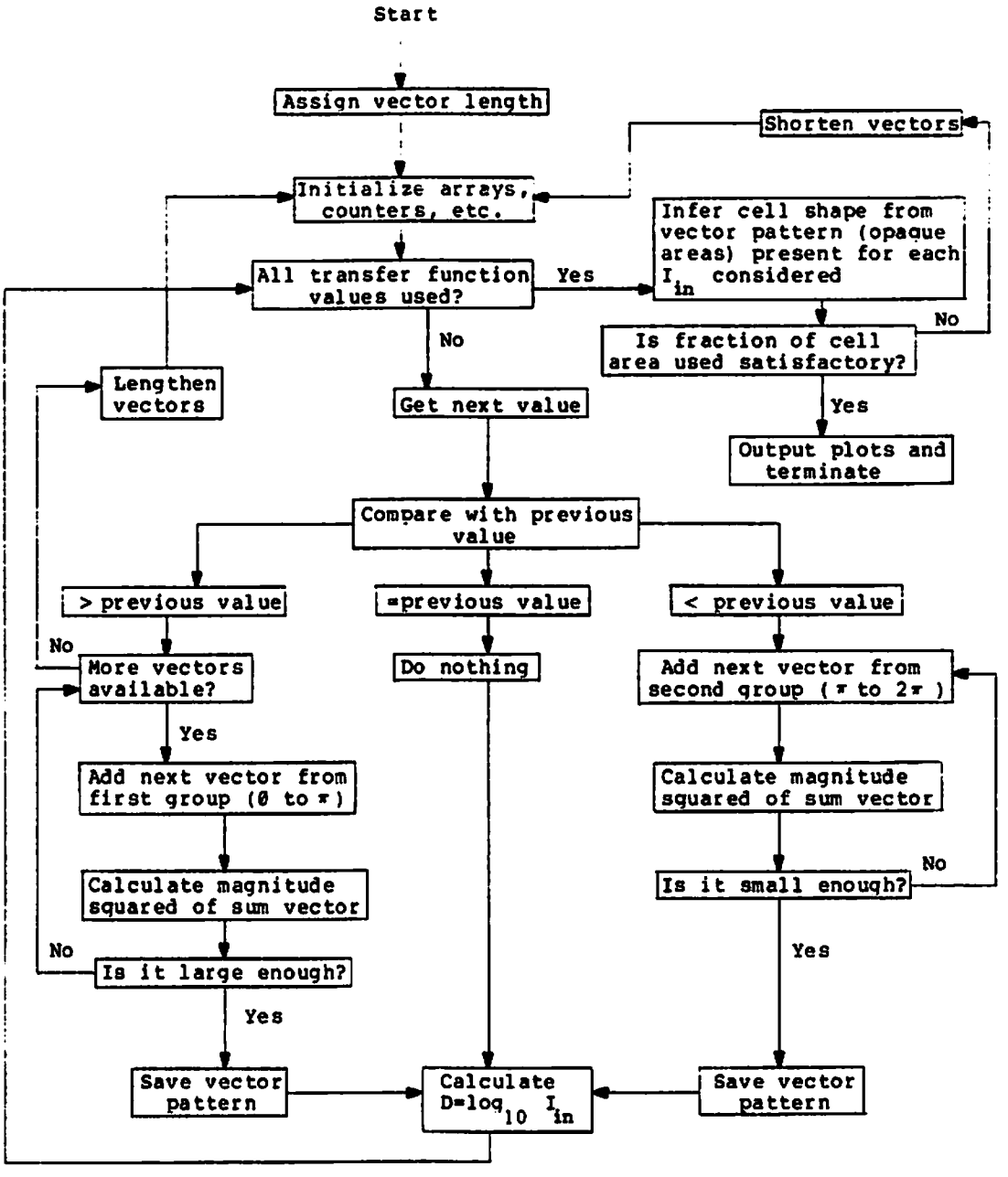

Figure 5-1. Non-monotonic halftone cell design algorithm.

thereby reduce the length of the sum vector. More vectors are added until the square of the length of the sum vector is decreased to a value less than the desired one. The next transfer function is then examined. This process is repeated for all remaining transfer function values.

The algorithm terminates in one of two ways. Either all the available vectors in the range from $\emptyset$ to π are used before all of the transfer function values are used, or all transfer function values are used and there are unused vectors remaining. The second situation implies that a portion of the halftone cell area is not being used. If this is the case, it must be decided if a sufficient fraction of the cell is being used, or if a better design is necessary. If it is necessary to try the design again due to either possibility, the vector lengths are all changed to a different value and the previously described procedure is repeated. If the algorithm terminates before using all of the transfer function, the vector lengths must be increased. Insufficient cell area utilization requires a decrease in the vector lengths.

The time required to arrive at a satisfactory solution depends on several factors. If the initial length chosen for the vectors is close to the value actually required, fewer iterations are necessary.

Increasing the number of vectors ℓ results in greater precision, but it takes longer to compute the cell shape.

5.3 Examples

Four representative examples have been calculated using the procedure described, and are shown in Fig. 5-2 to 5-5. It should be noted that the quantizer cell shape shown in Fig. 5-3 is not a particularly good choice. It is monotonic, and a more efficient monotonic cell using the zero order can be designed. The notch filter shown in Fig. 5-4 has been experimentally tested and is discussed further in chapter 7.

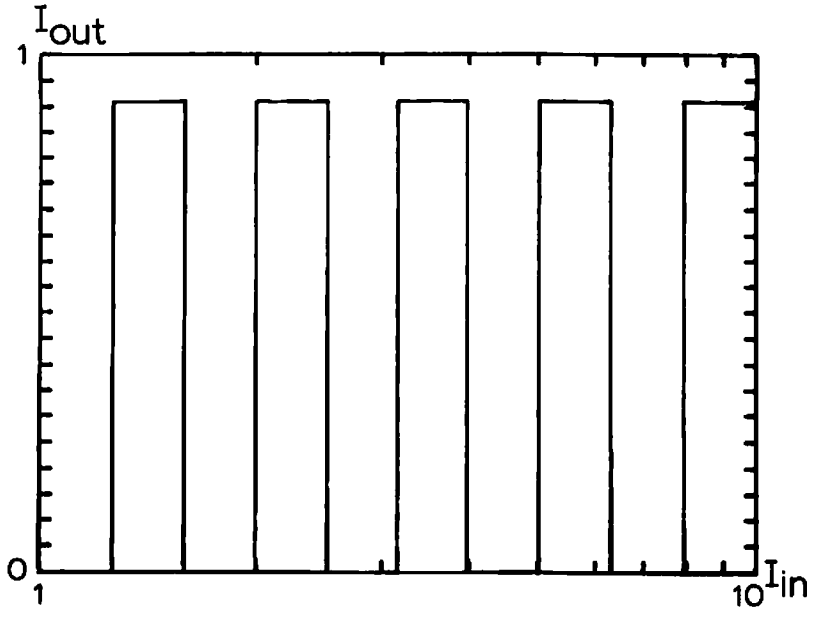

(a) Transfer function

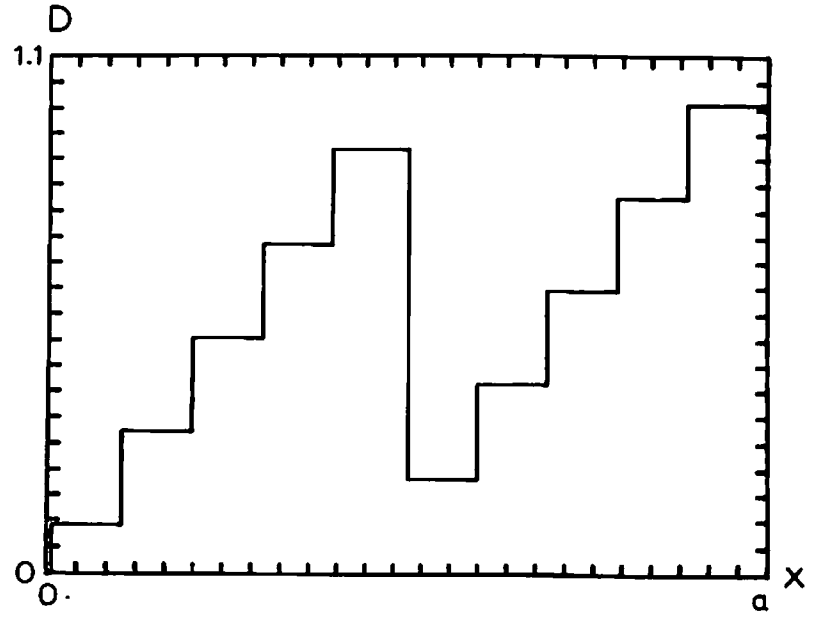

(b) Corresponding halftone cell shape

Figure 5-2. Five level slice.

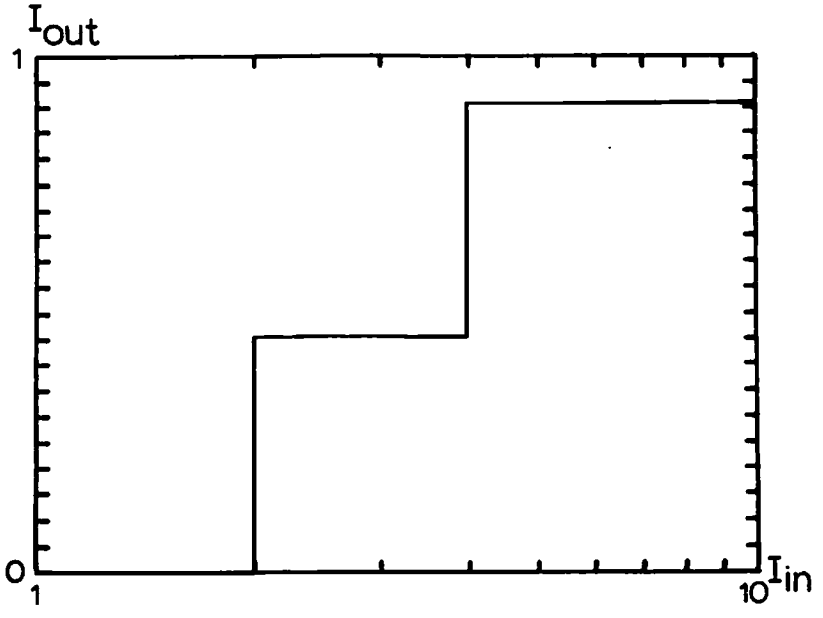

(a) Transfer function

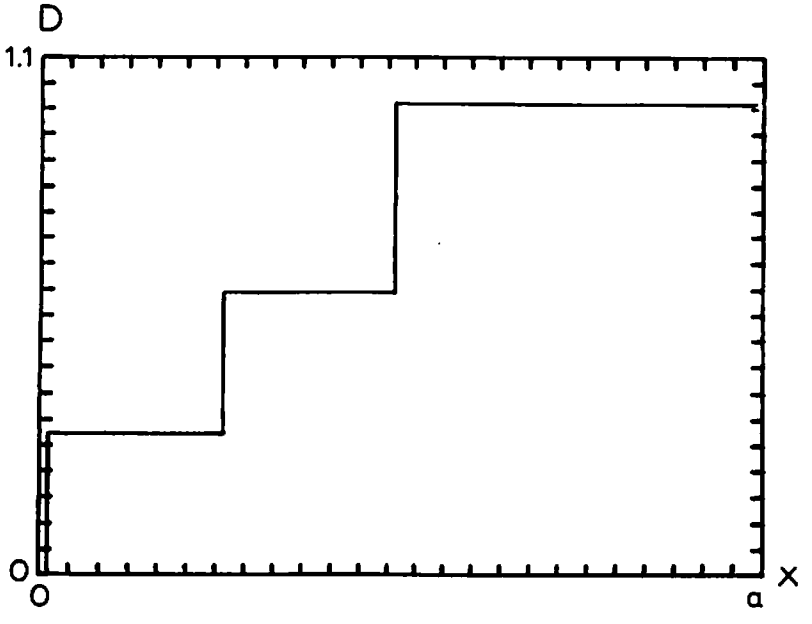

(b) Corresponding halftone cell shape

Figure 5-3. Quantizer

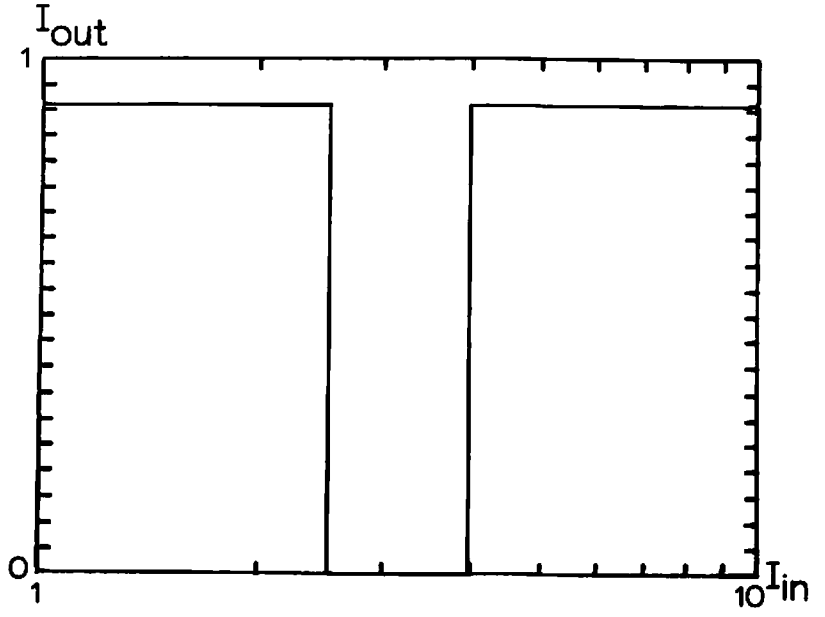

(a) Transfer function

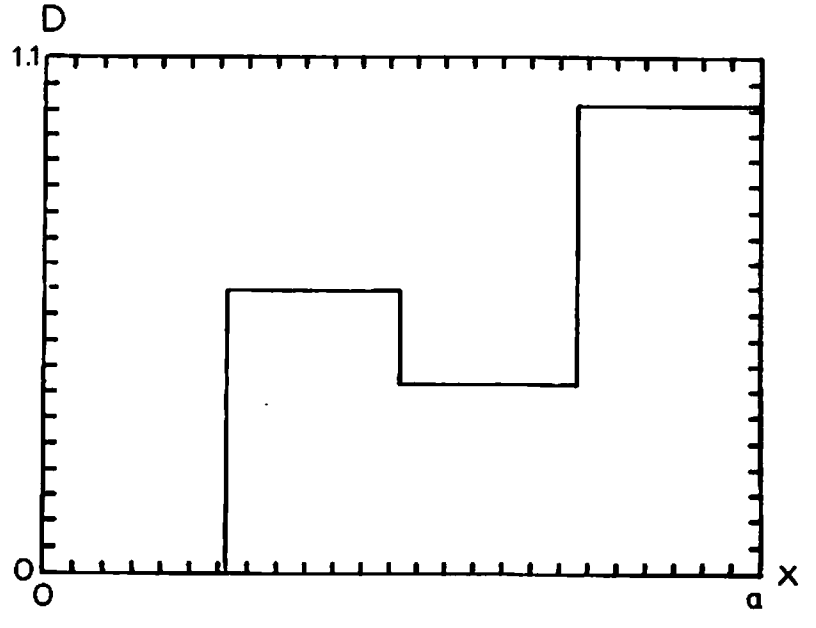

(b) Corresponding halftone cell shape

Figure 5-4. Notch filter

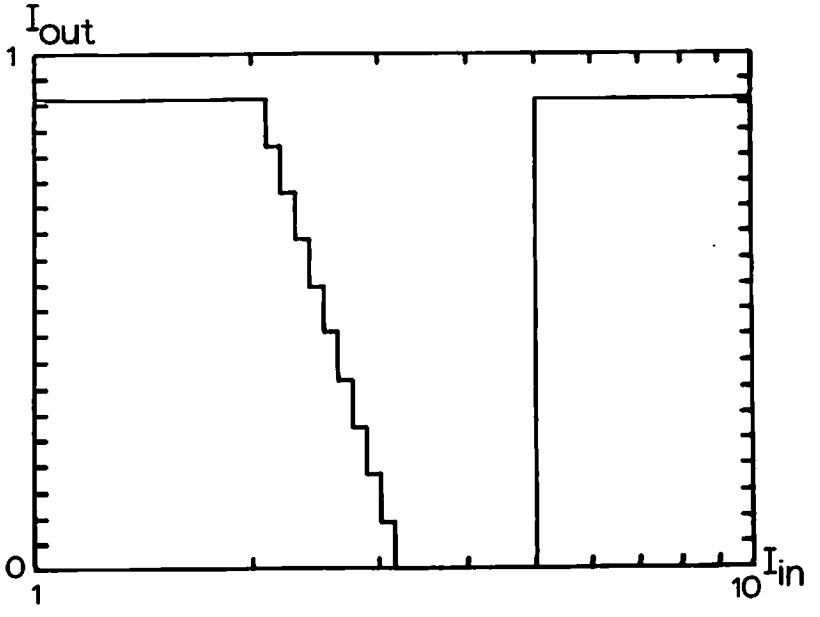

(a) Transfer function

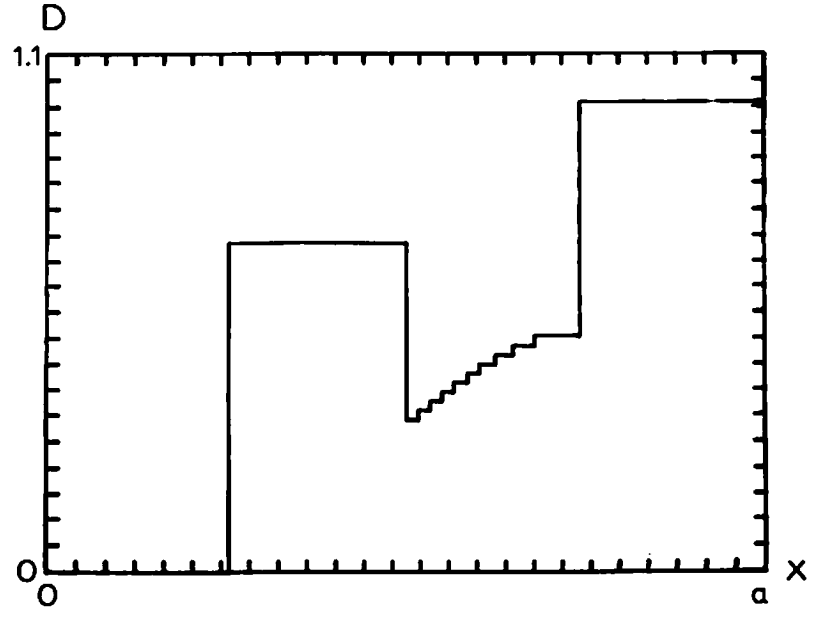

(b) Corresponding halftone cell shape

Figure 5-5. Edge tailored notch

CHAPTER 6

PRECOMPENSATION AND OTHER TOPICS

In some situations it is possible to modify the density profile of the halftone screen in advance so that some of the degradations due to non-ideal film are compensated. A technique for accomplishing this is described. As a separate topic, the possibility of bleaching the halftoned picture to arrive at a phase structure to be placed in the optical system is examined.

6.1 Precompensaton for Non-Ideal Film

If the qamma and saturation density of the copy film are non-ideal but known, it is possible in some situations to calculate a modified cell shape to accurately correct for these problems. An algorithm to perform these calculations has been developed. A block diagram is shown in Fig. 6-1. The first step is to calculate the ideal cell shape for the specified transfer function. The actual response degraded by the film characteristics is then calculated as discussed in chapter 4. Starting with

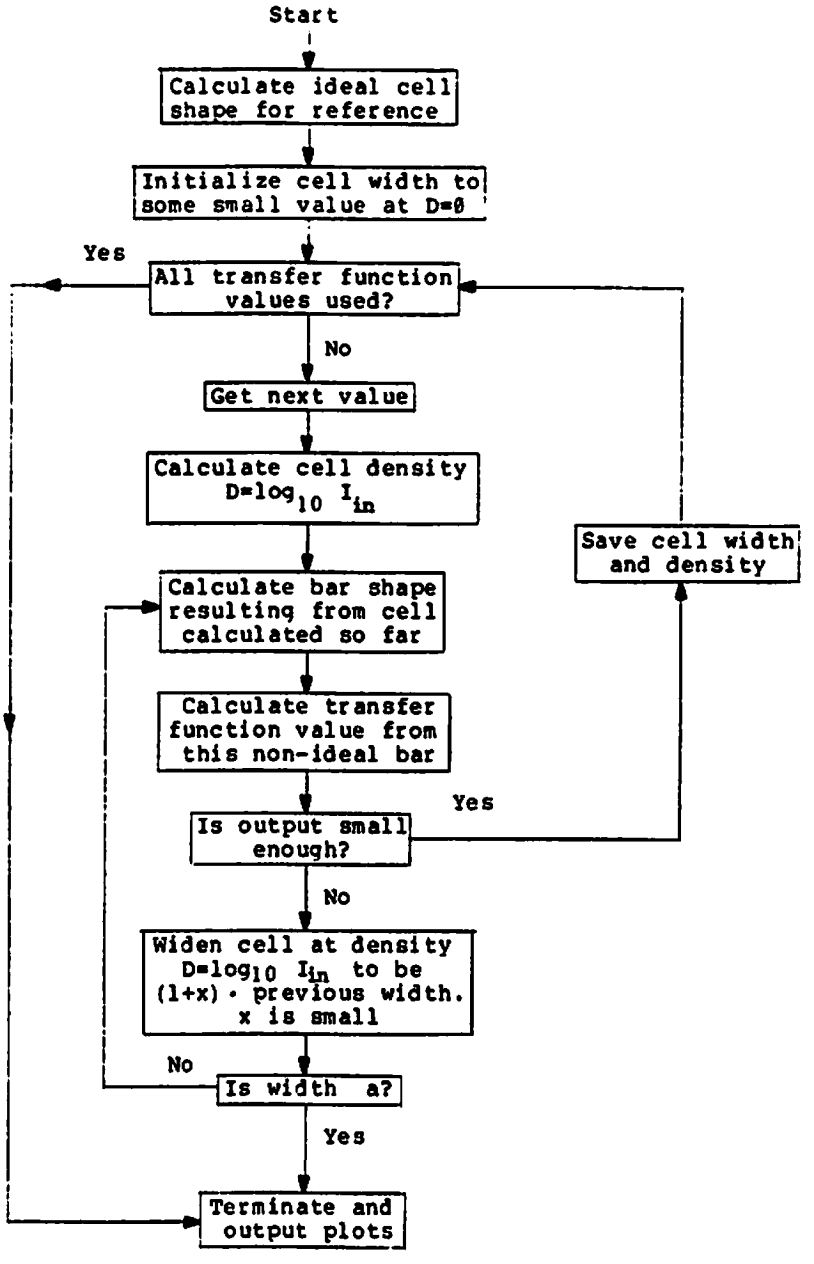

Figure 6-1. Zero order compensated cell algorithm for the one-film process.

the minimum input intensity the required change in bar width on the halftoned picture is calculated, taking into account the non-ideal film characteristics. The required cell width at the density corresponding to this input intensity can be determined from this calculated bar width. The process is repeated for larger values of I_{in} and the calculated width corresponds to the cell width at a density of $\log_{10} I_{in}$. The process terminates when the calculated bar width required exceeds the halftone cell size. This value of I_{in} determines the maximum cell density, which is given by $\log_{10} I_{in}$. A density vs. position plot of these calculated cell widths gives the cell shape required.

Precompensation does not work for flat portions or abrupt jump portions of the transfer function. Achieving a flat section requires the bar width and density on the halftoned picture to remain constant over a range of input intensities. An abrupt jump requires a rapid change in density over some portion of the copy film in response to a small change in input intensity. Neither of these is possible for a film with low gamma and saturation density.

Figures 6-2 to 6-5 show some transfer function and halftone cell shapes for a two decade one-film logarithmic response. A two-film situation could be handled in a

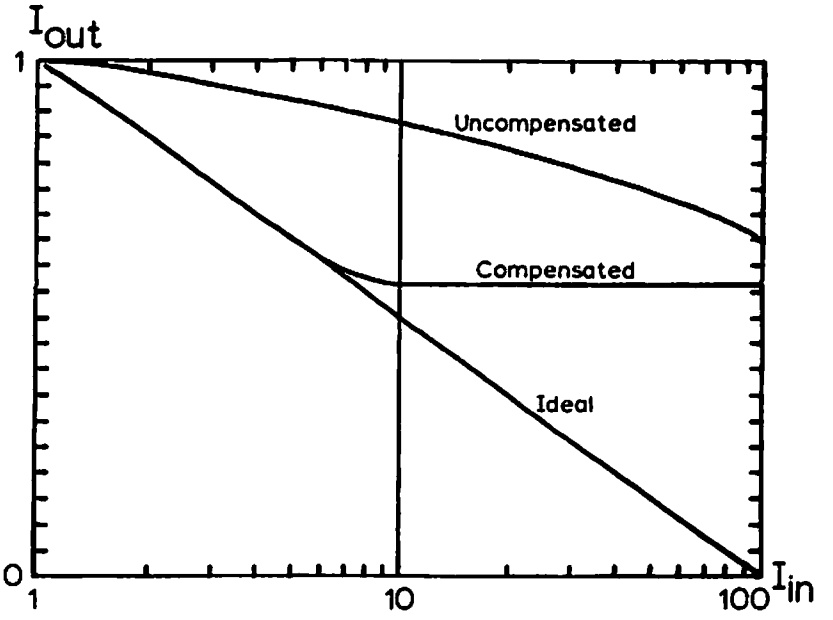

(a)

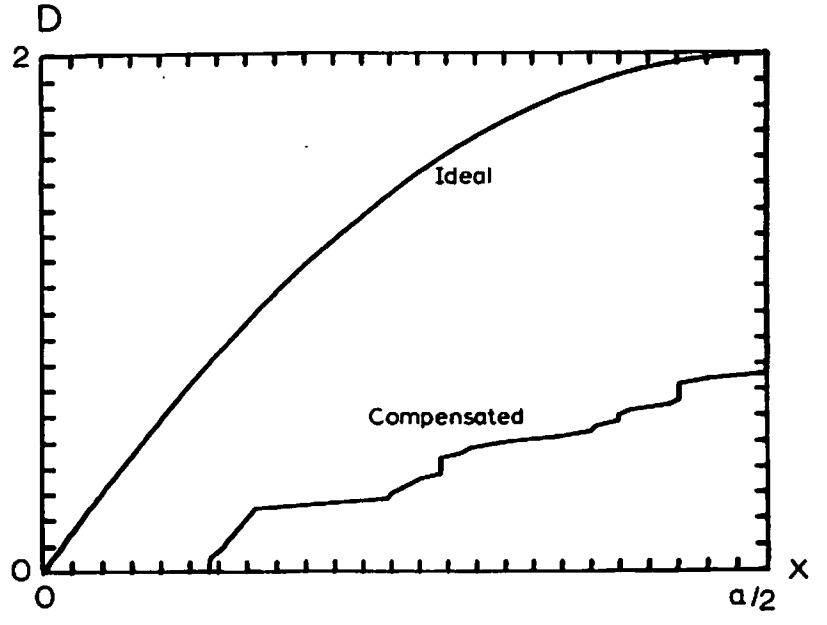

(b)

Figure 6-2. Two decade logarithm. $\gamma = 1$, $D_{sat} = .25$

(a) Ideal, uncompensated, and compensated transfer functions.

(b) Ideal and compensated halftone cell shapes.

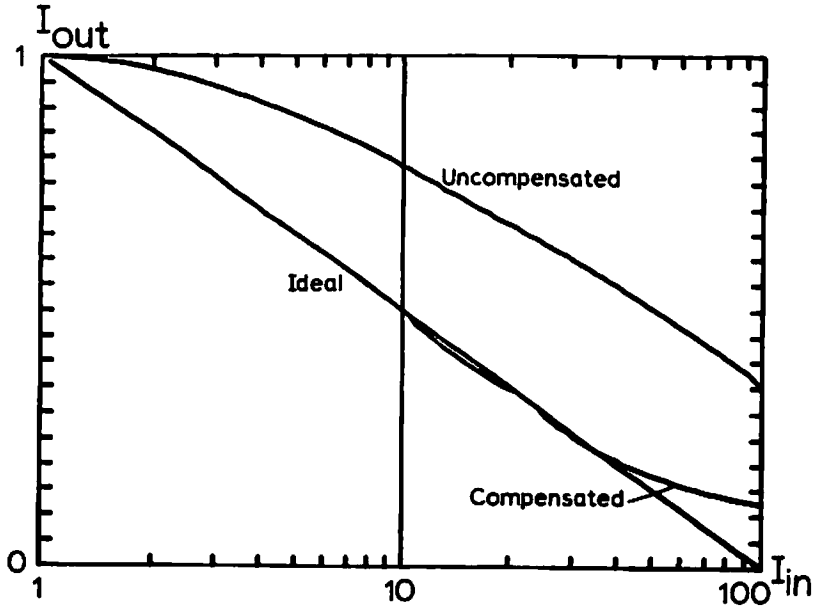

(a)

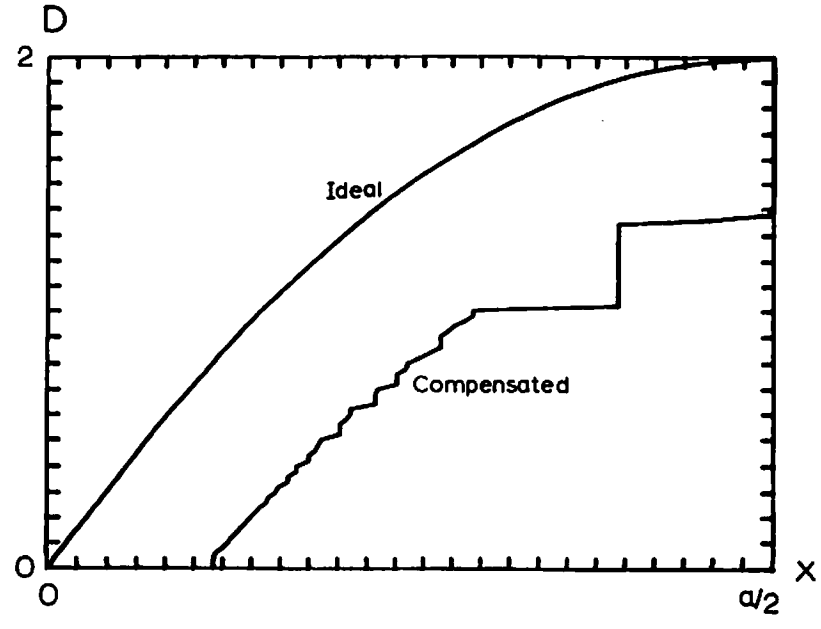

(b)

Figure 6-3. Two decade logarithm. $\gamma = 1$, $D_{sat} = 1$

(a) Ideal, uncompensated and compensated transfer functions.

(b) Ideal and compensated halftone cell shapes.

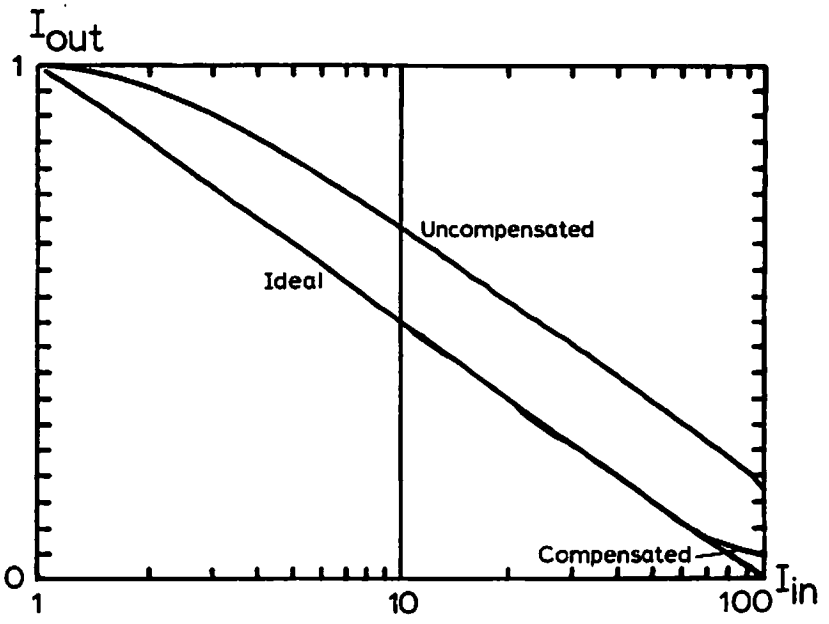

(a)

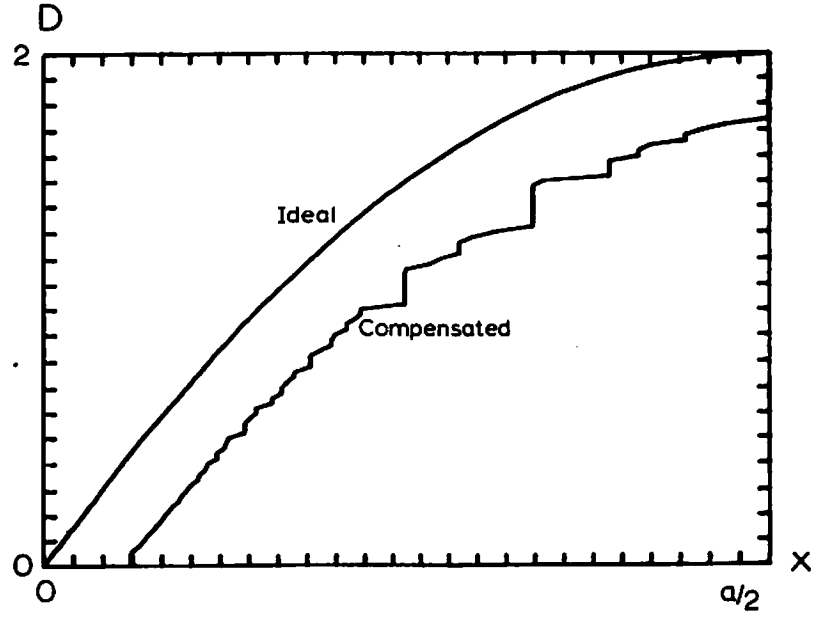

(b)

Figure 6-4. Two decade logarithm. $\gamma = 2$, $D_{sat} = 2$

(a) Ideal, uncompensated, and compensated transfer functions.

(b) Ideal and compensated halftone cell shapes.

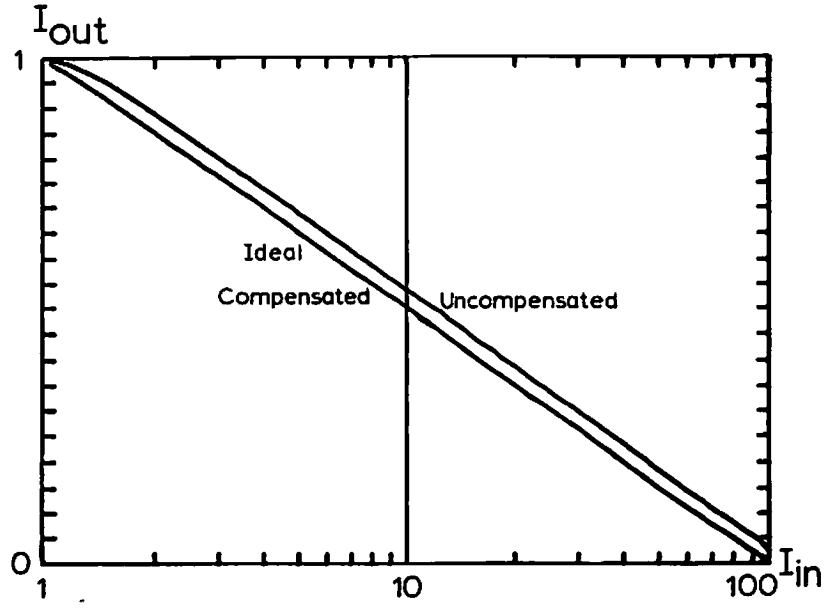

(a)

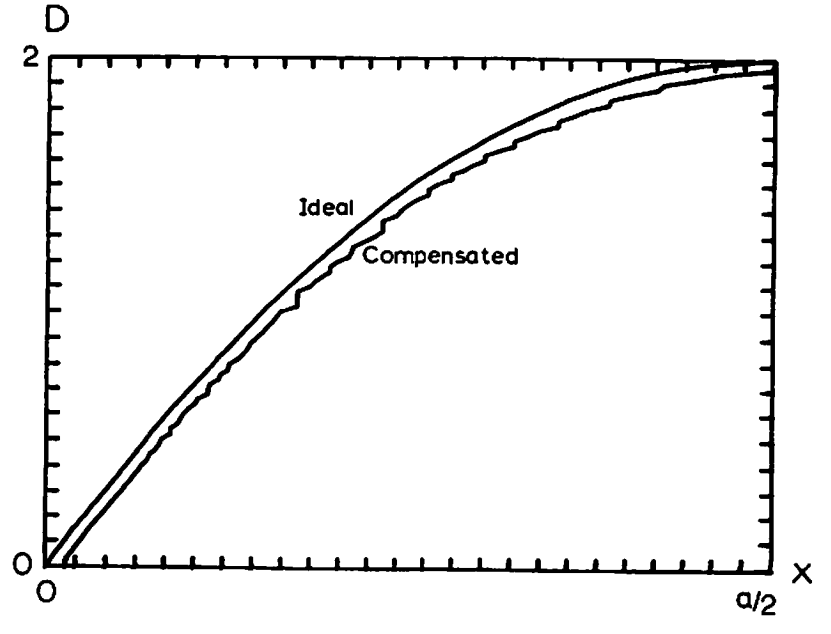

(b)

Figure 6-5. Two decade logarithm. $\gamma = 10$, $D_{sat} = 10$

(a) Ideal, uncompensated and compensated transfer functions.

(b) Ideal and compensated halftone cell shapes.

similar manner. Note that increasing gamma and D_{sat} results in a cell shape nearer to the ideal shape. Examining Fig. 6-4 shows that even for relatively low values of D_{sat} and gamma, a good approximation to the desired transfer function is possible, although the effective dynamic range is reduced.

6.2 Phase Halftoned Pictures

A possible variation on the procedure discussed in chapter 2 is to bleach the halftoned picture and use the resulting phase object as the input to the coherent optical system. The following analysis considers this situation. It is a somewhat modified version of that found at eq. (2.1) and following.

A single transparent phase shifting bar of width b in an opaque background can be represented as

$$v(x)=\exp(j\varphi)\cdot \mathrm{rect}(x/b) \quad . \tag{6.1}$$

An infinite one-dimensional array of such bars spaced a distance a apart on an opaque background can be represented as

$$u(x)=v(x)*((1/a)\cdot comb(x/a))$$
$$=exp(j\varphi)\cdot rect(x/b)*((1/a)\cdot comb(x/a)) \quad , \qquad (6.2)$$

and making the background unity transmission yields

$$t(x)=1-rect(x/b)*((1/a)\cdot comb(x/a))+u(x)$$
$$=1-(1-exp(j\varphi))\cdot rect(x/b)*((1/a)\cdot comb(x/a)) \qquad (6.3)$$

as the amplitude distribution in the input plane. Fourier transforming eq. (6.3) yields

$$\mathcal{F}\{t(x)\}=\delta(f_x)-(1-exp(j\varphi))\cdot (b\cdot sinc(bf_x)\cdot comb(af_x)) \quad . \qquad (6.4)$$

By replacing the comb function with a summation, eq. (6.4) becomes

$$\mathcal{F}\{t(x)\}=\delta(f_x)-(1-exp(j\varphi))\cdot(b/a)\cdot\sum_{n=-\infty}^{\infty}\delta(f_x-n/a)\cdot sinc(bf_x) \quad , \qquad (6.5)$$

the amplitude distribution in the Fourier transform plane.

Equation (6.5) is the general expression. The special cases of interest are $n=0$ and $n\neq 0$. Making these substitutions into eq. (6.5) gives

$$\mathcal{F}\{t(x)\}_{n=0} = \delta(f_x) \cdot (1-(b/a) \cdot (1-\exp(j\varphi))) \tag{6.6}$$

as the zero order component, and

$$\mathcal{F}\{t(x)\}_{n\neq 0} = (1-\exp(j\varphi)) \cdot (1/n\pi) \cdot \sin(\pi bn/a) \cdot \delta(f_x - n/a) \tag{6.7}$$

as the nth order component in the Fourier transform plane. The Fourier transforms of eq. (6.6) and (6.7) yield

$$\mathcal{F}\{\mathcal{F}\{t(x)\}_{n=0}\} = 1-(b/a) \cdot (1-\exp(j\varphi)) \tag{6.8}$$

as the amplitude in the output plane from the zero order component, and

$$\mathcal{F}\{\mathcal{F}\{t(x)\}_{n\neq 0}\} = (1-\exp(j\varphi)) \cdot (1/n\pi) \cdot \sin(\pi bn/a) \tag{6.9}$$

as the amplitude from the nth order component.

Examination of eq. (6.8) and (6.9) indicates that using phase allows non-monotonic response in the zero diffraction order and provides the potential for higher diffraction efficiency in non-zero diffraction orders, if the phase shift is chosen appropriately. However, the same transfer functions can be achieved by using an unbleached input halftoned picture made with a screen with

an appropriately chosen cell shape. There appears to be no reason to introduce the additional processing complexity. Also, slight errors in phase shift will cause the zero order transfer function to be different than expected, because the zero location will shift. In non-zero diffraction orders, phase errors can actually decrease the output as compared with an unbleached halftoned picture, if the phase shift is such that $|1-\exp(j\varphi)| < 1$.

CHAPTER 7

EXPERIMENTAL PROCEDURES AND RESULTS

7.1 Halftone Screen Production

Commercially available halftone screens can be used to achieve certain nonlinear transfer functions, such as the logarithm performed by Kato and Goodman [7-1,2]. There are various ways a screen can be made, such as by using a step and repeat camera, by making a defocused photographic copy of a ruled grating, by use of a plotting microdensitometer, or by optical filtering of binary gratings as used by Lohmann and Strand [7-3,4]. As demonstrated in previous chapters, achieving any control of the transfer function almost always requires halftone screens with cell shapes which are not commercially available.

Every halftone screen used in this work was custom made for the desired transfer function. For ease in fabrication, they were all one-dimensional gratings. The level slice screen was made by photographically duplicating a Ronchi ruling. A 200 line per inch Ronchi

ruling was contact printed onto Kodalith film which was then developed in diluted Dektol developer. This developing procedure yields a moderately low gamma on Kodalith and produces a screen with bars of equal width alternating between two different densities, as required. All the other screens were made on an Optronics plotting flatbed microdensitometer.

The procedure for making screens on the densitometer consists of placing the film, Kodak SO-427 sheet film in this case, emulsion side down on the glass plate in the scanning stage and having the computer write the desired pattern. The film is weighted by a dull black anodized aluminum plate to keep it flat. Line widths are selectable down to a minimum of 10 microns by appropriate choice of the substage aperture and focusing optics. The line spacing is always chosen to equal the line width, thus providing no pixel overlap. The exposed film is developed for the recommended time in D-19 developer.

Making halftone screens on a microdensitometer is quite slow, but it offers the necessary flexibility in screen parameters.

7.2 Initial Calibration

The microdensitometer requires a 10 bit input number for playback. To accurately make screens, the relationship between this input number and the final density on the SO-427 film must be known. This relationship was determined by making a 64 level grey scale with input numbers ranging from 0 to 1023 in steps of 16, thus spanning the available range. The film was then carefully processed and the densities were measured on the microdensitometer. The resulting data were plotted as density vs. input number and used as the reference thereafter. The readings taken were not very precise due to noise in the photomultiplier and/or associated circuitry. This noise also made it impossible to measure any densities greater than approximately 1.4. For this reason, no halftone screens with cells requiring densities substantially greater than 1.0 were constructed. The accuracy of those in the range from 0 to 1.0 D is also questionable, although the transfer functions obtained indicate that the errors are not too large in most cases. If more accurate readings of plotted densities could be made, overall dynamic ranges much better than 2 decades could be achieved using microdensitometer plotted halftone screens.

7.3 Making and Using the Halftoned Picture

The halftoned picture is made by contact printing the halftone screen and subject transparency on a piece of copy film and then processing the film. The copy film is placed emulsion side up on the base of an enlarger. The screen is placed emulsion side down on the copy film, and the subject transparency is placed emulsion side down on the screen. Finally, a piece of glass is placed on top of the three pieces of film to insure good contact. The enlarger provides the light for the exposure, which can be varied by changing the exposure time or lens aperture. Following exposure, the film is processed appropriately for the type being used.

After the film is dried, it is placed in a coherent optical system, in the front focal plane of a positive lens. The optical system is shown in Fig. 1-6 for an input made with a two-dimensional halftone screen. For an input made with a one-dimensional screen, the system itself is identical, but the Fourier transform plane has only a single row of spectral islands rather than a two-dimensional array of them. In the back focal plane, the diffraction order appropriate to the transfer function desired is selected by a small aperture. The diameter of the aperture is chosen to equal the spacing between

spectral islands so that the maximum amount of information contained in the diffraction order is passed, and all other diffraction orders are excluded. The order passed is retransformed by a second lens and the desampled output is available in the back focal plane of the second lens. It is this output which is photographed to give the pictures shown later in this chapter.

The transfer functions for which measured values are plotted, specifically the logarithm, exponential, and edge tailored bandpass, were measured by halftoning a step tablet, passing an unexpanded laser beam through the various steps on the halftoned picture and measuring the output intensity I_{out} in the appropriate diffraction order with an optical radiometer. I_{in} is calculated from the step density.

7.4 Specific Examples

This section discusses in some detail the transfer functions which were synthesized experimentally.

7.4.1 Level Slice

The halftone cell shape required for this function is calculated in chapter 3. The screen was made as mentioned

previously by contact printing a Ronchi ruling onto Kodalith film and developing in Dektol developer. The resulting halftone screen has approximately 8 lines per millimeter.

A one-film process using Kodalith film developed in Kodalith developer did not work well due to a tendency of the lines to bloom and merge together in the overexposed regions of the film. All the analysis made depends on the copy film holding line widths correctly, and the output in this case appears as if the trailing edge of the slice is sloped rather than abrupt. A wide slice is not possible due to the large exposure range involved.

Using 649-F film developed in D-8 or D-19 also proved unsatisfactory because the gamma was too low. The slice obtained was wider than desired, with sloping sides. The cause of this is visually apparent in a case where a step tablet was halftoned. Figure 7-1a is a photomicrograph of this halftoned step tablet. The grating structure which should be present only in one step is visible over 3 steps. The steps are .15 D apart on the step tablet. The output of the optical system for this case is a bright step with one less bright step on either side, and no output from any other step. This clearly indicates the sloping sides of the transfer function actually realized.

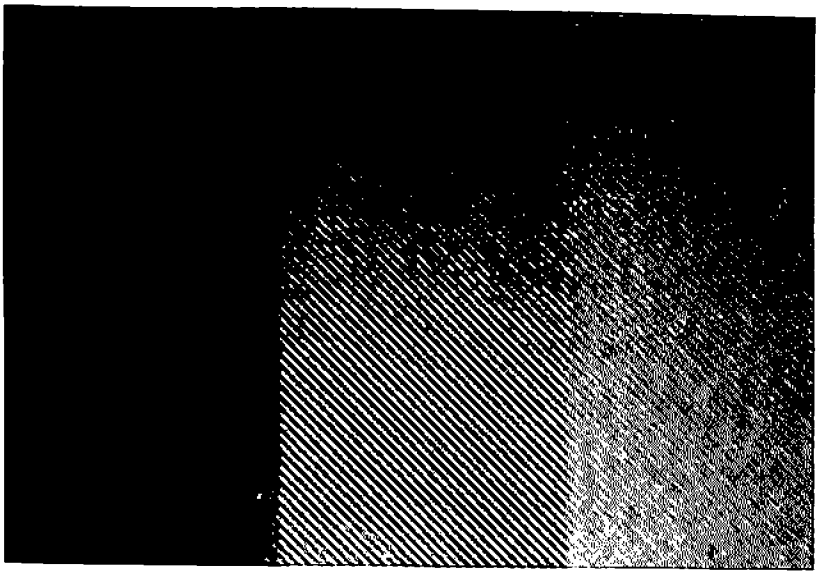

(a)

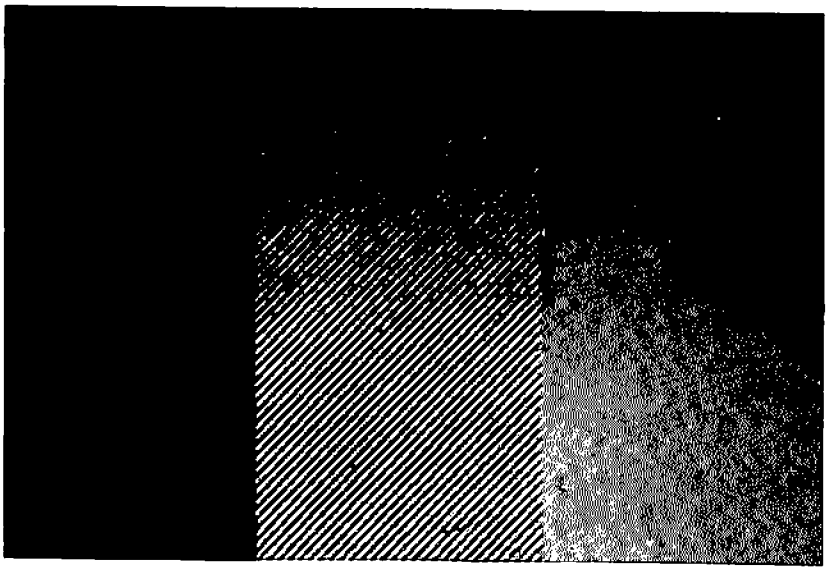

(b)

Figure 7-1. Photomicrograph of a section of a halftoned picture of a step tablet.
(a) One-film level slice.
(b) Two-film level slice.

Very little tendency for the lines to bloom was noted on the 649-F film.

A satisfactory solution is to use the two-film process with 649-F film as the first film and Kodalith film as the second. This exploits both the superior line holding characteristics of the 649-F and the high gamma of the Kodalith, by allowing only a rather narrow exposure range on the Kodalith. The exposure between the first and second film was adjusted so that only densities from Ø to approximately .2 on the 649-F passed enough light to expose the Kodalith. This small exposure range of less than two to one can be adequately handled by the Kodalith. The step tablet halftoned in this fashion yields output only in one step, clearly indicating the steepened sides on the transfer function. Figure 7-1b shows a photomicrograph of the two-film halftoned step tablet. Note that the grating structure is only visible in one step. An original input picture and level slices at two different levels are shown in Figures 7-2 and 7-3. Photomicrographs of a portion of the first and second films which produced Fig. 7-3a are shown in Fig. 7-4 and 7-5.

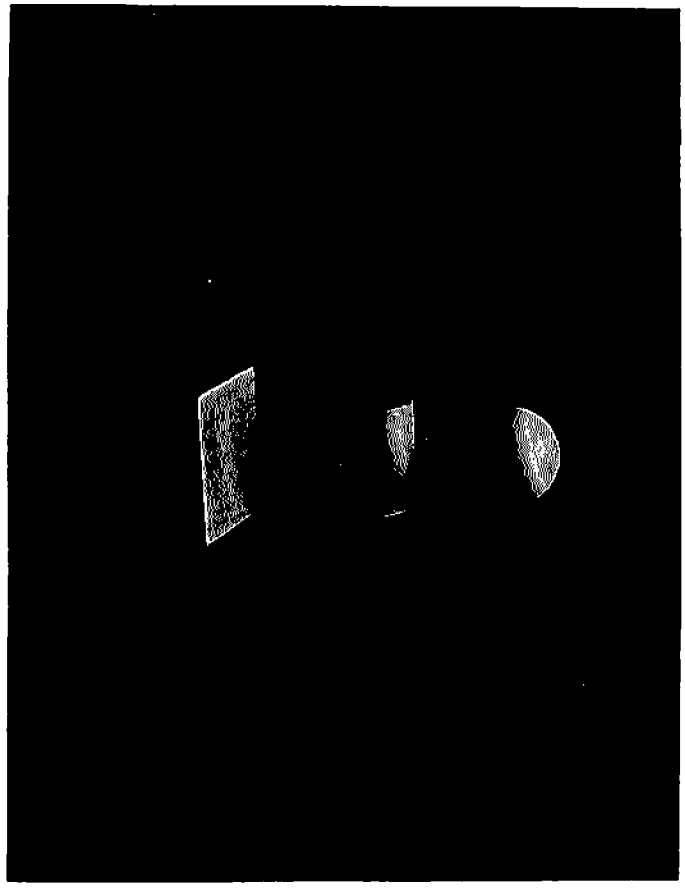

Figure 7-2. Geometrical figures used as system input.

(a)

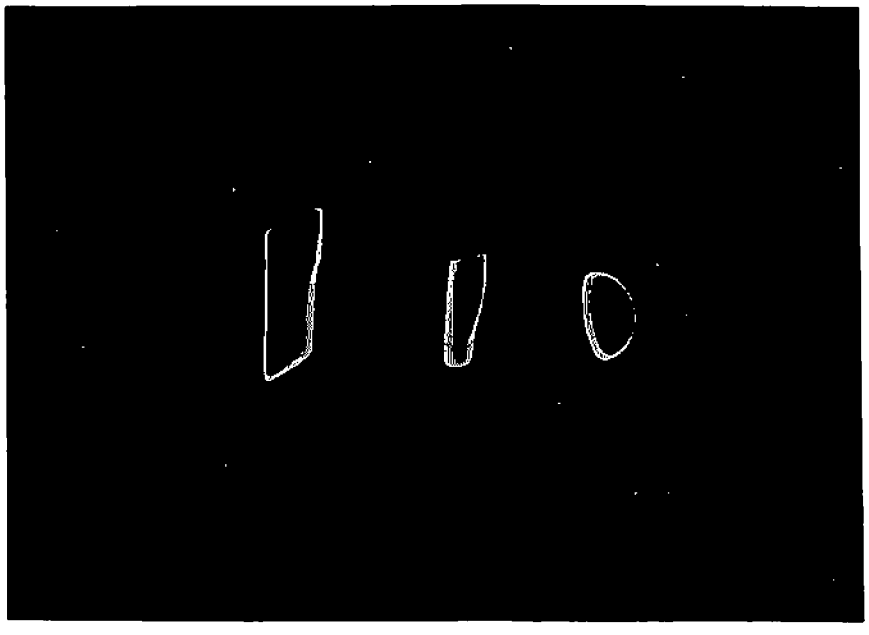

(b)

Figure 7-3. Two level slices of the geometrical figures.

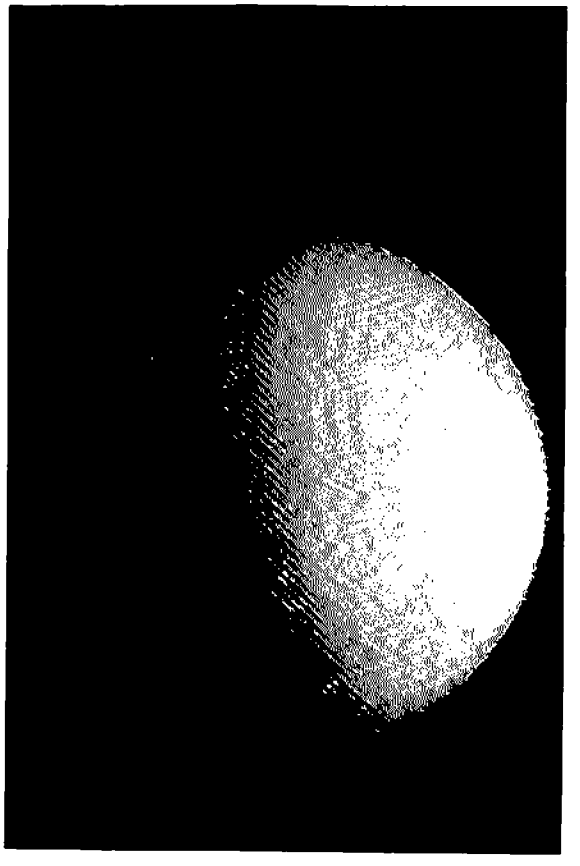

Figure 7-4. Photomicrograph of a section of the first film from a two film process.

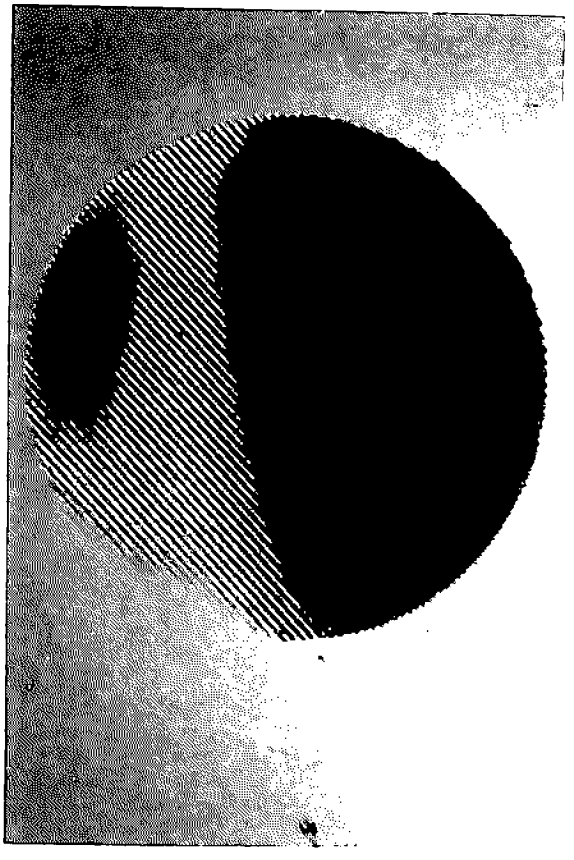

Figure 7-5. Photomicrograph of the same section as shown in Fig. 7-4, of the second film.

7.4.2 Monotonically Decreasing Logarithm

This halftone cell profile is calculated as indicated in chapter 3, except only over one decade of input range. The screen was made with the microdensitometer using a 10 micron aperture. The cells are non-symmetrical, each consisting of 25 scan lines. The resulting screen has 4 halftone cells per millimeter.

Due to the substantial time required to scan even a small area of film with a 10 micron aperture, the screen was made 1000 lines wide with 7000 pixels per line. This took approximately 2 hours. A step tablet was halftoned with this screen and the $I_{out}=h(I_{in})$ function measured. The result shown in Fig. 7-6 is quite linear over nearly the entire decade. The restriction to only one decade is due to the inability to accurately measure densities on the film greater than 1.0 with the particular microdensitometer available. This precludes using densities greater than 1.0 on the screen, and with 1.0 density as a maximum, only one decade of operation is possible.

The halftoned picture was made on Kodalith using the one-film process. Line blooming does not have much effect on the transfer function in this instance. The non-symmetrical cell causes blooming to occur

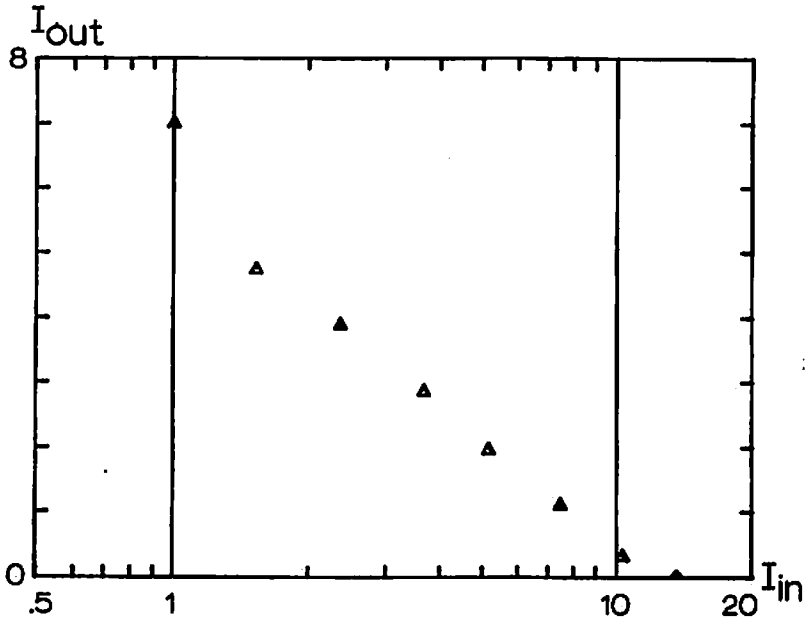

Figure 7-6. Output obtained from the logarithmic halftone screen.

preferentially on one edge of the bars on the halftoned picture. If the blooming displaces this edge by a fixed amount for all exposures above a certain level, it simply shifts the transfer function without changing its shape for all input intensities above this level; each I_{in} would have a fixed amount less I_{out} than expected. Blooming also causes I_{out} corresponding to I_{in} less than this fixed amount to be larger than expected from the rest of the measured values. As shown in Fig. 7-6, these effects occured experimentally. The point for I_{in} =1 falls above the line through the rest of the points. In addition, the base of the logarithm is not 10 as desired, probably due to errors in cell densities.

7.4.3 Monotonically Decreasing Exponential

The halftone cell is calculated as shown in chapter 3. The aperture size, resulting screen dimensions and scan time were the same as described in section 7.4.2 for the logarithm. The one-film process on Kodalith was used, and the measured transfer function is shown in Fig. 7-7. The fit to a straight line is quite good over 3 decades, and the base of the exponential is close to the desired 10.

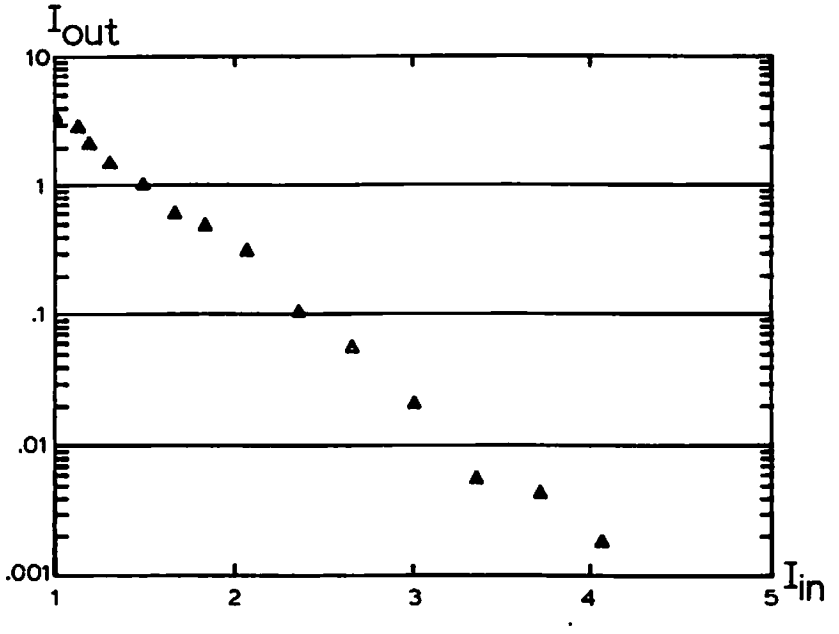

Figure 7-7. Output obtained from the exponential halftone screen.

7.4.4 Edge Tailored Bandpass

An edge tailored bandpass screen was designed using the procedure of chapter 3. Plots of the desired transfer function and calculated cell shape are shown in Fig. 7-8. The aperture size and screen dimensions are the same as for the logarithm. This screen was used on the step tablet to produce three halftoned pictures: one-film on Kodalith, one-film on 649-F, and two-film with 649-F first and Kodalith second. The measured output along the rising edge of the transfer function is shown for these three cases in Fig. 7-9, 7-10, and 7-11 respectively. None of these is precisely correct, due to line blooming on the Kodalith, finite gamma effects on the 649-F, or both. It is also possible that the cell shape is not totally correct due to calibration errors or processing variations.

This example serves to point out some of the difficulties in realizing a precise transfer function on photographic film.

7.4.5 Notch Filter

This function uses a non-monotonic halftone cell similar to that shown in Fig. 5-3. A cell made exactly as

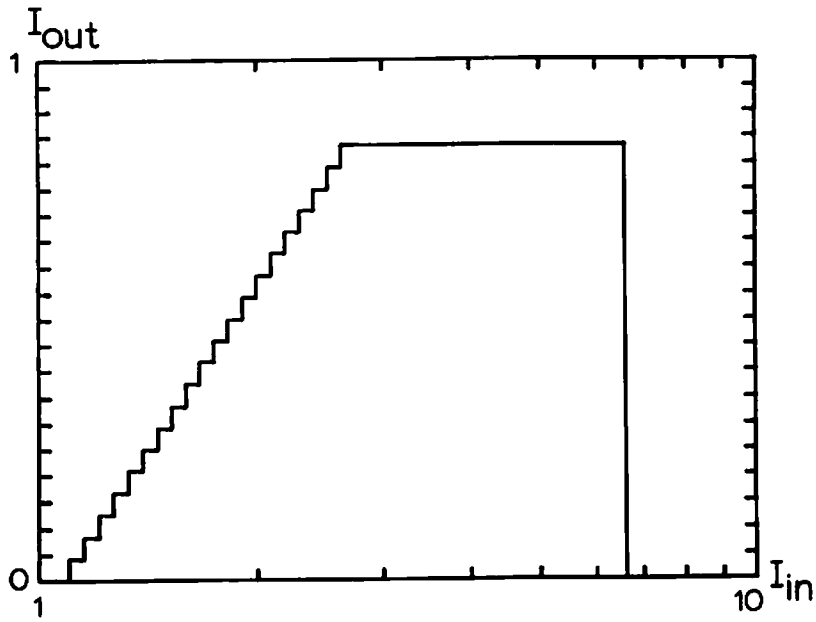

(a)

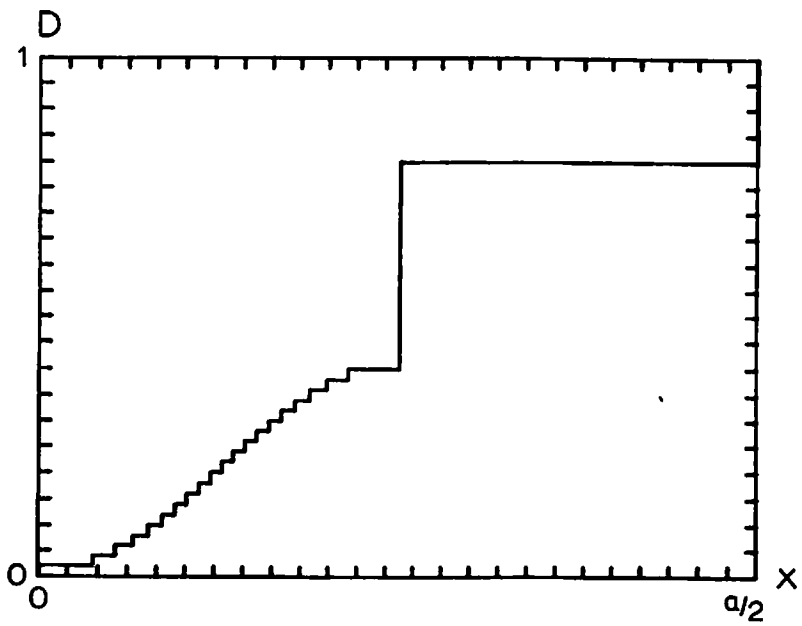

(b)

Figure 7-8. (a) Edge tailored bandpass transfer function.
(b) Corresponding halftone cell shape.

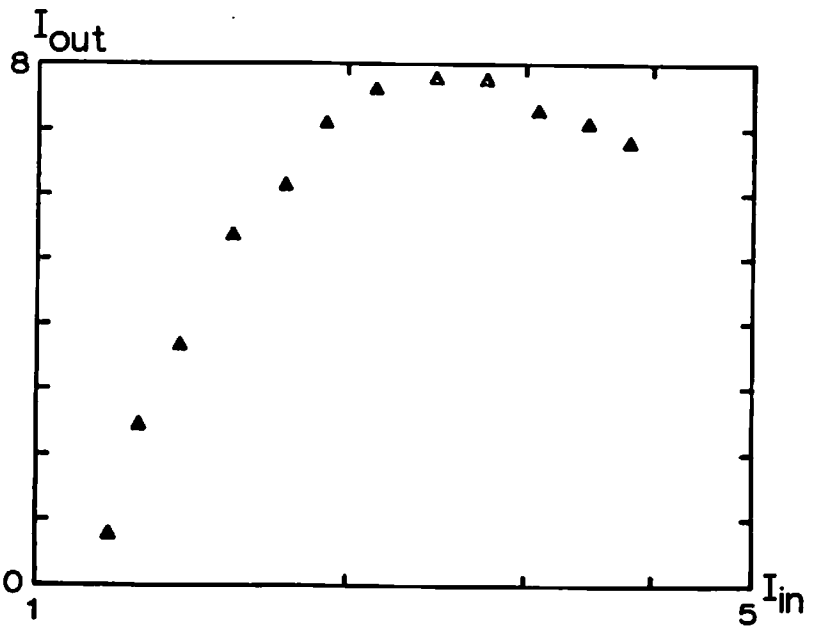

Figure 7-9. Edge tailored bandpass output using the one-film process on Kodalith film.

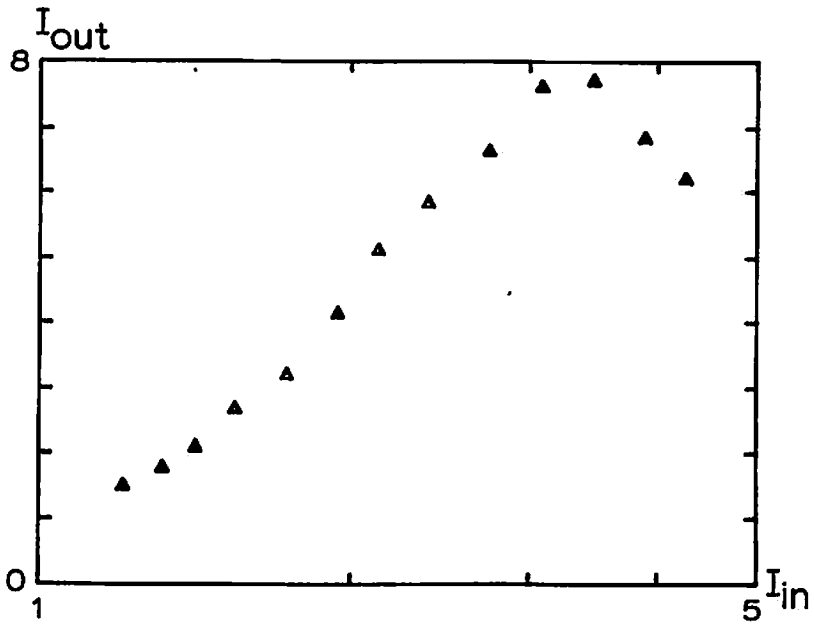

Figure 7-10. Edge tailored bandpass output using the one-film process on 649-F film.

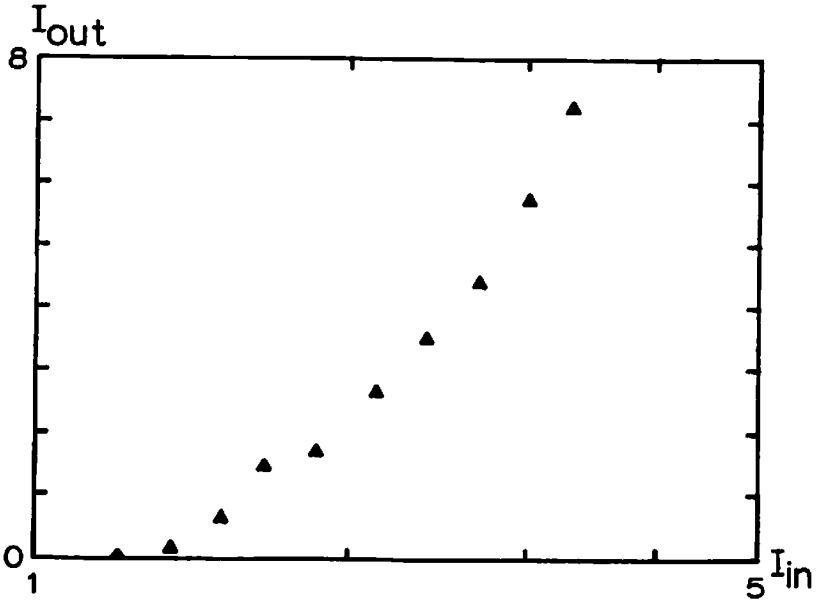

Figure 7-11. Edge tailored bandpass output using the two-film process with 649-F film first and Kodalith film second.

shown in Fig. 5-3 does not work well with the one-film process on Kodalith film. The reason for this is that the lines on the copy film tend to bloom on one edge, the edge with the least dense cell bar adjacent to it. A way of eliminating this problem is to use a halftone cell in which all the active areas are separated by opaque bars. Such a cell is shown in Fig. 7-12.

This halftone screen is used in the first diffraction order, and the halftoned picture was made using the one-film process on Kodalith. The effect of the dense bars separating the active areas is to cause any line blooming due to overexposure to occur symmetrically. The screen was made with a 28 micron aperture, and was 2000 pixels square.

Input intensities above the copy film threshold I', but less than $10^{D1} \cdot I'$ will produce bars in the 0 to a/8 range on the film, yielding some diffraction into the first order. Intensities in the range $10^{D1} \cdot I'$ to $10^{D2} \cdot I'$ will produce bars on the film in the ranges 0 to a/8 and a/2 to 5a/8. This range of inputs effectively doubles the spatial frequency and reduces the first order diffraction to zero. Input intensities between $10^{D2} \cdot I'$ and $10^{D3} \cdot I'$ will yield three bars, lying in the range 0 to a/8, a/4 to 3a/8, and a/2 to 5a/8. In this range some diffraction

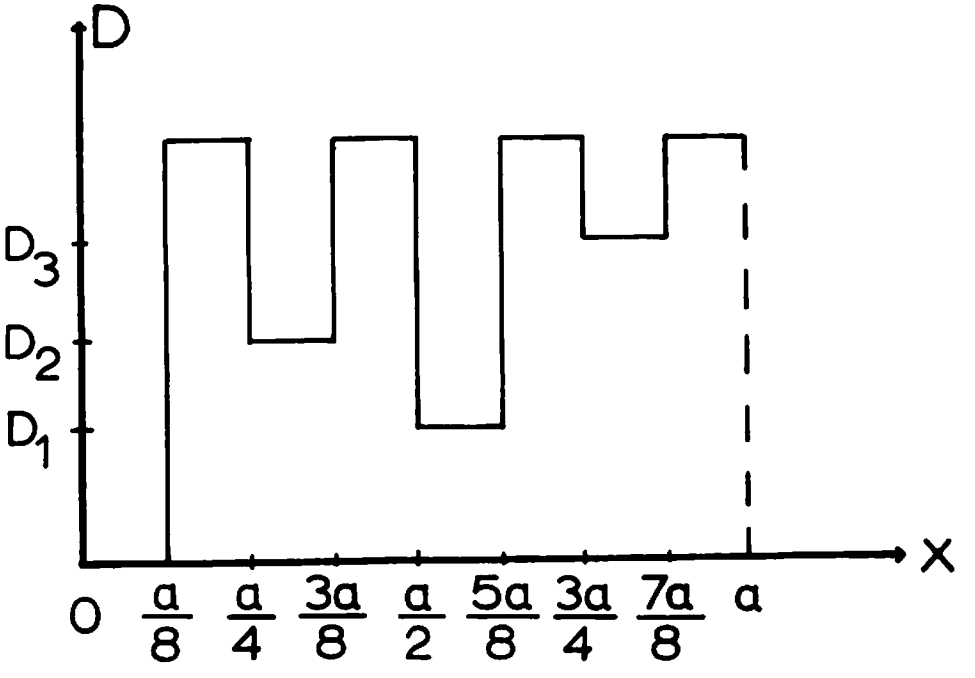

Figure 7-12. Halftone cell profile for notch filtering.

into the first order occurs. The effect of this halftone screen is to exclude all intensities between $10^{D_1} \cdot I'$ and $10^{D_2} \cdot I'$.

A photomicrograph of the halftoned picture of a corner of the rectangular solid of Fig. 7-3 is shown in Fig. 7-13. Note the different grating structure generated for the three different input intensities. Figure 7-14 shows a notch filtered version of the original picture in Fig. 7-3. A photomicrograph of a small section of the screen used for the notch filtering is shown in Fig. 7-15.

7.4.6 Quantizer

In the interest of simplicity, a quantizer screen with only 3 quantization levels was constructed. This screen represents an interesting exception to the analysis in previous chapters. The cell is non-monotonic, but it is different from the cell in Fig. 5-2 and uses the second diffraction order rather than the first. The cell profile is shown in Fig. 7-16.

Low input intensities, less than $10^{D_1} \cdot I'$ will yield no bar structure on the copy film and hence no second order diffraction. Medium input intensities, between $10^{D_1} \cdot I'$ and $10^{D_2} \cdot I'$ will yield bars of width a/8 spaced a

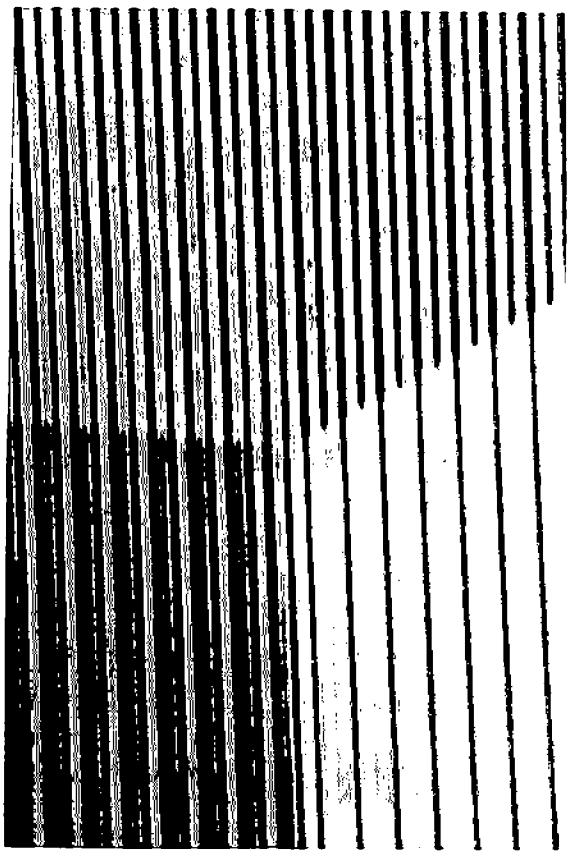

Figure 7-13. Photomicrograph of a portion of the notch filter halftoned picture of the geometrical figures.

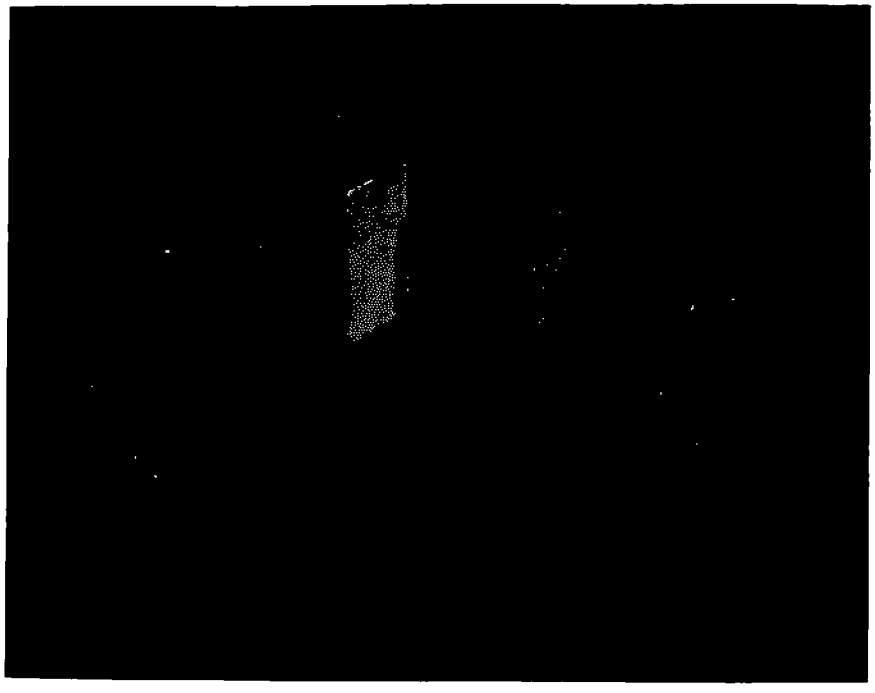

Figure 7-14. Notch filtered geometrical figures.

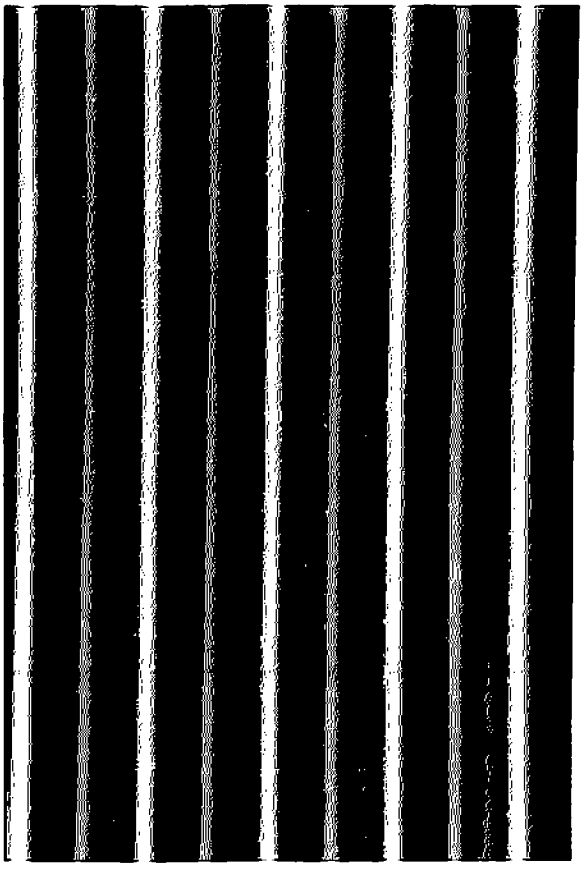

Figure 7-15. Photomicrograph of a small section of the notch filter halftone screen.

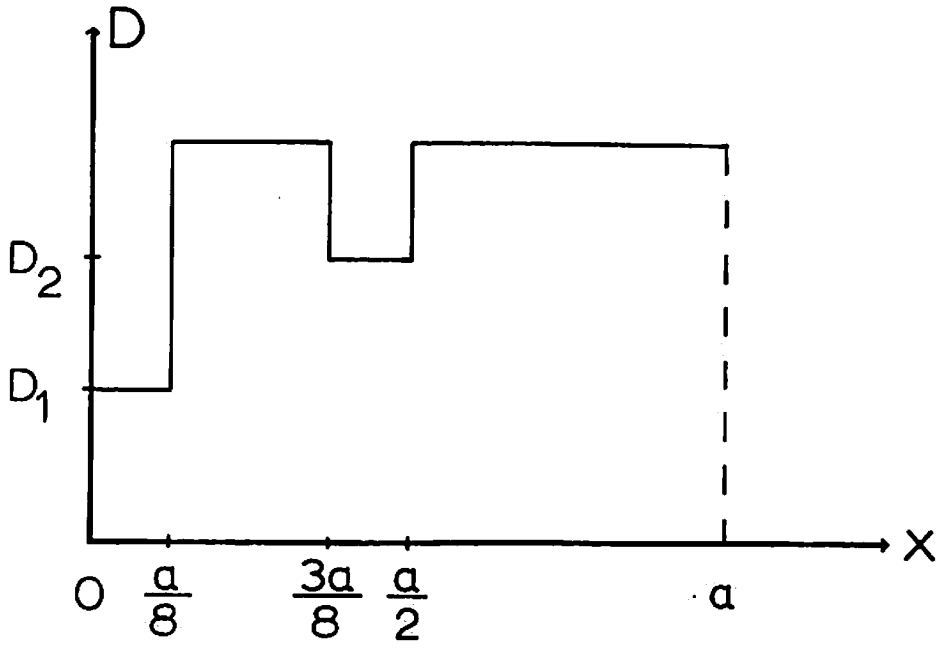

Figure 7-16. Cell profile for a three level quantizer.

distance a apart. High input intensities, larger than $10^{D_2} \cdot I'$, will yield two bars of width a/8 in each cell area separated by a/4.

Using the geometrical approach presented in chapter 5, the output can be determined as follows. Using the second order corresponds to having vectors evenly spaced in angle between 0 and 4π radians. Because the entire bar structure falls in only one half of the cell width, the range from 2π to 4π can be ignored. Intensities less than $10^{D_1} \cdot I'$ yield no bars, and consequently no second order diffraction. One bar, coming from the midrange of input intensities corresponds to vectors from 0 to $\pi/2$ summing to provide a vector length of some amount x at $\pi/4$ radians. Two bars corresponds to the previous case plus vectors from the range $3\pi/2$ to 2π. Adding these additional vectors makes a resultant vector of length $\sqrt{2}\,x$ at 0 radians. The output intensity is the square of these values, so the three intensity values are 0, x^2, and $2x^2$. This process is shown pictorally in Fig. 7-17.

A screen such as shown in Fig. 7-16 was made on the microdensitometer using a 28 micron aperture and a 2000 pixel square scan. It was used with the one-film process on Kodalith. The reason for using a screen such as this rather than a simple quantizer in the zero order, or one

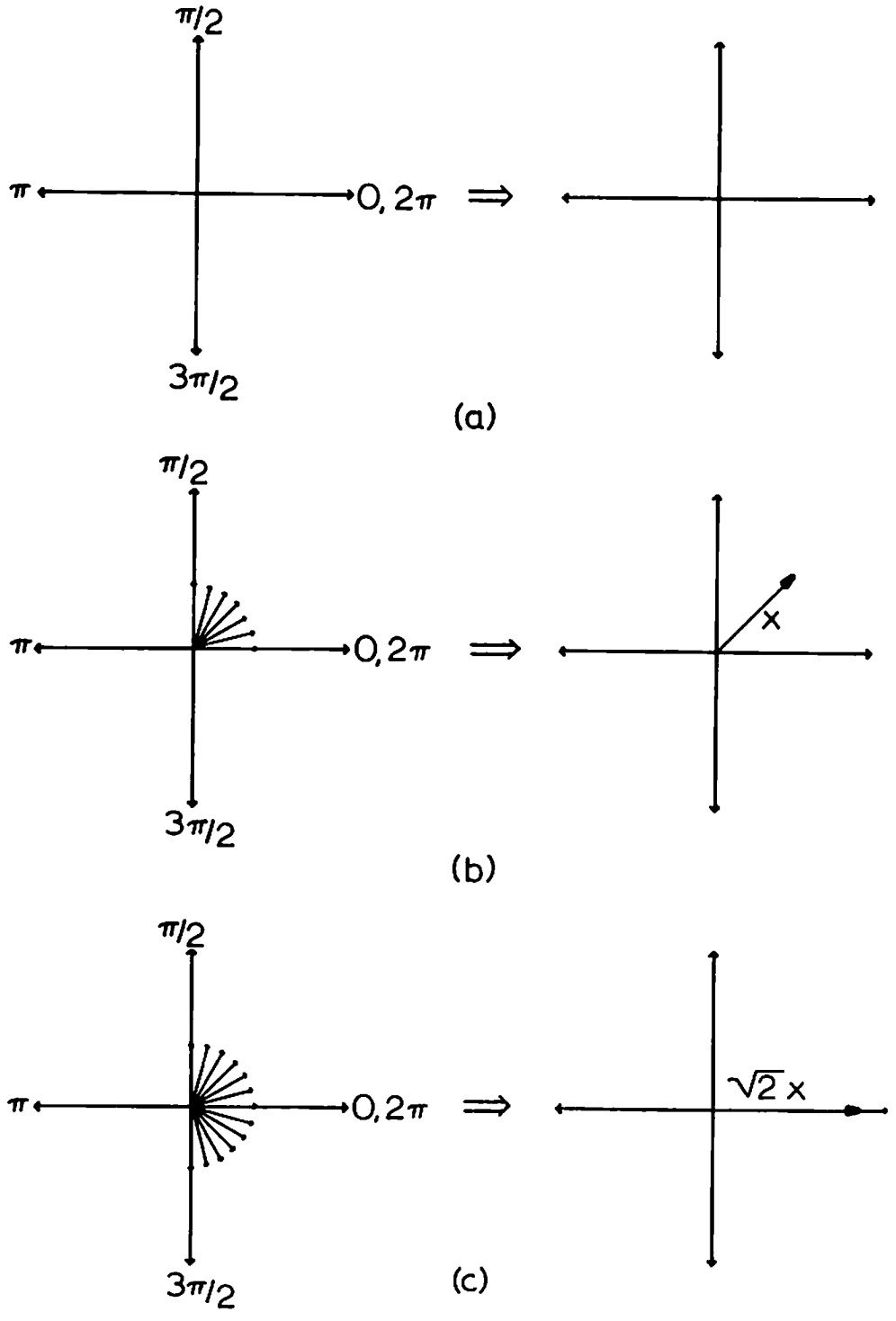

Figure 7-17. Diagram of the vector addition used to calculate the output from the quantizer screen.

such as in Fig. 5-2 in the first order is that this screen produces a halftoned picture whose diffracted amplitude is much less sensitive to slight line blooming due to overexposure. It depends not so much on the precise width of the line as on how many lines there are. This results in a much more distinct quantization effect. A quantized version of Fig. 7-3 is shown in Fig. 7-18. The result is particularly visible on the face of the cylinder, showing a decrease through the three output quantization levels.

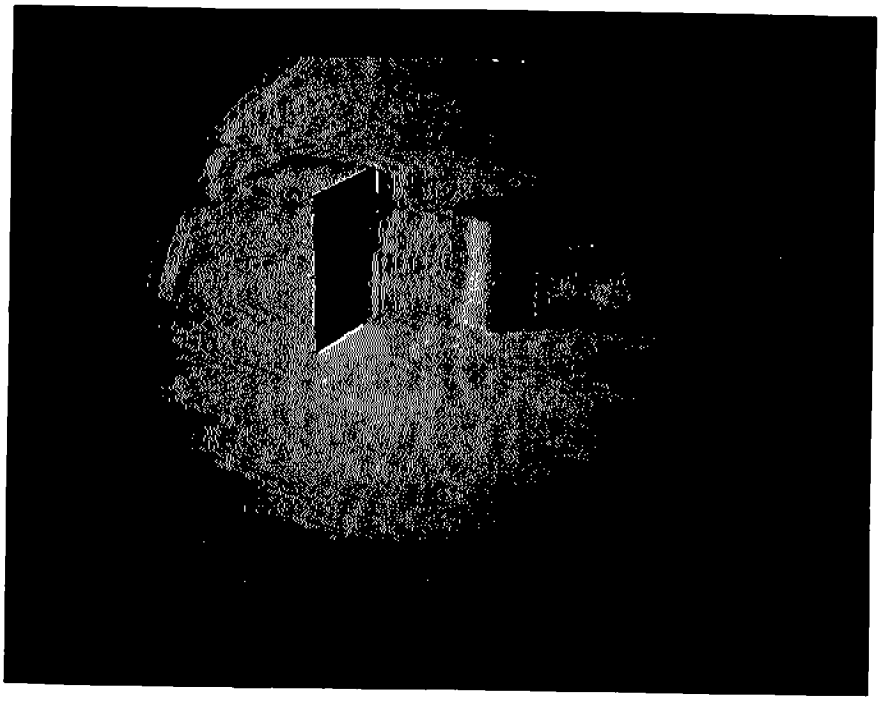

Figure 7-18. Quantized geometrical figures.

CHAPTER 8

CONCLUSIONS AND TOPICS FOR FURTHER RESEARCH

In this dissertation an analysis of nonlinear optical processing by halftone screen preprocessing has been made. The technique is very general, allowing arbitrary transfer functions to be achieved with either monotonic or non-monotonic cells. An exact algorithm for synthesizing monotonic cells has been presented, with illustrative examples. In general there exists no unique solution to the synthesis problem for non-monotonic cells; however an algorithm which yields a solution of arbitrarily high accuracy was presented. Non-monotonic cells are frequently to be preferred to monotonic cells for abrupt jump types of transfer functions because they are somewhat less sensitive to line blooming problems on the copy film. Consideration was given to the effect on the transfer function of non-ideal film in the halftone process. It was discovered that finite gamma and saturation density degrade the transfer function, with the greatest problem occuring at sharp jumps in the transfer function. These sharp jumps become rounded rather than sharp. A technique

for compensating for the resulting degradations which is applicable in many cases was presented. The precompensation technique works for smooth curves, but at the cost of a somewhat decreased dynamic range. Better films with a high gamma and less tendency to bloom in the overexposed areas are needed to improve the performance of the halftone method.

Several theoretical topics seem worthy of further effort. The analysis of the non-ideal film situation for non-monotonic halftone cells should be considered. These cells are attractive because of the greater power present in the first diffraction order and the decreased sensitivity to blooming due to overexposure. The use of more than one diffraction order, and the placement of amplitude and/or phase shifting masks in the various orders would probably yield interesting results. For example, it might be possible to synthesize a wide variety of different transfer functions by using the appropriate combination of diffraction orders, each appropriately phase delayed and amplitude scaled. The proper choice of the halftone cell shape to yield the maximum variety and range of possible functions would be an interesting problem. It might prove possible to devise a halftone screen which would yield several transfer functions of interest in different diffraction orders. This screen

might be two-dimensional and multiple orders could be used. It could also be capable of yielding these various transfer functions simultaneously.

The feasibility of the halftone technique has been experimentally verified. The performance limitations are the halftone screen itself and the medium used to record the halftoned picture. A technique for fabricating complex halftone screens accurately is necessary if the full potential of this method is to be realized. Since this need be done only once for each transfer function, speed is not a primary consideration. The scanning microdensitometer approach was not found to be sufficiently accurate for precise work, though this is perhaps not generally true for all microdensitometers. Alternatives such as the shifted grating method or a step and repeat camera could be considered. The non-ideal characteristics of the recording medium are a serious limitation. In addition to finite gamma and saturation density, the film requires several minutes to process.

In any practical system, the photographic film must be replaced by some sort of real-time optical element. This would make real-time or near real-time operation possible. Two possibilities are the liquid crystal light valve [8-1] and the PROM device [8-2]. Either device has

been designed for wide range inputs and consequently has a relatively low gamma (approximately 2.0 in the case of the liquid crystal device). They are not ideal binary thresholding devices, and will therefore not yield ideal results, but some type of compensation is probably possible. The halftone technique is an attractive one for these devices because it does not require variable device characteristics to achieve different transfer functions. It is a challenge to develop high gamma devices with a large saturation density now that a demonstrated real-time need has been found.

As an example of how a real-time nonlinear processing system might be constructed, consider a situation in which an outdoor scene must be nonlinearly processed. This could be accomplished with the following procedure: 1.) Image the scene onto the halftone screen, 2.) Image the screen onto an incoherent-to-coherent conversion device with a high gamma characteristic, and 3.) Process the coherent light as indicated in chapter 1 to yield the output. This accomplishes the processing at an operating speed limited only by the response time of the active optical element.

In conclusion, the halftone technique is a very versatile, flexible technique to consider for performing

nonlinear analog operations on two-dimensional data. It would be applicable in any situation where the halftone screen can be made and the precision of digital processing is not required. The other factor which should be considered is that the digital method requires scanning the input data with some sort of analog device in the beginning. It is therefore also limited by the precision achievable in an analog system. As a final note, this optical technique in common with other optical techniques is very much less expensive to implement than a digital system to perform the same task.

REFERENCES

[1-1] J. W. Goodman, Introduction to Fourier Optics, McGraw-Hill, New York, 1968.

[1-2] K. T. Stalker and S. H. Lee, "Use of Nonlinear Optical Elements in Optical Information Processing", J. Opt. Soc. Am., vol. 64, page 545, 1974.

[1-3] S. H. Lee, "Optical Processing with Nonlinearity and Feedback", Proceedings Electro-Optics/International Laser Conference 1975, Anaheim, California, pp. 22-30, 1975.

[1-4] S. H. Lee, "Mathematical Operations by Optical Processing", Optical Engineering, vol. 13, pp. 196-207, 1974.

[1-5] N. H. Farhat, "Nonlinear Optical Data Processing and Filtering: A Feasibility Study", IEEE Trans. Computers, vol. C-24, pp. 443-448, 1975.

[1-6] J. D. Armitage and A. W. Lohmann, "Theta Modulation in Optics", Applied Optics, vol. 4, pp. 399-403, 1965.

[1-7] J. Schwider and R. Burow, "Nonlinearities in Image Holography", J. Opt. Soc. Am., vol. 60, page 1421, 1970.

[1-8] Goodman, chapt. 7.

[1-9] Goodman, pp. 21-25.

[1-10] M. Marquet, "Dehalftoning of Negatives by Optical Filtering", Optica Acta, vol. 6, pp. 404-405, 1959.

[1-11] M. Marquet and J. Tsujiuchi, "Interpretation of Particular Aspects of Dehalftoned Images", Optica Acta, vol. 8, pp. 267-277, 1961.

[1-12] H. Kato and J. W. Goodman, "Nonlinear Transformations and Logarithmic Filtering in Coherent Optical Systems", Optics Communications, vol. 8, pp. 378-381, 1973.

[1-13] H. Kato and J. W. Goodman, "Nonlinear Filtering in Coherent Optical Systems Through Halftone Screen Processes", Applied Optics, vol. 14, pp. 1813-1824, 1975.

[1-14] T. C. Strand, "Non-monotonic Non-linear Image Processing Using Halftone Techniques", Optics Communications, vol. 15, pp. 60-65, 1975.

[1-15] A. W. Lohmann and T. C. Strand, "Nonlinear Optical Image Processing", Proceedings Optical Society of America Topical Meeting on Image Processing, Asilomar, California, February 1976.

[1-16] A. W. Lohmann and T. C. Strand, "Analog-to Digital Conversion of Pictures with Optical Means", Proceedings Electro-Optics/International Laser Conference 1975, Anaheim, Calif., pp. 16-21, 1975.

[1-17] H. K. Liu, J. W. Goodman, and J. Chan, "Equidensitometry by Coherent Optical Filtering", submitted to Applied Optics.

[1-18] A. A. Sawchuk and S. R. Dashiell, "Nonmonotonic Nonlinearities in Optical Processing", Proceedings IEEE 1975 International Optical Computing Conference, Washington, D. C., pp. 73-76, April, 1975.

[1-19] S. R. Dashiell and A. A. Sawchuk, "Optical Synthesis of Nonlinear Nonmonotonic Functions", J. Opt. Soc. Am., vol. 65, page 1177, 1975.

[1-20] S. R. Dashiell and A. A. Sawchuk, "Optical Synthesis of Nonlinear Nonmonotonic Functions", Optics Communications, vol. 15, pp. 66-70, 1975.

[1-21] S. R. Dashiell and A. A. Sawchuk, "Analysis and Synthesis of Nonlinear Optical Processing", Proceedings Electro-Optics/International Laser Conference 1975, Anaheim, California, pp. 9-15, 1975.

[1-22] S. R. Dashiell and A. A. Sawchuk, "Synthesis of Nonlinear Nonmonotonic Functions in Optical Image Processing", Proceedings Optical Society of America Topical Meeting on Image Processing, Asilomar, California, February 1976.

[2-1] Goodman, pp. 21-25.

[2-2] D. Kermisch and P. G. Roetling, "Fourier Spectrum of Halftone Images", J. Opt. Soc. Am., vol. 65, pp. 716-723, 1975.

[2-3] Goodman, page 14.

[2-4] Goodman, chapter 7.

[3-1] A. V. Oppenheim, R. W. Schaefer, and T. G. Stockham, Jr., "Nonlinear Filtering of Multiplied and Convolved Signals", Proc. IEEE, vol. 56, pp. 1264-1291, 1968.

[3-2] H. C. Andrews, A. G. Tescher, and R. P. Kruger, "Image Processing by Digital Computer", IEEE Spectrum, vol. 9, no. 7, pp. 20-32, 1972.

[3-3] A. A. Sawchuk and S. R. Dashiell, "Nonmonotonic Nonlinearities in Optical Processing", Proceedings IEEE 1975 International Optical Computing Conference, Washington, D. C., pp. 73-76, April, 1975.

[4-1] G. A. Korn and T. M. Korn, Mathematical Handbook for Scientists and Engineers, Second Edition, McGraw-Hill, New York, page 902, 1968.

[7-1] H. Kato and J. W. Goodman, "Nonlinear Transformations and Logarithmic Filtering in Coherent Optical Systems", Optics Communications, vol. 8, pp. 378-381, 1973.

[7-2] H. Kato and J. W. Goodman, "Nonlinear Filtering in Coherent Optical Systems Through Halftone Screen Processes", Applied Optics, vol. 14, pp. 1813-1824, 1975.

[7-3] T. C. Strand, "Non-monotonic Non-linear Image Processing Using Halftone Techniques", Optics Communications, vol. 15, pp. 60-65, 1975.

[7-4] A. W. Lohmann and T. C. Strand, "Analog-to Digital Conversion of Pictures with Optical Means", Proceedings Electro-Optics/International Laser Conference 1975, Anaheim, Calif., pp. 16-21, 1975.

[8-1] T. D. Beard, W. P. Bleha, S-Y. Wong, Appl. Phys. Lett., vol. 22, pp. 90-92, 1973.

[8-2] S. Iwasa and J. Feinleib, "The PROM Device in Optical Processing Systems", Optical Engineering, vol. 13, pp. 235-242, 1974.